Khakalo, Sergei; Niiranen, Jarkko

Form II of Mindlin's second strain gradient theory of elasticity with a simplification: for materials and structures from nano- to macro-scales

Published in:
European Journal of Mechanics A: Solids

DOI:
10.1016/j.euromechsol.2018.02.013

Published: 01/09/2018

Document Version
Peer-reviewed accepted author manuscript, also known as Final accepted manuscript or Post-print

Form II of Mindlin's second strain gradient theory of elasticity with a simplification: For materials and structures from nano- to macro-scales

Article *in* European Journal of Mechanics - A/Solids · April 2018

DOI: 10.1016/j.euromechsol.2018.02.013

CITATIONS
3

READS
74

2 authors:

Sergei Khakalo
Aalto University
17 PUBLICATIONS **56** CITATIONS
SEE PROFILE

Jarkko Niiranen
Aalto University
44 PUBLICATIONS **264** CITATIONS
SEE PROFILE

Form II of Mindlin's second strain gradient theory of elasticity with a simplification: for materials and structures from nano- to macro-scales

Sergei Khakalo* and Jarkko Niiranen*

*Aalto University, School of Engineering, Department of Civil Engineering, P.O. Box 12100, 00076 AALTO, Finland.

February 22, 2018

Abstract

The fundamental equations for Form II of Mindlin's second strain gradient elasticity theory for isotropic materials are first derived. A corresponding simplified formulation is then proposed, with six and two higher-order material parameters for the strain and kinetic energy, respectively. This simplified model is still capable of accounting for free surface effects and surface tension arising in second strain gradient continua. Within the simplified model, at first, surface tension effects appearing in nano-scale solids near free boundaries are analyzed. Next, a thin strip under tension and shear is considered and closed-form solutions are provided for analyzing the free surface effects. Expressions for effective Poisson's ratio and effective shear modulus are proposed and found to be size-dependent. Most importantly, for each model problem a stability analysis is accomplished disallowing non-physical solutions (befallen but not exclusively disputed in a recent Form I article). Finally, a triangular macro-scale lattice structure of trusses is shown, as a mechanical metamaterial, to behave as a second strain gradient continuum. In particular, it is shown that initial stresses prescribed on boundaries can be associated to one of the higher-order material parameters, modulus of cohesion, giving rise to surface tension. For completeness, a numerical free vibration eigenvalue analysis is accomplished for both a fine-scale lattice model and the corresponding second-order continuum via standard and isogeometric finite element simulations, respectively, completing the calibration procedure for the higher-order material parameters. The eigenvalue analysis confirms the necessity of the second velocity gradient terms in the kinetic energy density.

Keywords: second strain gradient elasticity, third displacement gradient elasticity, stability analysis, surface effects, surface tension, size effects, nano-structures, mechanical metamaterials, architectured materials, lattice structures, effective material moduli, dispersion relation

1 Introduction

Material modelling, in its broad meaning, is a fundamental task to be accomplished in order to adequately describe and predict the mechanical behaviour of solids. Although all materials are known to have a discrete nature, real physical systems can be modelled by the classical theories of continuum mechanics introduced and at first developed by such famous names as Piola, Poisson, Navier, Cauchy, and many others. The classical continuum models assume that the characteristic length scale of the material, e.g., grain or inhomogeneity size, is much smaller than the representative volume of the underlying averaging principles. This assumption is not necessarily valid, however, when modelling, on one hand, micro- and nano-scale objects such as MEMS or NEMS, or on the other hand, meso- and macro-scale discrete systems such as mechanical metamaterials or lattice structures. At nano-scale, due to the increasing surface-to-volume ratio, most materials demonstrate a very strong size-dependent behaviour. As reported in many works (see [1] and [2], for instance), atoms lying near a free surface are in the presence of different bindings than atoms in the bulk due to a redistribution of the underlying

electronic charges leading to different values of elastic moduli in the surface region and in the bulk. As an example, it has been experimentally observed that nano-wires can be relatively stiffer [3, 4, 5] or softer [6, 7] than the corresponding bulk material. It has been reported as well that the surface tension can lead to a liquid-like pseudoelasticity for sub-10-nm crystalline silver particles [8]. At micro-scale, the size-dependent material behaviour is typically caused by interactions of molecular chains in polymers [9] or grains in polycrystals and granular materials [10, 11, 12]. At meso- or macro-scale, the characteristic length scale, especially in lattice structures, is associated to the size of the elementary cell or representative volume element of the system.

In order to incorporate the material length scale into continuum models, a family of generalized continuum theories has been developed during the past century: couple-stress theories [13, 14, 15], strain gradient theories [16, 17, 18], micromorphic theories [19, 20, 16], multipolar theories [21], continua with surface elasticity [22, 23, 24] and non-local theories [25] (see [26, 27, 28, 29], for references and detailed overviews). In the first-order strain gradient theories, by including the second gradient of displacements [13, 16] or equivalently the first gradient of strains [18] into Helmholtz free energy density function, it is possible to distinguish the surface layer from the bulk material – unlike in [22, 23] where the bulk material is covered by a membrane-like surface of zero thickness governed by a constitutive law. As a matter of fact, the corresponding higher-order boundary conditions become responsible for the surface effects. In the isotropic case, in particular, there appears five higher-order material coefficients in addition to the classical material moduli. By utilizing atomistic approaches, or *ab initio* simulations, these additional material parameters have been determined in [30, 31, 32], for instance. The atomistic representation of the strain gradient elasticity tensors has been provided very recently in [33]. Besides, for the identification of strain gradient coefficients both heuristic methods [34, 35] and homogenization approaches [36] can be found in the literature.

In 1965, Mindlin [17] showed that by including the third gradient of displacements into the strain energy density function the surface tension can arise in isotropic, centrosymmetric, linearly elastic solids (as a consequence of the initial, homogeneous, self-equilibrating triple stresses). Earlier at the same year, it had been reported by Toupin and Gazis [37] that such an effect appears within the first strain gradient theory only for non-centrocymmetric materials. The third gradient of displacements brings eleven additional material parameters to the model, giving eighteen elastic moduli in total, determined via atomistic calculations in [38, 39] (2013). The need of the third gradient of displacements – providing a linear term in the second gradient of strains (responsible for surface tension) and coupling terms between strains and their second gradients (responsible for free surface effects) in the strain energy density – has been quite recently (2016) reconsidered for isotropic solids by Cordero et al. in [40]. The present contribution can be considered as a critical amendment, complement and extension of [40] as detailed in what follows. It should be noticed that Mindlin's work [17] has been extended to geometrically non-linear case with energetic boundaries by Javili et al. in [29] (2013).

The class of the so-called simplified models of strain gradient elasticity, to which the core of the present work belongs as well, has been developed in order (1) to reduce the number of higher-order material parameters and (2) to derive analytical solutions for model problems. The simplified first strain gradient model including only one additional material constant was originally proposed by Vardoulakis et al. in [41] and Altan and Aifantis in [42], and later extended to the second strain gradient models by others (see [43], for instance). A hierarchy of the simplified isotropic first strain gradient models is presented in [44], whereas the higher-order inertia effects are addressed in [45, 46], for instance. The reduced strain gradient models have been applied in a variety of applications: for regularizing singularities and stress concentrations [41, 43, 47, 48, 49, 50, 51, 52], for nano- and micro-structures [11, 53] and for granular materials [12], in particular. Furthermore, the strain gradient theories have been adopted and developed for modelling numerous mechanical metamaterials [54, 55, 56, 57, 58, 59] – providing exceptional properties not observed in natural materials.

Regarding computational methods, a number of works can be found for the first strain gradient models as detailed in an overview in [60]. For the second strain gradient models, however, only three related works exist: in [40], the finite element formulation is based on [61] where the second strain gradient theory is obtained as a special case of a second-order micromorphic model; the second strain gradient elasticity theory with second velocity gradient inertia is implemented via conforming, isogeometric Galerkin methods for two-dimensional problems in [62], and for static three-dimensional problems in [63].

The present paper focuses on (1) the theoretical fundamentals, (2) model problems and (3) applications of Mindlin's second strain gradient elasticity theory involving the second velocity gradient inertia. First of all, we distinguish two forms of the strain energy density (Form I and Form II; cf. [18]) and introduce a general Form II second strain gradient elasticity model which is based on enriching the strain energy density by the first and second gradients of strains, instead of the second and third gradients of displacements as proposed by Mindlin in his Form I model [17]. In case of linearly elastic isotropic materials, we define the strain energy density and derive the corresponding constitutive relations – not explicitly revealed before. The core of the present work is, however, in proposing a simplified Form II model which, along with the Lamé parameters, contains six and two higher-order material moduli in the strain energy density and kinetic energy, respectively, and is still able to account for free surface effects and surface tension. Accordingly, besides the model proposal the main novelties and findings of the present work are detailed below:

(i) A set of stability analyses for the higher-order material parameters is performed (insufficiently accomplished in the related earlier study [40] considering a Form I model). It is demonstrated how non-admissible parameter values violating the positive definiteness of the strain energy lead to singular solutions resulting in absolutely non-physical material behaviour befallen but not disputed in [40], rather endorsed by a vague argumentation and leaving the question open: "The relevance of the proposed parameters and the possible need for higher order regularisation remain open questions which require a thorough analysis of the well-posedness of the associated variational problem" [40]. Our analysis resolves the parameter issue and removes the regularization question, and hence impugns many of the results presented in [40].

(ii) Both free surface effects and surface tension are captured in the model problems of nano-objects in tension and shear. The size dependency of the related effective shear modulus and effective Poisson's ratio is demonstrated as well.

(iii) A fairly general macro-scale lattice structure is shown to behave as a second strain gradient continuum – albeit the analysis remains valid for such a mechanical metamaterial at any length scale – approving that the critical higher-order effects encountered are not limited to nano-scale alone (primarily considered by [40] and the other related references [17, 38, 39]).

(iv) Steps towards the identification and distinguishment for the role of different higher-order parameters provides understanding of their influence on the effective material properties. This knowledge finally offers tools for designing mechanical metamaterials with desired properties.

This article is organized as follows: In Section 2, by utilizing Hamilton's principle, the stress equation of motion and boundary conditions are recalled. The Form II strain energy and constitutive equations are then derived for isotropic materials and a simplified variant of the model is proposed. In Section 3, surface tension in solids is analyzed by considering two model problems and including stability analyses guaranteeing physical solutions. Sections 4 and 5 are devoted to surface effects arising in a thin strip under tensile and shear loadings, respectively, including stability analyses. Section 6 analyzes a fairly general lattice structure, as an axample of architectured second gradient metamaterials, and serves as a confirmation for the effects observed in Sections 3, 4 and 5. Section 7 discusses the results with some concluding remarks.

Tensor notation. The boldface letters are used for denoting vectors or tensors of any rank. In the tensor product notation the multiplication sign $\otimes$ is omitted: $\nabla\boldsymbol{u} = \nabla \otimes \boldsymbol{u} = u_{j,i}\boldsymbol{e}_i\boldsymbol{e}_j$, for instance, where $\boldsymbol{e}_i$, $i = 1, 2, 3$, form the basis of an orthogonal Cartesian coordinate system. Scalar products between vectors or tensors of the same rank are defined as follows:

$$\boldsymbol{n}\cdot\boldsymbol{u} = n_i u_i, \quad \boldsymbol{\tau} : \boldsymbol{\varepsilon} = \tau_{ij}\varepsilon_{ij}, \quad \boldsymbol{\tau}\cdot\cdot\boldsymbol{\varepsilon} = \tau_{ij}\varepsilon_{ji},$$

$$\nabla\boldsymbol{\tau} \vdots \nabla\boldsymbol{\varepsilon} = \tau_{jk,i}\varepsilon_{jk,i}, \quad \nabla\nabla\boldsymbol{\tau} :: \nabla\nabla\boldsymbol{\varepsilon} = \tau_{ks,ij}\varepsilon_{ks,ij}.$$

Scalar products between tensors of different rank are defined as

$$\boldsymbol{n}\cdot\boldsymbol{\sigma} = n_i\sigma_{ij}\boldsymbol{e}_j, \quad \boldsymbol{nn} : \nabla\boldsymbol{\tau} = n_i n_j \tau_{jk,i}\boldsymbol{e}_k, \quad \boldsymbol{nnn} \vdots \nabla\nabla\boldsymbol{\tau} = n_i n_j n_k \tau_{ks,ij}\boldsymbol{e}_s.$$

Above, Einstein's summation convention has been used for the indices.

2 Basic equations of the second strain gradient elasticity

In this section, we first utilize Hamilton's principle and derive the equation of motion in terms of force quantities and boundary conditions of the second strain gradient elasticity theory. The expressions for natural boundary conditions include the higher-order inertia terms as observed in [16] within the first strain gradient theory. Next, we introduce the Mindlin's strain energy density of Form II for isotropic materials and derive the corresponding constitutive equations. Finally, we propose a simplified form of the corresponding higher-order continuum theory which, unlike the existing simplified models, is able to account for the free surface effects.

For derivations, we apply direct tensor notation. The corresponding expressions written with index notation are collected in Appendix B.

2.1 Stress equation of motion and boundary conditions

Let us consider Hamilton's principle for an independent displacements variation $\delta\boldsymbol{u}$ between fixed limits of $\boldsymbol{u}$ at times t_0 and t_1 [64] in the form

$$\delta\int_{t_0}^{t_1}(\mathscr{T}-\mathscr{W})dt+\int_{t_0}^{t_1}\delta W_1 dt=0, \tag{1}$$

where $\mathscr{T}$ and $\mathscr{W}$ are the total kinetic and strain energies in a volume Ω:

$$\mathscr{T}=\int_{\Omega}T d\Omega, \quad \mathscr{W}=\int_{\Omega}W d\Omega \tag{2}$$

and δW_1 stands for the variation of the work done by external forces.

It is assumed that kinetic energy density T is a function of velocity and its first and second gradients, whereas strain energy density W contains kinematical variables $\boldsymbol{\varepsilon}_1$, $\boldsymbol{\varepsilon}_2$ and $\boldsymbol{\varepsilon}_3$:

$$T=T(\dot{\boldsymbol{u}},\nabla\dot{\boldsymbol{u}},\nabla\nabla\dot{\boldsymbol{u}}), \quad W=W(\boldsymbol{\varepsilon}_1,\boldsymbol{\varepsilon}_2,\boldsymbol{\varepsilon}_3). \tag{3}$$

Originally, the second strain gradient elasticity theory has been formulated by Mindlin [17] with

$$\boldsymbol{\varepsilon}_1=\boldsymbol{\varepsilon}=\frac{1}{2}(\nabla\boldsymbol{u}+\boldsymbol{u}\nabla), \quad \boldsymbol{\varepsilon}_2=\nabla\nabla\boldsymbol{u}, \quad \boldsymbol{\varepsilon}_3=\nabla\nabla\nabla\boldsymbol{u}, \tag{4}$$

corresponding to a Form I strain gradient elasticity theory [18]. In this work, we consider Form II strain gradient elasticity theory implying that

$$\boldsymbol{\varepsilon}_2=\nabla\boldsymbol{\varepsilon}, \quad \boldsymbol{\varepsilon}_3=\nabla\nabla\boldsymbol{\varepsilon}, \tag{5}$$

which is supposed to be an extension of works [17] and [18]. As in [17], the case of infinitesimal strains is considered.

Next, the variation of the total kinetic energy (for guidance, see [64]) is derived in the form

$$\delta\int_{t_0}^{t_1}\mathscr{T}dt=-\int_{t_0}^{t_1}\int_{\Omega}(\dot{\boldsymbol{p}}_1\cdot\delta\boldsymbol{u}+\dot{\boldsymbol{p}}_2:\nabla\delta\boldsymbol{u}+\dot{\boldsymbol{p}}_3\vdots\nabla\nabla\delta\boldsymbol{u})d\Omega dt, \tag{6}$$

where $\boldsymbol{p}_1$, standing for the ordinary momentum, and $\boldsymbol{p}_2$ and $\boldsymbol{p}_3$, denoting the higher-order momentum tensors, are defined as the derivatives of the kinetic energy density with respect to the corresponding work conjugates, i.e., $\dot{\boldsymbol{u}}$, $\nabla\dot{\boldsymbol{u}}$ and $\nabla\nabla\dot{\boldsymbol{u}}$, as

$$\boldsymbol{p}_1=\frac{\partial T}{\partial\dot{\boldsymbol{u}}}, \quad \boldsymbol{p}_2=\frac{\partial T}{\partial(\nabla\dot{\boldsymbol{u}})}, \quad \boldsymbol{p}_3=\frac{\partial T}{\partial(\nabla\nabla\dot{\boldsymbol{u}})}. \tag{7}$$

The variation of the total strain energy takes the form

$$\delta\int_{t_0}^{t_1}\mathscr{W}dt=\int_{t_0}^{t_1}\int_{\Omega}(\boldsymbol{\tau}_1:\delta\boldsymbol{\varepsilon}_1+\boldsymbol{\tau}_2\vdots\delta\boldsymbol{\varepsilon}_2+\boldsymbol{\tau}_3::\delta\boldsymbol{\varepsilon}_3)d\Omega dt, \tag{8}$$

where the Cauchy (or Cauchy-like) stress $\boldsymbol{\tau}_1$, the work conjugate of (ordinary) strain $\boldsymbol{\varepsilon}$, and the double and triple stresses $\boldsymbol{\tau}_2$ and $\boldsymbol{\tau}_3$, the work conjugate of the higher-order kinematical variables $\boldsymbol{\varepsilon}_2$ and $\boldsymbol{\varepsilon}_3$, respectively, are defined as

$$\boldsymbol{\tau}_1 = \frac{\partial W}{\partial \boldsymbol{\varepsilon}_1}, \quad \boldsymbol{\tau}_2 = \frac{\partial W}{\partial \boldsymbol{\varepsilon}_2}, \quad \boldsymbol{\tau}_3 = \frac{\partial W}{\partial \boldsymbol{\varepsilon}_3}. \tag{9}$$

Now, by assuming the variation of work done by external forces in the form

$$\int_{t_0}^{t_1} \delta W_1 dt = \int_{t_0}^{t_1} \left[\int_{\Omega} \boldsymbol{f} \cdot \delta \boldsymbol{u} d\Omega + \int_{\partial\Omega_1} \boldsymbol{t}_1 \cdot \delta \boldsymbol{u} dS + \int_{\partial\Omega_2} \boldsymbol{t}_2 \cdot (\boldsymbol{n} \cdot \nabla \delta \boldsymbol{u}) dS + \int_{\partial\Omega_3} \boldsymbol{t}_3 \cdot (\boldsymbol{n} \cdot \nabla)^2 \delta \boldsymbol{u} dS \right] dt, \tag{10}$$

where for simplicity all possible edge and wedge forces are omitted (cf. [17, 65, 45]), one can derive the stress equation of motion of a 3D solid within the second strain gradient elasticity theory (see [65, 45])

$$\nabla \cdot \boldsymbol{\sigma} + \boldsymbol{f} = \dot{\boldsymbol{p}}_1 - \nabla \cdot \dot{\boldsymbol{p}}_2 + \nabla\nabla : \dot{\boldsymbol{p}}_3 \quad \text{in } \Omega \tag{11}$$

with $\boldsymbol{\sigma}$ denoting the so-called total [41], or balancing, stress tensor which is expressed in terms of the Cauchy, double and triple stresses as

$$\boldsymbol{\sigma} = \boldsymbol{\tau}_1 - \nabla \cdot \boldsymbol{\tau}_2 + \nabla\nabla : \boldsymbol{\tau}_3. \tag{12}$$

It should be mentioned that there is a discussion on the Cauchy and total stresses to be a candidate on a role of true stresses since the physical meaning of these two stresses is still an open question. In [66, 65], it is reported that the total stresses play the role of Cauchy stresses which for the bulk part of a material satisfy the Cauchy theorem. In [49], however, it is demonstrated that serious problems arise with the total stresses. For a deep discussion on the validity of the Cauchy theorem in higher order elasticity theories, the reader is invited to see the pioneering work from Seppecher and dell'Isola [67], see also [68].

Within the second strain gradient elasticity, the traction, or natural, boundary conditions are expressed as

$$\begin{aligned} \partial\Omega_1 : \quad & \boldsymbol{t}_1 = \boldsymbol{n} \cdot \boldsymbol{\sigma} + \mathbf{L} \cdot [\boldsymbol{n} \cdot (\boldsymbol{\tau}_2 - \nabla \cdot \boldsymbol{\tau}_3) + \mathbf{L} \cdot (\boldsymbol{n} \cdot \boldsymbol{\tau}_3) - (\nabla_s \boldsymbol{n}) \cdot (\boldsymbol{n}\boldsymbol{n} : \boldsymbol{\tau}_3)] \\ & + \boldsymbol{n} \cdot (\dot{\boldsymbol{p}}_2 - \nabla \cdot \dot{\boldsymbol{p}}_3) - \nabla_s \cdot (\boldsymbol{n} \cdot \dot{\boldsymbol{p}}_3) + (\nabla_s \cdot \boldsymbol{n}) \boldsymbol{n}\boldsymbol{n} : \dot{\boldsymbol{p}}_3, \end{aligned} \tag{13}$$

$$\begin{aligned} \partial\Omega_2 : \quad & \boldsymbol{t}_2 = \boldsymbol{n}\boldsymbol{n} : (\boldsymbol{\tau}_2 - \nabla \cdot \boldsymbol{\tau}_3) + \boldsymbol{n} \cdot [\mathbf{L} \cdot (\boldsymbol{n} \cdot \boldsymbol{\tau}_3)] + \mathbf{L} \cdot (\boldsymbol{n}\boldsymbol{n} : \boldsymbol{\tau}_3) \\ & + \boldsymbol{n}\boldsymbol{n} : \dot{\boldsymbol{p}}_3, \end{aligned} \tag{14}$$

$$\partial\Omega_3 : \quad \boldsymbol{t}_3 = \boldsymbol{n}\boldsymbol{n}\boldsymbol{n} \vdots \boldsymbol{\tau}_3, \tag{15}$$

with $\mathbf{L} = \boldsymbol{n}(\nabla_s \cdot \boldsymbol{n}) - \nabla_s$ and $\nabla_s = (\mathbf{I} - \boldsymbol{n}\boldsymbol{n}) \cdot \nabla$ (see [17]). It can be seen that on a par with ordinary traction force $\boldsymbol{t}_1$, the work conjugate of displacement $\boldsymbol{u}$, there appear double and triple traction forces $\boldsymbol{t}_2$ and $\boldsymbol{t}_3$, the work conjugates of the first and second normal derivatives of the displacements, respectively. Moreover, due to the first and second velocity gradients included in the kinetic energy density (3), the ordinary and double traction forces are enriched by higher-order inertia terms.

The essential boundary conditions are given as

$$\boldsymbol{u} = \boldsymbol{u}_1, \quad \boldsymbol{n} \cdot \nabla \boldsymbol{u} = \boldsymbol{u}_2, \quad (\boldsymbol{n} \cdot \nabla)^2 \boldsymbol{u} = \boldsymbol{u}_3, \tag{16}$$

where $\boldsymbol{u}_i$ are the prescribed functions on the corresponding Dirichlet boundary parts $\partial\Omega_{u_i}$, $i = 1, 2, 3$. Here, $\boldsymbol{n}$ denotes the unit vector normal to the domain boundary, ∇ stands for Hamilton's nabla-operator and $\mathbf{I}$ is the isotropic unit tensor of second rank.

As a note, it should be mentioned that initial conditions are not highlighted here.

2.2 Constitutive equations

For a linear elastic anisotropic non-centrosymmetric (see the definition of centrosymmetry in [69]) second strain gradient solid, the strain energy density is assumed to be a quadratic function in terms

of strains, first-order and second-order gradients of strains of the form

$$\begin{aligned} W = &\frac{1}{2}\boldsymbol{\varepsilon}_1 : {}^4\mathbf{C} : \boldsymbol{\varepsilon}_1 + \frac{1}{2}\boldsymbol{\varepsilon}_2 \vdots {}^6\mathbf{A} \vdots \boldsymbol{\varepsilon}_2 + \frac{1}{2}\boldsymbol{\varepsilon}_3 :: {}^8\mathbf{B} :: \boldsymbol{\varepsilon}_3 \\ &+ \boldsymbol{\varepsilon}_1 : {}^5\mathbf{D} \vdots \boldsymbol{\varepsilon}_2 + \boldsymbol{\varepsilon}_1 : {}^6\mathbf{C} :: \boldsymbol{\varepsilon}_3 + \boldsymbol{\varepsilon}_2 \vdots {}^7\mathbf{D} :: \boldsymbol{\varepsilon}_3 \\ &+ {}^3\mathbf{D} \vdots \boldsymbol{\varepsilon}_2 + {}^4\mathbf{B} :: \boldsymbol{\varepsilon}_3, \end{aligned} \tag{17}$$

where ${}^n\mathbf{A}$, ${}^n\mathbf{B}$, ${}^n\mathbf{C}$, ${}^n\mathbf{D}$ denote the stiffness tensors of the nth rank. The first two lines in expression (17) have been considered by Lazar [43], whereas the third line with terms linear in $\boldsymbol{\varepsilon}_2$ and $\boldsymbol{\varepsilon}_3$ (inspired by Mindlin's linear term, see [17]) complements the strain energy density (17) to a general case of a linear elastic anisotropic second strain gradient solid.

For a centrosymmetric isotropic (later isotropic, for brevity) second strain gradient solid, expression (17) is reduced by eliminating terms containing the stiffness tensors of odd rank (${}^3\mathbf{D}$, ${}^5\mathbf{D}$, ${}^7\mathbf{D}$) giving

$$\begin{aligned} W = &\frac{1}{2}\boldsymbol{\varepsilon}_1 : {}^4\mathbf{C} : \boldsymbol{\varepsilon}_1 + \frac{1}{2}\boldsymbol{\varepsilon}_2 \vdots {}^6\mathbf{A} \vdots \boldsymbol{\varepsilon}_2 + \frac{1}{2}\boldsymbol{\varepsilon}_3 :: {}^8\mathbf{B} :: \boldsymbol{\varepsilon}_3 \\ &+ \boldsymbol{\varepsilon}_1 : {}^6\mathbf{C} :: \boldsymbol{\varepsilon}_3 + {}^4\mathbf{B} :: \boldsymbol{\varepsilon}_3. \end{aligned} \tag{18}$$

Next, we distinguish two forms for the strain energy density:

$$W = W(\boldsymbol{\varepsilon}_1, \boldsymbol{\varepsilon}_2, \boldsymbol{\varepsilon}_3) = \tilde{W}(\boldsymbol{\varepsilon}, \nabla\nabla\boldsymbol{u}, \nabla\nabla\nabla\boldsymbol{u}) = \hat{W}(\boldsymbol{\varepsilon}, \nabla\boldsymbol{\varepsilon}, \nabla\nabla\boldsymbol{\varepsilon}), \tag{19}$$

where $\tilde{W}$ corresponds to Form I of the second strain gradient elasticity (cf. [17, 18]), while $\hat{W}$ stands for Form II which is explicitly written below. For the same displacement field $\boldsymbol{u}$, both formulations are equivalent with the following relations between the variables (cf. [18], pp. 110–111):

$$\begin{aligned} \nabla\nabla\boldsymbol{u} &= \nabla\boldsymbol{\varepsilon} - \boldsymbol{\varepsilon}\nabla + \nabla\boldsymbol{\varepsilon} \vdots {}^6\mathbf{I}, \\ \nabla\nabla\nabla\boldsymbol{u} &= \nabla\nabla\boldsymbol{\varepsilon} - \nabla\boldsymbol{\varepsilon}\nabla + \nabla\nabla\boldsymbol{\varepsilon} :: {}^8\mathbf{I}_1. \end{aligned} \tag{20}$$

For the isotropic materials, the strain energy density of Form II can be explicitly expressed as

$$\begin{aligned} \hat{W} = &\frac{1}{2}\lambda(\mathrm{tr}\boldsymbol{\varepsilon})^2 + \mu\boldsymbol{\varepsilon} : \boldsymbol{\varepsilon} + \hat{a}_1(\nabla\cdot\boldsymbol{\varepsilon})\cdot\nabla(\mathrm{tr}\boldsymbol{\varepsilon}) + \hat{a}_2\nabla(\mathrm{tr}\boldsymbol{\varepsilon})\cdot\nabla(\mathrm{tr}\boldsymbol{\varepsilon}) \\ &+ \hat{a}_3(\nabla\cdot\boldsymbol{\varepsilon})\cdot(\nabla\cdot\boldsymbol{\varepsilon}) + \hat{a}_4\nabla\boldsymbol{\varepsilon} \vdots \nabla\boldsymbol{\varepsilon} + \hat{a}_5\nabla\boldsymbol{\varepsilon} \vdots \boldsymbol{\varepsilon}\nabla \\ &+ \hat{b}_1(\Delta\mathrm{tr}\boldsymbol{\varepsilon})^2 + \hat{b}_2\nabla\nabla(\mathrm{tr}\boldsymbol{\varepsilon}) : \nabla\nabla(\mathrm{tr}\boldsymbol{\varepsilon}) + \hat{b}_3\Delta\boldsymbol{\varepsilon} : \nabla\nabla(\mathrm{tr}\boldsymbol{\varepsilon}) \\ &+ \hat{b}_4\Delta\boldsymbol{\varepsilon} : \Delta\boldsymbol{\varepsilon} + \hat{b}_5\nabla\cdot\boldsymbol{\varepsilon}\nabla : \nabla\boldsymbol{\varepsilon}\cdot\nabla + \hat{b}_6\nabla\nabla\boldsymbol{\varepsilon} :: \nabla\nabla\boldsymbol{\varepsilon} + \hat{b}_7\nabla\nabla\boldsymbol{\varepsilon} :: \nabla\boldsymbol{\varepsilon}\nabla \\ &+ \hat{c}_1(\mathrm{tr}\boldsymbol{\varepsilon})\Delta(\mathrm{tr}\boldsymbol{\varepsilon}) + \hat{c}_2\boldsymbol{\varepsilon} : \nabla\nabla(\mathrm{tr}\boldsymbol{\varepsilon}) + \hat{c}_3\boldsymbol{\varepsilon} : \Delta\boldsymbol{\varepsilon} + \hat{b}_0\Delta(\mathrm{tr}\boldsymbol{\varepsilon}). \end{aligned} \tag{21}$$

The relations between Form I and Form II second strain gradient elasticity theories, based on (20), are given in Appendix A. It should be mentioned that due to the compatibility conditions $\nabla\times\boldsymbol{\varepsilon}\times\nabla = 0$ expression (21) can take other equivalent forms, for instance, term $\Delta(\mathrm{tr}\boldsymbol{\varepsilon})$ is equal to and can be replaced by $\nabla\nabla : \boldsymbol{\varepsilon}$ as long as strains are compatible.

As within Form I, in addition to two classical Lamé parameters μ and λ, the strain energy density contains sixteen additional higher-order elastic moduli. The five coefficients $\hat{a}_i$ which appear in Toupin's and Mindlin's strain gradient theory [13, 16] relate to the first gradient of strains and have dimension of force. The seven parameters $\hat{b}_i$ relate to the second gradient of strains and have dimension of force times squared length. The three parameters $\hat{c}_i$ relate to the cross-terms with respect to strains and second gradient of strains and have dimension of force. The coefficient b_0, with the dimension of force, is a modulus of cohesion (see the discussion in [17]).

For the given strain energy density (21), the constitutive relations (9) are explicitly defined as

$$\begin{aligned}
\hat{\boldsymbol{\tau}}_1 &= 2\mu\boldsymbol{\varepsilon} + \lambda(\mathrm{tr}\boldsymbol{\varepsilon})\mathbf{I} + \hat{c}_1\Delta(\mathrm{tr}\boldsymbol{\varepsilon})\mathbf{I} + \hat{c}_2\nabla\nabla(\mathrm{tr}\boldsymbol{\varepsilon}) + \hat{c}_3\Delta\boldsymbol{\varepsilon},\\
\hat{\boldsymbol{\tau}}_2 &= \hat{a}_1(\mathbf{I}\nabla(\mathrm{tr}\boldsymbol{\varepsilon}) + \nabla\cdot\boldsymbol{\varepsilon}\mathbf{I})\cdot\cdot\,{}^4\mathbf{I} + 2\hat{a}_2\nabla(\mathrm{tr}\boldsymbol{\varepsilon})\mathbf{I}\\
&\quad + 2\hat{a}_3\mathbf{I}\nabla\cdot\boldsymbol{\varepsilon}\cdot\cdot\,{}^4\mathbf{I} + 2\hat{a}_4\nabla\boldsymbol{\varepsilon} + 2\hat{a}_5\boldsymbol{\varepsilon}\nabla\cdot\cdot\,{}^4\mathbf{I},\\
\hat{\boldsymbol{\tau}}_3 &= 2\hat{b}_1\Delta(\mathrm{tr}\boldsymbol{\varepsilon})\mathbf{II} + 2\hat{b}_2\nabla\nabla(\mathrm{tr}\boldsymbol{\varepsilon})\mathbf{I} + \hat{b}_3(\mathbf{I}\nabla\nabla(\mathrm{tr}\boldsymbol{\varepsilon}) + \Delta\boldsymbol{\varepsilon}\mathbf{I})\\
&\quad + 2\hat{b}_4\mathbf{I}\Delta\boldsymbol{\varepsilon} + 2\hat{b}_5\nabla\cdot\boldsymbol{\varepsilon}\mathbf{I}\nabla :: {}^8\mathbf{I} + \hat{b}_7(\nabla\boldsymbol{\varepsilon}\nabla + \nabla\nabla\boldsymbol{\varepsilon} :: {}^8\mathbf{I}_1) :: {}^8\mathbf{I}\\
&\quad + 2\hat{b}_6\nabla\nabla\boldsymbol{\varepsilon} + \hat{c}_1(\mathrm{tr}\boldsymbol{\varepsilon})\mathbf{II} + \hat{c}_2\boldsymbol{\varepsilon}\mathbf{I} + \hat{c}_3\mathbf{I}\boldsymbol{\varepsilon} + \hat{b}_0\mathbf{II},
\end{aligned} \tag{22}$$

where ${}^4\mathbf{I}$, ${}^6\mathbf{I}$, ${}^8\mathbf{I}_1$ and ${}^8\mathbf{I}$ stand for the isotropic tensors of fourth, sixth and eighth rank, respectively, and are defined as ${}^4\mathbf{I} = \frac{1}{2}(\boldsymbol{e}_i\boldsymbol{e}_j\boldsymbol{e}_i\boldsymbol{e}_j + \boldsymbol{e}_i\boldsymbol{e}_j\boldsymbol{e}_j\boldsymbol{e}_i)$, ${}^6\mathbf{I} = \boldsymbol{e}_i\boldsymbol{e}_j\boldsymbol{e}_k\boldsymbol{e}_j\boldsymbol{e}_i\boldsymbol{e}_k$, ${}^8\mathbf{I}_1 = \boldsymbol{e}_i\boldsymbol{e}_j\boldsymbol{e}_m\boldsymbol{e}_n\boldsymbol{e}_i\boldsymbol{e}_n\boldsymbol{e}_j\boldsymbol{e}_m$, ${}^8\mathbf{I} = \frac{1}{4}(\boldsymbol{e}_i\boldsymbol{e}_j\boldsymbol{e}_m\boldsymbol{e}_n\boldsymbol{e}_i\boldsymbol{e}_j\boldsymbol{e}_m\boldsymbol{e}_n + \boldsymbol{e}_i\boldsymbol{e}_j\boldsymbol{e}_m\boldsymbol{e}_n\boldsymbol{e}_j\boldsymbol{e}_i\boldsymbol{e}_m\boldsymbol{e}_n + \boldsymbol{e}_i\boldsymbol{e}_j\boldsymbol{e}_m\boldsymbol{e}_n\boldsymbol{e}_i\boldsymbol{e}_j\boldsymbol{e}_n\boldsymbol{e}_m + \boldsymbol{e}_i\boldsymbol{e}_j\boldsymbol{e}_m\boldsymbol{e}_n\boldsymbol{e}_j\boldsymbol{e}_i\boldsymbol{e}_n\boldsymbol{e}_m)$.

2.3 A simplified Form II model of the second strain gradient elasticity

For parameters $\hat{a}_i$ and $\hat{b}_i$, we adopt the simplifications proposed in [43, 65], where non-zero coefficients $\hat{a}_2$, $\hat{a}_4$ and $\hat{b}_2$, $\hat{b}_6$ are expressed in terms of Lamé parameters by introducing, respectively, two length-scale parameters l_a and l_b with the dimensions of length:

$$\begin{aligned}
\hat{a}_1 = \hat{a}_3 = \hat{a}_5 = 0, \quad \hat{a}_2 = \frac{1}{2}\lambda l_a^2, \quad \hat{a}_4 = \mu l_a^2\\
\hat{b}_1 = \hat{b}_3 = \hat{b}_4 = \hat{b}_5 = \hat{b}_7 = 0, \quad \hat{b}_2 = \frac{1}{2}\lambda l_b^4, \quad \hat{b}_6 = \mu l_b^4.
\end{aligned} \tag{23}$$

Parameters $\hat{c}_i$, $i = 1, 2, 3$, and $\hat{b}_0$, instead, are kept in the model implying a new simplified strain gradient elasticity model. Here and in what follows (see Appendix A) $\hat{c}_i = \tilde{c}_i = c_i$, $i = 1, 2, 3$, and $\hat{b}_0 = \tilde{b}_0 = b_0$. The simplified second strain gradient elasticity theory, through the strain energy density, reads as

$$\begin{aligned}
W &= \frac{1}{2}\lambda(\mathrm{tr}\boldsymbol{\varepsilon})^2 + \mu\boldsymbol{\varepsilon} : \boldsymbol{\varepsilon} + l_a^2\big(\frac{1}{2}\lambda\nabla(\mathrm{tr}\boldsymbol{\varepsilon})\cdot\nabla(\mathrm{tr}\boldsymbol{\varepsilon}) + \mu\nabla\boldsymbol{\varepsilon} \vdots \nabla\boldsymbol{\varepsilon}\big)\\
&\quad + l_b^4\big(\frac{1}{2}\lambda\nabla\nabla(\mathrm{tr}\boldsymbol{\varepsilon}) : \nabla\nabla(\mathrm{tr}\boldsymbol{\varepsilon}) + \mu\nabla\nabla\boldsymbol{\varepsilon} :: \nabla\nabla\boldsymbol{\varepsilon}\big)\\
&\quad + c_1(\mathrm{tr}\boldsymbol{\varepsilon})\Delta(\mathrm{tr}\boldsymbol{\varepsilon}) + c_2\boldsymbol{\varepsilon} : \nabla\nabla(\mathrm{tr}\boldsymbol{\varepsilon}) + c_3\boldsymbol{\varepsilon} : \Delta\boldsymbol{\varepsilon} + b_0\Delta(\mathrm{tr}\boldsymbol{\varepsilon}).
\end{aligned} \tag{24}$$

The corresponding constitutive relations (22), deprived of hats, take the simplified form

$$\begin{aligned}
\boldsymbol{\tau}_1 &= 2\mu\boldsymbol{\varepsilon} + \lambda(\mathrm{tr}\boldsymbol{\varepsilon})\mathbf{I} + c_1\Delta(\mathrm{tr}\boldsymbol{\varepsilon})\mathbf{I} + c_2\nabla\nabla(\mathrm{tr}\boldsymbol{\varepsilon}) + c_3\Delta\boldsymbol{\varepsilon},\\
\boldsymbol{\tau}_2 &= l_a^2\big(2\mu\nabla\boldsymbol{\varepsilon} + \lambda\nabla(\mathrm{tr}\boldsymbol{\varepsilon})\mathbf{I}\big),\\
\boldsymbol{\tau}_3 &= l_b^4\big(2\mu\nabla\nabla\boldsymbol{\varepsilon} + \lambda\nabla\nabla(\mathrm{tr}\boldsymbol{\varepsilon})\mathbf{I}\big) + c_1(\mathrm{tr}\boldsymbol{\varepsilon})\mathbf{II} + c_2\boldsymbol{\varepsilon}\mathbf{I} + c_3\mathbf{I}\boldsymbol{\varepsilon} + b_0\mathbf{II}.
\end{aligned} \tag{25}$$

By assuming constant μ and λ, stresses $\boldsymbol{\tau}_i$ as well as total stress $\boldsymbol{\sigma}$ can be expressed in the form

$$\boldsymbol{\tau}_1 = \boldsymbol{\tau}_0 + c_1\Delta(\mathrm{tr}\boldsymbol{\varepsilon})\mathbf{I} + c_2\nabla\nabla(\mathrm{tr}\boldsymbol{\varepsilon}) + c_3\Delta\boldsymbol{\varepsilon}, \tag{26}$$

$$\boldsymbol{\tau}_2 = l_a^2\nabla\boldsymbol{\tau}_0, \tag{27}$$

$$\boldsymbol{\tau}_3 = l_b^4\nabla\nabla\boldsymbol{\tau}_0 + c_1(\mathrm{tr}\boldsymbol{\varepsilon})\mathbf{II} + c_2\boldsymbol{\varepsilon}\mathbf{I} + c_3\mathbf{I}\boldsymbol{\varepsilon} + b_0\mathbf{II}, \tag{28}$$

$$\boldsymbol{\sigma} = (1 - l_a^2\Delta + l_b^4\Delta\Delta)\boldsymbol{\tau}_0 + (2c_1 + c_2)\Delta(\mathrm{tr}\boldsymbol{\varepsilon})\mathbf{I} + c_2\nabla\nabla(\mathrm{tr}\boldsymbol{\varepsilon}) + 2c_3\Delta\boldsymbol{\varepsilon}, \tag{29}$$

where $\boldsymbol{\tau}_0 = 2\mu\boldsymbol{\varepsilon} + \lambda(\mathrm{tr}\boldsymbol{\varepsilon})\mathbf{I}$. It is worth noting that when coupling parameters disappear ($c_i = 0$) constitutive law (26) immediately takes the standard form, i.e., the Hooke's law, whereas the double, triple and total stresses, following (27), (28) and (29), coincide with the corresponding ones considered in [43, 65].

For kinetic energy density T, we adopt the simplified form proposed in [65] which includes only two additional higher-order length-scale parameters d_1 and d_2:

$$T = \frac{1}{2}\rho(\dot{\boldsymbol{u}}\cdot\dot{\boldsymbol{u}} + d_1^2\nabla\dot{\boldsymbol{u}} : \nabla\dot{\boldsymbol{u}} + d_2^4\nabla\nabla\dot{\boldsymbol{u}} \vdots \nabla\nabla\dot{\boldsymbol{u}}). \tag{30}$$

The positive definiteness of the kinetic energy density as a quadratic form implies the following inequalities: $\rho > 0$, $d_1^2 > 0$ and $d_2^4 > 0$. With the given kinetic energy density (30), the momenta (7) posses the following constitutive forms:

$$\boldsymbol{p}_1 = \rho \dot{\boldsymbol{u}}, \quad \boldsymbol{p}_2 = \rho d_1^2 \nabla \dot{\boldsymbol{u}}, \quad \boldsymbol{p}_3 = \rho d_2^4 \nabla\nabla \dot{\boldsymbol{u}}, \tag{31}$$

which for constant density ρ can be expressed in terms of momentum $\boldsymbol{p}_1$ as $\boldsymbol{p}_2 = d_1^2 \nabla \boldsymbol{p}_1$ and $\boldsymbol{p}_3 = d_2^4 \nabla\nabla \boldsymbol{p}_1$.

For the strain energy density (24), stability conditions in terms of elastic moduli are touched in the next sections in reduced forms. It is worth noting, however, that expression (24) can not be rigorously considered as a quadratic form due to the term linear in $\nabla\nabla\boldsymbol{\varepsilon}$.

3 Surface tension effects in 1D models

In this section, we utilize the proposed simplified second strain gradient model in order to study surface tension which is critical in solids when the surface to volume ratio is large enough. As reported in [17], such effects can be captured by including a term linear in second gradient of strains into the strain energy density. It is also mentioned that four additional material constants with dimension of length arising in the displacement equation of equilibrium ([17], eq. (25)) can be real or complex.

As example problems, we consider a body occupying the half-space and a thin layer with surface tension. These two examples should be considered as a continuation and extension of the study in [40] since, most importantly, we accomplish a critical parameter analysis which was omitted in [40] leading to unphysical material behaviour. By selecting different material parameter values, we demonstrate that the solution becomes singular if the strain energy density is not positively defined. For acceptable material constants, we present the displacement, strain and stress profiles caused by non-zero surface tension. Finally, we analyze and compare the Cauchy and total stress distributions in the problems.

3.1 A half-space with surface tension

Let us consider a half space $x \geq 0$ in a Cartesian $x,\ y,\ z$-coordinate system (cf. [17]) occupied by an elastic continuum governed by the second strain gradient theory of simplified Form II formulated in (24). With zero body and traction forces, the elastic continuum is supposed to be deformed only due to non-zero surface tension. Let us assume that all variables have non-zero components only in the x-direction leading to the displacements and strains of the form

$$\boldsymbol{u} = u(x)\boldsymbol{e}_x, \quad \boldsymbol{\varepsilon} = \varepsilon_{xx}(x)\boldsymbol{e}_x\boldsymbol{e}_x, \quad \text{with } \nabla = \boldsymbol{e}_x \partial/\partial x. \tag{32}$$

Accordingly, strain energy density (24) takes the form

$$W = \frac{1}{2}(2\mu + \lambda)(\varepsilon_{xx}^2 + l_a^2 \varepsilon_{xxx}^2 + l_b^4 \varepsilon_{xxxx}^2 + 2c\varepsilon_{xx}\varepsilon_{xxxx}) + b_0 \varepsilon_{xxxx}, \tag{33}$$

where $c = (c_1 + c_2 + c_3)/(2\mu + \lambda)$. The corresponding stability conditions read as

$$2\mu + \lambda > 0, \quad l_a^2 > 0, \quad l_b^4 > 0, \quad l_b^4 > c^2. \tag{34}$$

For the strain energy density defined in (33), the active stresses can be written as

$$\begin{aligned} \tau_{xx} &= \frac{\partial W}{\partial \varepsilon_{xx}} = (2\mu + \lambda)(\varepsilon_{xx} + c\varepsilon_{xxxx}), \\ \tau_{xxx} &= \frac{\partial W}{\partial \varepsilon_{xxx}} = (2\mu + \lambda) l_a^2 \varepsilon_{xxx}, \\ \tau_{xxxx} &= \frac{\partial W}{\partial \varepsilon_{xxxx}} = (2\mu + \lambda)(l_b^4 \varepsilon_{xxxx} + c\varepsilon_{xx}) + b_0. \end{aligned} \tag{35}$$

With the kinematical assumptions $\varepsilon_{xx} = u'$, $\varepsilon_{xxx} = \varepsilon'_{xx} = u''$ and $\varepsilon_{xxxx} = \varepsilon''_{xx} = u'''$, stresses (35) can be expressed in terms of displacements as

$$\begin{aligned} \tau_{xx} &= (2\mu + \lambda)(u' + cu'''), \\ \tau_{xxx} &= (2\mu + \lambda) l_a^2 u'', \\ \tau_{xxxx} &= (2\mu + \lambda)(l_b^4 u''' + cu') + b_0. \end{aligned} \tag{36}$$

By substituting the stresses above into the stress equation of equilibrium given in (11), one can derive the displacement governing equation of the form

$$\big(u-(l_a^2-2c)u''+l_b^4u''''\big)''=0 \tag{37}$$

or equivalently as

$$(1-l_1^2\frac{d^2}{dx^2})(1-l_2^2\frac{d^2}{dx^2})\frac{d^2u}{dx^2}=0, \tag{38}$$

where

$$l_{1,2}^2=\frac{1}{2}\big(l_a^2-2c\pm\sqrt{(l_a^2-2c)^2-4l_b^4}\big). \tag{39}$$

The natural boundary conditions (13)–(15) at surface $x=0$ with stresses defined in (36) take the form

$$\begin{aligned}
&\boldsymbol{t}_1\cdot\boldsymbol{e}_x=(2\mu+\lambda)(u-(l_a^2-2c)u''+l_b^4u'''')'=0,\\
&\boldsymbol{t}_2\cdot\boldsymbol{e}_x=(2\mu+\lambda)((l_a^2-c)u''-l_b^4u'''')=0,\\
&\boldsymbol{t}_3\cdot\boldsymbol{e}_x=(2\mu+\lambda)(l_b^4u'''+cu')+b_0=0.
\end{aligned} \tag{40}$$

It should be noted that the governing equation (37) with the first traction boundary condition from (40) alone can be rewritten in terms of the total stress as $\sigma'=0$ with $\sigma=0$ at $x=0$, which obviously requires that the total stress equals to zero.

The general solution of the differential equation (38) can be derived in the form

$$u(x)=A_1e^{-x/l_1}+A_2e^{-x/l_2}+A_3e^{x/l_1}+A_4e^{x/l_2}+A_5x+A_6. \tag{41}$$

Since the solution must vanish at infinity, we set $A_3=0$, $A_4=0$, $A_5=0$, $A_6=0$, whereas according to boundary conditions (40) the rest coefficients take the form

$$A_1=\frac{b_0}{2\mu+\lambda}\frac{l_1^2(l_2^2+c)}{l_1(l_2^2+c)^2-l_2(l_1^2+c)^2},\quad A_2=-A_1\frac{l_2^2(l_1^2+c)}{l_1^2(l_2^2+c)}. \tag{42}$$

It can be seen that solution (41) is non-trivial as long as modulus of cohesion b_0 is non-zero. For further calculations, the classical material constants are set to $E=140$ GPa and $\nu=0.3$, the modulus of cohesion is defined by equation $b_0/(2\mu+\lambda)=0.1l_a^2$, while the rest of the parameters are varied.

It is worth noting that by setting relations $l_a^2=\bar{a}/(2\mu+\lambda)$, $l_b^4=\bar{b}/(2\mu+\lambda)$ and $c=\bar{c}/(2\mu+\lambda)$, where $\bar{a}=2(\tilde{a}_1+\tilde{a}_2+\tilde{a}_3+\tilde{a}_4+\tilde{a}_5)$, $\bar{b}=2(\tilde{b}_1+\tilde{b}_2+\tilde{b}_3+\tilde{b}_4+\tilde{b}_5+\tilde{b}_6+\tilde{b}_7)$ and $\bar{c}=\tilde{c}_1+\tilde{c}_2+\tilde{c}_3$, one can immediately retrieve the solution derived by Mindlin in 1965 [17]. On the other hand, by letting the change of parameters to be $l_a^2=L_1^2/2$, $l_b^4=L_1^2L_2^2/2$ and $c=L_1^2\eta/2$, where $L_1^2=\bar{a}/(\mu+\lambda/2)$, $L_2^2=\bar{b}/\bar{a}$ and $\eta=\bar{c}/\bar{a}$, we immediately follow the notation and solution proposed in [40].

Let us next analyze the parameter space depicted in Fig. 1 where the ordinate is ratio c/l_a^2 and abscissa is l_b^4/l_a^4. In order to be consistent with [40], we organize Fig. 1 as follows: the purple area (zone "1") corresponds to an exponentially decreasing solution at infinity. For this case, lengths l_1 and l_2, defined in (39), are real numbers, i.e., $\Im(l_1,l_2)=0$. The orange area (zone "2") is associated to the solution which oscillates without decaying (not vanishing at infinity) and hence has no physical meaning. In this case, l_1 and l_2 are imaginary, i.e., $\Re(l_1,l_2)=0$. The yellow area (zone "3") relates to the oscillating solution which exponentially decreases towards infinity. In this zone, l_1 and l_2 are complex numbers, i.e., $\Re(l_1,l_2)\neq 0$ and $\Im(l_1,l_2)\neq 0$. These three zones are separated by a blue line defined according to (39) as $4(l_b/l_a)^4=(1-2c/l_a^2)^2$.

Next, the skew hatched area corresponds to a convex strain energy density. This area is bounded by a black line which according to (34) is prescribed as $(l_b/l_a)^4=(c/l_a^2)^2$. Finally, the parameter diagram is supplemented by a "singularity" area, or domain of singular solutions, which (for the current problem) is represented as red curve implicitly defined as $l_1(l_2^2+c)^2=l_2(l_1^2+c)^2$. For the parameter values lying on this line, the displacements of the free surface $x=0$ become singular, which is illustrated in Fig. 2a. Here, the free surface displacements (red solid lines) are plotted as a function

of ratio c/l_a^2, i.e., along the path $l_b^4/l_a^4 = 2$ indicated as green dashed line in Fig. 1. It can bee seen that by crossing the "singularity" zone (asymptotes $c/l_a^2 \approx -1.85$ and $c/l_a^2 \approx 1.85$ in Fig. 2a) the displacements tend to plus or minus infinity depending on the approaching path. In Fig. 2b, the displacements, as a function of x-coordinate, are presented for $c/l_a^2 = -3$, $c/l_a^2 = -2$, $c/l_a^2 = -1.855$, $c/l_a^2 = -1.84$ and $c/l_a^2 = -1.82$ highlighting this feature (cf. Fig. 6 of [40]).

It is worth noting that since there are no characteristic lengths in this half-space problem the "singularity" area appears as a line. In the next subsection, it is shown that with a layer thickness as a characteristic length the "singularity" zone becomes a domain.

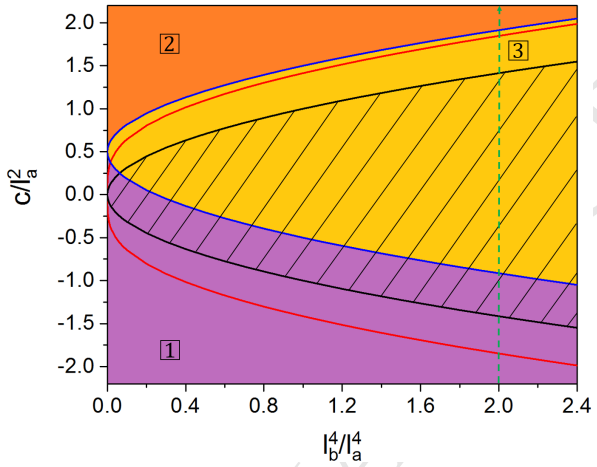

Figure 1: Parameter diagram for the half-space problem. Zones "1", "2" and "3" (investigated in [40]) are supplemented by a domain of singular solutions represented by a red line. Green dashed line $l_b^4/l_a^4 = 2$ defines the parameter path for Fig. 2a.

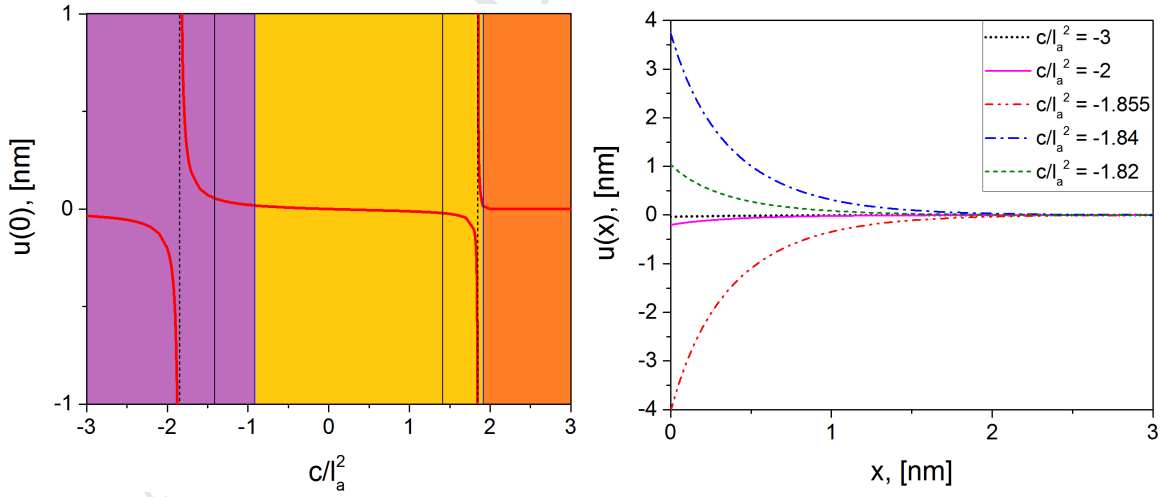

(a) (b)

Figure 2: Half-space problem: Singular solution for $l_b^4/l_a^4 = 2$. (a) Displacement of free surface $x = 0$ as a function of ratio c/l_a^2. (b) Distribution of the displacements in the x-direction for different values of c/l_a^2.

For parameters taken from the domain of convex strain energy density, the displacement, strain and stress profiles are shown in Fig. 3. With $l_b^4/l_a^4 = 2$, it can be seen in Fig. 3 (top) that $c/l_a^2 = 0$ and $c/l_a^2 = 1.4$ correspond to oscillating solutions which decay towards infinity, while $c/l_a^2 = -1.4$ relates to an exponentially decreasing displacement.

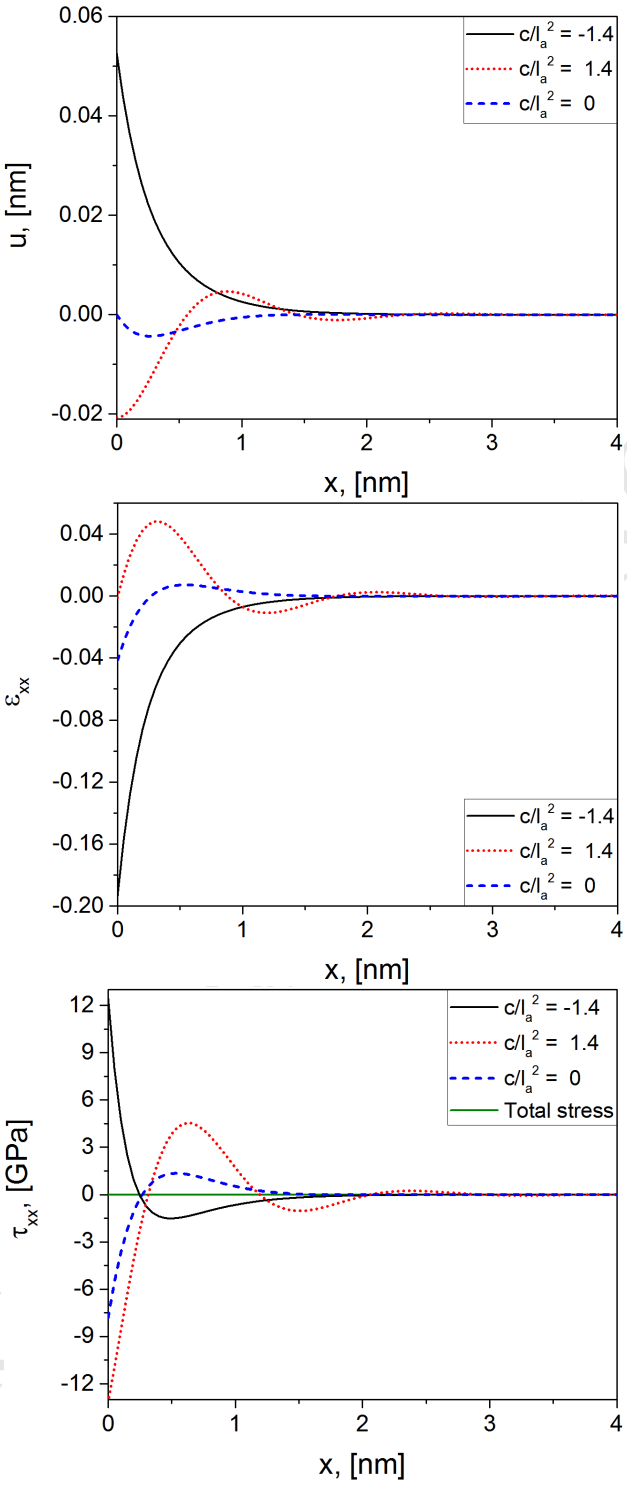

Figure 3: Half-space problem: Profiles of the displacements (top), strains (middle) and stresses (bottom) localized around the surface for parameters lying in the domain of convex strain energy density.

For $c/l_a^2 = 0$, surface $x = 0$ becomes fixed ($u(0) = 0$), whereas the interior points undergo non-zero displacements.

It is worth noting that for compressive strain in Fig. 3 (middle) the corresponding Cauchy stress in Fig. 3 (bottom) can be tensile and vice versa, which is due to the presence of coupling parameter c in the constitutive relation (35) (first line). A special attention should be paid to the fact that the

total stress (being equal to zero) represents the unstressed state of the bulk material leaving the free surface effects uncaptured. The Cauchy stress, however, is able to describe the stressed state of the thin boundary layer caused by the surface tension. As can be seen in Fig. 3 (bottom), the Cauchy stress is localized near the free surface and then rapidly approaches the zero total stress (after a couple of nanometers in this example).

3.2 A thin strip with surface tension

As a second example, let us consider a thin strip infinite in the y- and z-directions with thickness h in the x-direction. As in the previous subsection, this problem is considered to be one-dimensional with the assumptions and derivations in (32)–(39) remaining valid. The boundaries $x = \pm h/2$ of the strip are free of loadings leading to the boundary conditions of the form (40). As a result, displacement field (41) is determined by constants

$$
\begin{aligned}
A_3 &= -\frac{1}{2}\frac{b_0}{2\mu+\lambda}\frac{l_1^2(l_2^2+c)}{\sinh(\gamma_1)\big(l_1(l_2^2+c)^2\coth(\gamma_1)-l_2(l_1^2+c)^2\coth(\gamma_2)\big)},\\
A_4 &= -A_3\frac{l_2^2(l_1^2+c)\sinh(\gamma_1)}{l_1^2(l_2^2+c)\sinh(\gamma_2)},\\
A_1 &= -A_3, \quad A_2 = -A_4, \quad A_5 = 0, \quad A_6 = 0,
\end{aligned}
\tag{43}
$$

where $\gamma_i = h/(2l_i)$, $i = 1, 2$.

The parameter space depicted in Fig. 4a exactly coincides with the one constructed in the previous subsection except the domain of singular solutions. This zone (hatched by vertical red lines) is spread between the boundary of the domain of convex strain energy density (black solid line prescribed as $(l_b/l_a)^4 = (c/l_a^2)^2$) and the "singularity" curve (red solid line implicitly defined as $l_1(l_2^2+c)^2 = l_2(l_1^2+c)^2$) reflecting the fact that the thickness of the strip acts as a characteristic length in this problem. In other words, for any set of parameters lying in the domain of singular solutions there exists a critical thickness h^* such that the displacements of the free surfaces ($x = \pm h/2$) become singular, which is shown in Fig. 4b for $c/l_a^2 = -1.8$ and $l_b^4/l_a^4 = 2$. It can be seen that the displacements of surface $x = h/2$, plotted as a function of thickness h for $l_a = 1,\ 5,\ 10$ nm, tend to plus or minus infinity (depending on the approaching path) along with the corresponding asymptote. The depicted asymptotes $h^* \approx 6.98,\ 34.87,\ 69.75$ (black dashed lines in Fig. 4b) are defined as the critical thicknesses for $l_a = 1,\ 5,\ 10$ nm, respectively. The same behaviour is observed for any point taken from the domain of singular solutions (as chosen in Fig. 8a of [40] without any physical or mathematical reasoning).

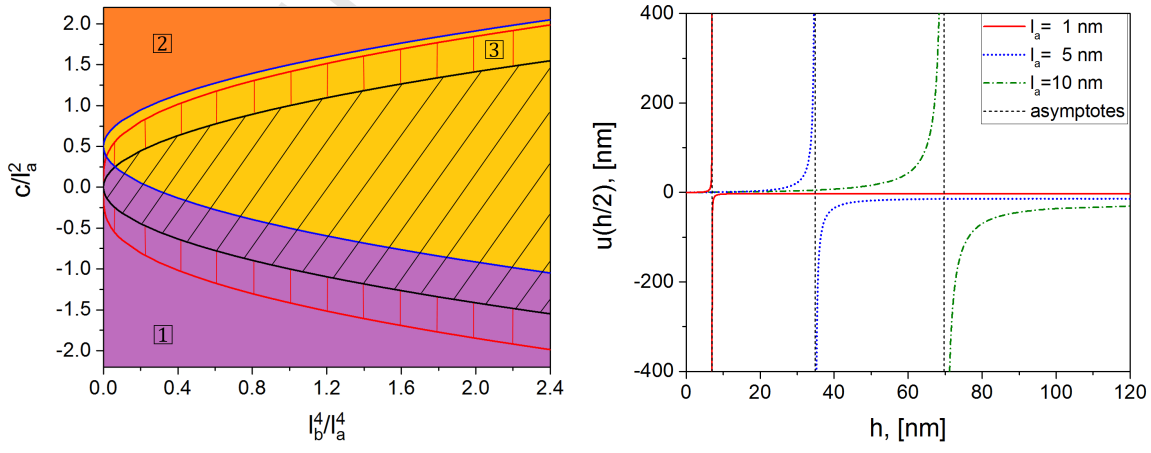

(a) (b)

Figure 4: Thin strip. (a) Parameter space: Zones "1", "2" and "3" (investigated in [40]) are supplemented by the domain of singular solutions hatched with vertical red lines. (b) Singular solution for $c/l_a^2 = -1.8$ and $l_b^4/l_a^4 = 2$: Displacements of surface $x = h/2$ are plotted as a function of thickness h for $l_a = 1,\ 5,\ 10$ nm.

For the parameters lying in the domain of convex strain energy density ($l_b^4/l_a^4 = 2$ and $c/l_a^2 = \pm 1.4$), the displacement, strain and stress profiles are presented in Fig. 5 for $h = 2,\ 5,\ 10$ nm.

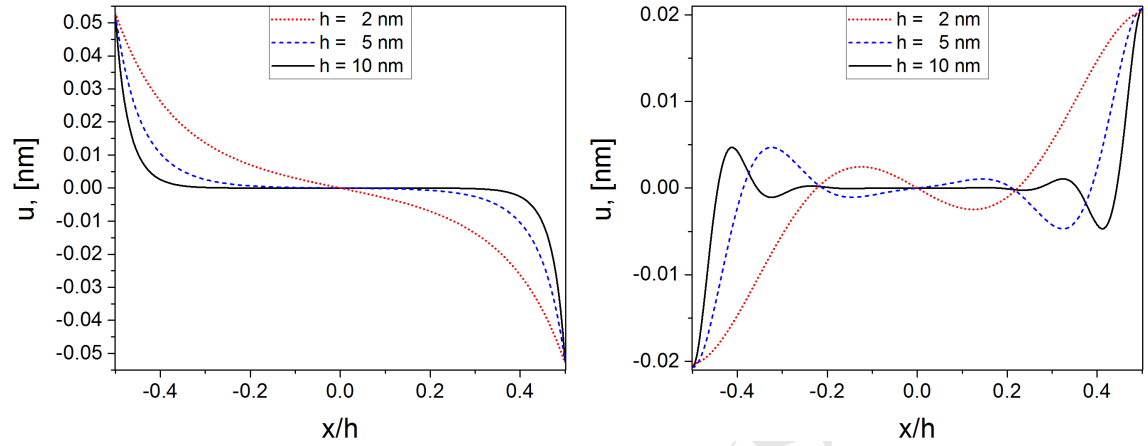

(a) Displacement profiles for $c/l_a^2 = -1.4$ (left) and $c/l_a^2 = 1.4$ (right)

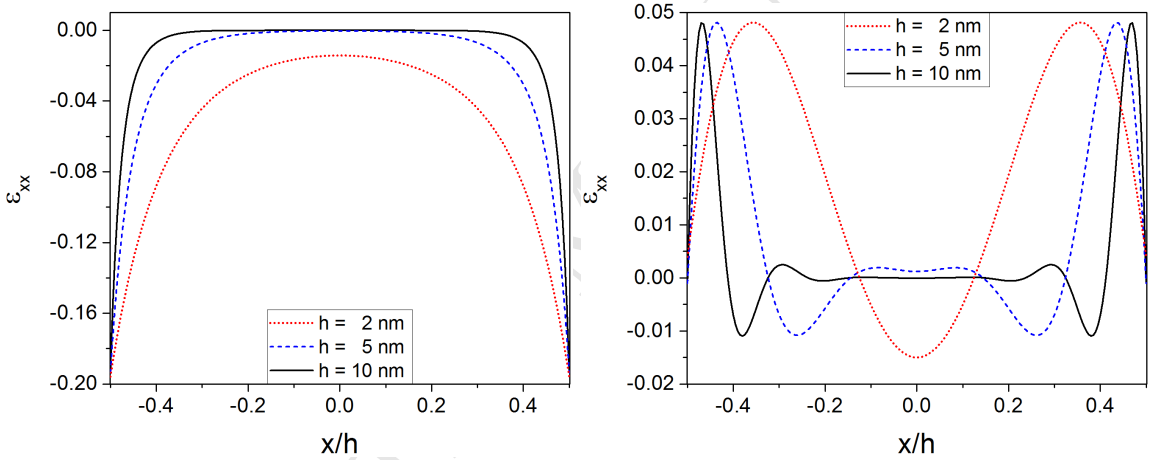

(b) Strain profiles for $c/l_a^2 = -1.4$ (left) and $c/l_a^2 = 1.4$ (right)

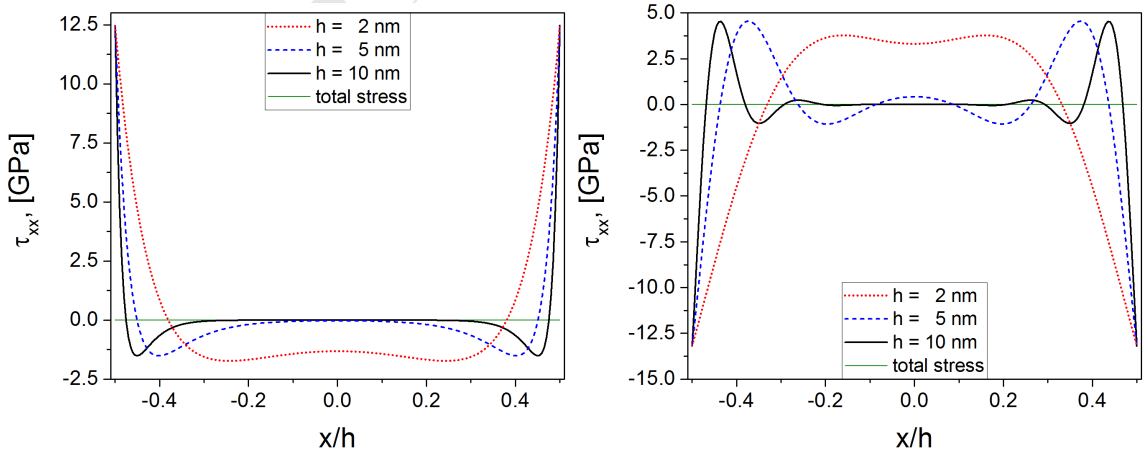

(c) Stress profiles for $c/l_a^2 = -1.4$ (left) and $c/l_a^2 = 1.4$ (right)

Figure 5: Thin strip. Displacement, strain and stress profiles for $c/l_a^2 = -1.4$ (left column) and $c/l_a^2 = 1.4$ (right column) with $l_b^4/l_a^4 = 2$.

It can be seen that the displacements have an exponential character for parameters taken from zone "1" ($c/l_a^2 = -1.4$), whereas for parameters lying in zone "3" ($c/l_a^2 = 1.4$) the displacements are

oscillating. The free surface effects are localized near the boundaries as the thickness increases with respect to the higher-order material parameters. It should be mentioned that when the thickness is large enough the Cauchy stress approaches the corresponding total stress (which is equal to zero) in the bulk part of the strip.

4 Surface effects in tension/compression

In this section, we focus on the free surface effects which occur in a strip long enough upon tension or compression. Here, we intentionally choose the lengths and higher order parameters to be of nano-scale since the effect of free surfaces on the material behaviour is well known (observed) in the solids at nano scale.

First, we (make general assumptions regarding the displacement and strain fields and then) derive a closed form solution. Second, we provide a parameter analysis, i.e., by selecting different higher-order parameters c_i we consider all possible scenarios of the non-classical material reaction upon tension or compression. For non-acceptable material parameter values, we conclude and demonstrate that there exist critical values of a strip width for which the material behaviour becomes absolutely non-physical, i.e., solution becomes singular (cf. Section 5 in [40]). Lastly, we introduce the measure for the effective Poisson's ratio and present its size-dependency.

4.1 Derivation of a closed-form solution

The strip is considered to be thin enough and can be hence represented as a 2D rectangular domain with length L and width h. The problem of interest is schematically drawn in Fig. 21a. The bottom end ($y = 0$) is clamped (singly or fully, see [60] to follow the notation). The prescribed displacement or traction loading is applied to the upper end ($y = L$). The side boundaries are free of loadings. The origin of a Cartesian coordinate system is placed such that the ordinate axis lies on the middle line (see Fig. 21a). The mechanical behaviour is governed by the second strain gradient model proposed in Subsection 2.3 with the classical material parameters μ and λ and higher-order ones l_a, l_b and c_i, $i = 1, 2, 3$.

Let us consider the region far from the strip ends where the influence of the end boundaries is negligible. Therefore, we suppose the displacement field to be of the form

$$\boldsymbol{u} = u(x)\boldsymbol{e}_x + v(y)\boldsymbol{e}_y, \quad \text{where } v(y) = Ay + B, \tag{44}$$

with constants A and B and unit vectors $\boldsymbol{e}_x$ and $\boldsymbol{e}_y$. The corresponding strain field is of the form

$$\boldsymbol{\varepsilon} = \varepsilon_{xx}(x)\boldsymbol{e}_x\boldsymbol{e}_x + \varepsilon_{yy}(y)\boldsymbol{e}_y\boldsymbol{e}_y, \quad \text{where } \varepsilon_{yy}(y) = A. \tag{45}$$

The yy-component of the far away strain field is assumed to be constant as in the classical case, i.e., in case of applied displacement U_0

$$\varepsilon_{yy}(y) = U_0/L, \tag{46}$$

or in case of applied loading P

$$\varepsilon_{yy}(y) = \frac{2\mu + \lambda}{4\mu(\mu + \lambda)}P. \tag{47}$$

Within these assumptions, the strain energy density (24) takes the following form:

$$\begin{aligned} W = \frac{1}{2}\big(&2\mu(\varepsilon_{xx}^2 + \varepsilon_{yy}^2) + \lambda(\varepsilon_{xx} + \varepsilon_{yy})^2 + l_a^2(2\mu + \lambda)\varepsilon_{xxx}^2 + l_b^4(2\mu + \lambda)\varepsilon_{xxxx}^2\big) \\ &+ \bar{c}\varepsilon_{xx}\varepsilon_{xxxx} + c_1\varepsilon_{yy}\varepsilon_{xxxx}, \end{aligned} \tag{48}$$

where $\bar{c} = c_1 + c_2 + c_3$. The positive definiteness condition of the strain energy density as a quadratic form requires that the material parameters fulfil the following stability conditions

$$2\mu > |\lambda| - \lambda, \quad l_a^2 > 0, \quad 4l_b^4\mu(2\mu + \lambda)(\mu + \lambda) > (c_1^2 + \bar{c}^2)(2\mu + \lambda) - 2c_1\bar{c}\lambda. \tag{49}$$

It is worth noting that within the present problem formulation the strain energy density contains cross-parameters c_i as their combination $\bar{c}$ and parameter c_1 alone, which gives three possible scenarios: either $\bar{c} \neq 0$ and $c_1 = 0$, $\bar{c} = 0$ and $c_1 \neq 0$ or $\bar{c} \neq 0$ and $c_1 \neq 0$ (to be discussed in the next subsection).

The components of the stresses which give contribution to the one-dimensional governing equation of the problem are defined as the derivatives of the strain energy density

$$\begin{aligned} \tau_{xx} &= \frac{\partial W}{\partial \varepsilon_{xx}} = (2\mu + \lambda)\varepsilon_{xx} + \lambda\varepsilon_{yy} + \bar{c}\varepsilon_{xxxx}, \\ \tau_{xxx} &= \frac{\partial W}{\partial \varepsilon_{xxx}} = l_a^2(2\mu + \lambda)\varepsilon_{xxx}, \\ \tau_{xxxx} &= \frac{\partial W}{\partial \varepsilon_{xxxx}} = l_b^4(2\mu + \lambda)\varepsilon_{xxxx} + \bar{c}\varepsilon_{xx} + c_1\varepsilon_{yy}. \end{aligned} \tag{50}$$

By utilizing the kinematical assumptions, the strain components are written as

$$\varepsilon_{xx} = u', \quad \varepsilon_{xxx} = \varepsilon'_{xx} = u'', \quad \varepsilon_{xxxx} = \varepsilon''_{xx} = u''' \tag{51}$$

and the stress components take the form

$$\begin{aligned} \tau_{xx} &= (2\mu + \lambda)(u' + cu''') + \lambda\varepsilon_{yy}, \\ \tau_{xxx} &= l_a^2(2\mu + \lambda)u'', \\ \tau_{xxxx} &= (2\mu + \lambda)(l_b^4 u''' + cu') + c_1\varepsilon_{yy}, \end{aligned} \tag{52}$$

with the corresponding total stress

$$\sigma_{xx} = (2\mu + \lambda)(u' + (2c - l_a^2)u''' + l_b^4 u'''') + \lambda\varepsilon_{yy}, \tag{53}$$

where $c = \bar{c}/(2\mu + \lambda)$ and prime indicates the derivative with respect to x-argument.

The resulting displacement equation of equilibrium can be written in the form

$$(1 - l_1^2\frac{d^2}{dx^2})(1 - l_2^2\frac{d^2}{dx^2})\frac{d^2\bar{u}}{dx^2} = 0, \tag{54}$$

where

$$l_{1,2}^2 = \frac{1}{2}\big(l_a^2 - 2c \pm \sqrt{(l_a^2 - 2c)^2 - 4l_b^4}\big). \tag{55}$$

Here, it is useful to introduce a displacement variable

$$\bar{u}(x) = u(x) + \frac{\lambda}{2\mu + \lambda}\varepsilon_{yy}x \tag{56}$$

which is a perturbation of the classical solution due to the free surface effect. The general solution of the differential equation (54) takes the known form

$$\bar{u}(x) = A_1 e^{-x/l_1} + A_2 e^{-x/l_2} + A_3 e^{x/l_1} + A_4 e^{x/l_2} + A_5 x + A_6. \tag{57}$$

By substituting this solution with (56) into (53), it can be seen that $\sigma_{xx} = 0$ which means that the total stress does not appear within this problem formulation by analogy to the Cauchy stress within the classical model.

Free surface conditions imply the absence of applied loadings, which is formally expressed as

$$\begin{aligned} \boldsymbol{t}_1 \cdot \boldsymbol{e}_x &= (2\mu + \lambda)(\bar{u} + (2c - l_a^2)\bar{u}'' + l_b^4\bar{u}'''')' = 0, \\ \boldsymbol{t}_2 \cdot \boldsymbol{e}_x &= (2\mu + \lambda)((l_a^2 - c)\bar{u}'' - l_b^4\bar{u}'''') = 0, \\ \boldsymbol{t}_3 \cdot \boldsymbol{e}_x &= (2\mu + \lambda)(l_b^4\bar{u}''' + c\bar{u}') + (c_1 - \lambda c)\varepsilon_{yy} = 0 \end{aligned} \tag{58}$$

at $x = \pm h/2$ and results in the following expressions for the solution constants A_i:

$$\begin{aligned} A_3 &= -\frac{1}{2}\frac{(c_1-\lambda c)\varepsilon_{yy}}{2\mu+\lambda}\frac{l_1^2(l_2^2+c)}{\sinh(\gamma_1)\big(l_1(l_2^2+c)^2\coth(\gamma_1)-l_2(l_1^2+c)^2\coth(\gamma_2)\big)}, \\ A_4 &= -A_3\frac{l_2^2(l_1^2+c)\sinh(\gamma_1)}{l_1^2(l_2^2+c)\sinh(\gamma_2)}, \\ A_1 &= -A_3, \quad A_2 = -A_4, \quad A_5 = 0, \quad A_6 = 0, \end{aligned} \tag{59}$$

where $\gamma_i = h/(2l_i)$, $i = 1, 2$.

It is notable that the boundary conditions (58) and constants A_i coincide with those of Subsection 3.2 if parameter b_0 is replaced by $(c_1 - \lambda c)\varepsilon_{yy}$. As in the case of thin strip with surface tension (see Subsection 3.2), it means that non-classical contribution $\bar{u}$ disappears from the total solution $u(x)$ in (56) when either $c_i = 0$, $i = 1, 2, 3$, or $c_1 = \lambda c$, leading to the classical solution of the form

$$u(x) = u_0(x) = -\frac{\lambda}{2\mu+\lambda}\varepsilon_{yy}x. \tag{60}$$

4.2 Parameter study

In this subsection, we provide a parameter analysis by demonstrating how the choice of the cross-parameters c_i affects the behaviour of the model. The classical material constants are taken to be $E = 140$ GPa and $\nu = 0.3$. The non-classical parameters are set to be $l_a = 0.5$ nm and $l_b = 1$ nm with six pairs of c and c_1: (1) $c = -0.7$ nm^2, $c_1 = 0$; (2) $c = 0.7$ nm^2, $c_1 = 0$; (3) $c = 0$, $c_1/\lambda = -1$ nm^2; (4) $c = 0$, $c_1/\lambda = 1$ nm^2; (5) $c = -0.7$ nm^2, $c_1/\lambda = -1$ nm^2; (6) $c = 0.7$ nm^2, $c_1/\lambda = 1$ nm^2, leading to three possible non-classical material reactions. All selected parameter values satisfy stability conditions (49). Width values are set to be $h = 5,\ 20,\ 50$ nm.

Of special interest is the distribution of the displacements across the strip width, presented in Fig. 6. The ordinate is the normalized displacement $u(x)/u_0(h/2)$, while the abscissa is the dimensionless coordinate $2x/h$. The first possible scenario is illustrated in Figs. 6a and 6b with $c = \pm 0.7$ nm^2 and $c_1 = 0$, where the side boundary undergoes larger deformation than the corresponding classical one. Cross-parameter c with negative sign leads to exponentially decaying solution, while the positive value of c makes the solution to decay with oscillations.

The second variant is shown in Figs. 6c and 6d with $c = 0$ and $c_1/\lambda = \mp 1$ nm^2. It is remarkable that the deformation of the side boundaries is not sensitive to the presence of free surfaces (does not differ from the classical one), while the effect concentrates inside the material. The third case for $c = -0.7$ nm^2, $c_1/\lambda = -1$ nm^2 and $c = 0.7$ nm^2, $c_1/\lambda = 1$ nm^2 is presented in Figs. 6e and 6f, where the side boundary undergoes smaller deformations than the corresponding classical one. The decaying character remains identical to the first case with respect to the sign of cross-parameter c. The deformation of the strip side boundaries as a function of strip width is used in the next subsection for calculating the effective Poisson's ratio which is found to be size-dependent.

The corresponding normalized strains $\varepsilon_{xx}(x)/u_0'(x)$ against dimensionless coordinate $2x/h$ are depicted in Fig. 7. Decaying character can be explicitly detected with respect to the cross-parameters sign. The profiles of the xx-stress components are collected in Fig. 8. The non-zero Cauchy stresses reach the maximum/minimum (depending on the parameter values) at the boundaries, whereas the total stresses are equal to zero as well as the stresses within the classical theory.

A common fact to all these plots is that the surface effect is localized near the boundary while the strip width becomes larger, whereas the bulk solution lies on the corresponding classical one.

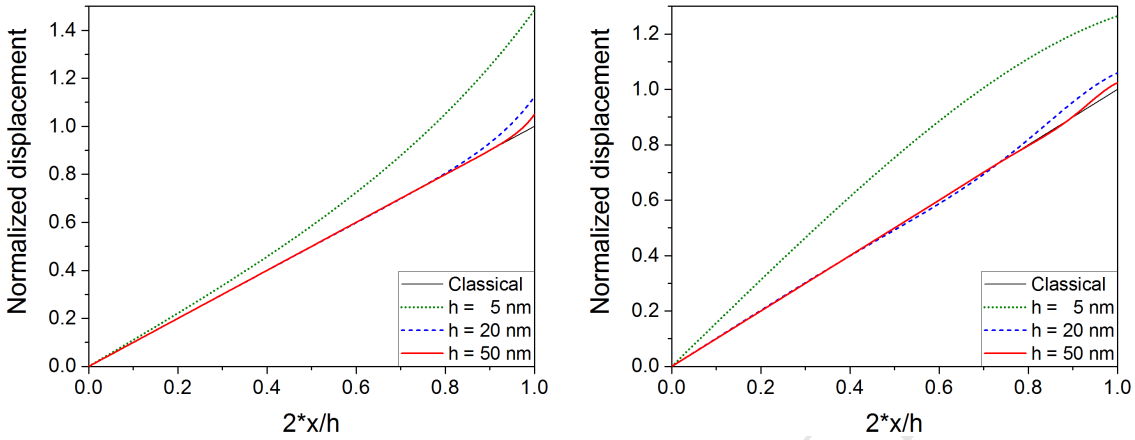

(a) $c = -0.7$ nm^2, $c_1 = 0$

(b) $c = 0.7$ nm^2, $c_1 = 0$

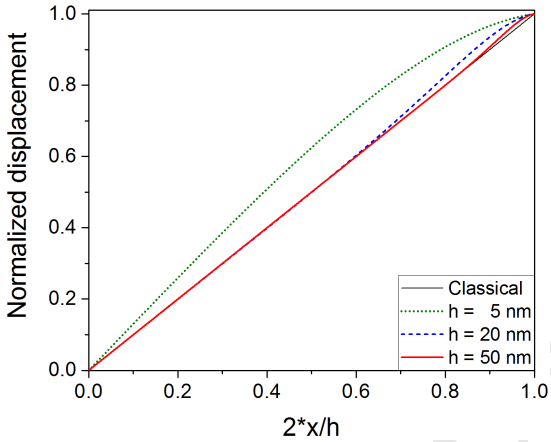

(c) $c = 0$, $c_1/\lambda = -1$ nm^2

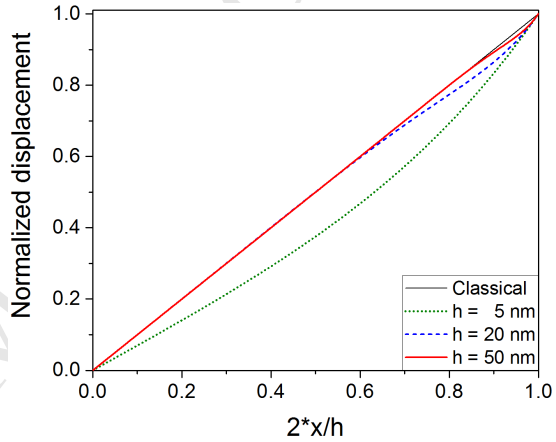

(d) $c = 0$, $c_1/\lambda = 1$ nm^2

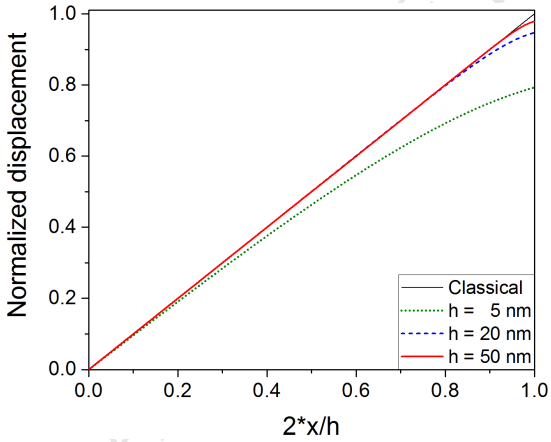

(e) $c = -0.7$ nm^2, $c_1/\lambda = -1$ nm^2

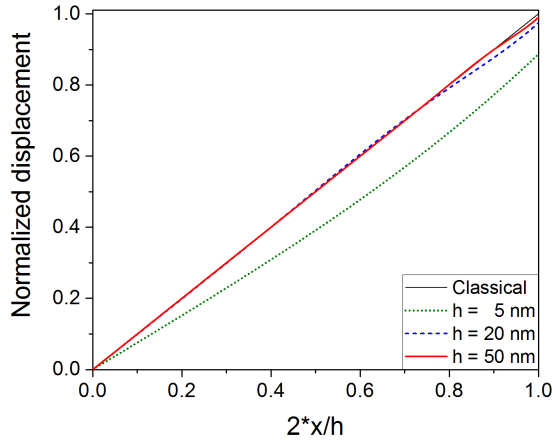

(f) $c = 0.7$ nm^2, $c_1/\lambda = 1$ nm^2

Figure 6: Normalized displacement profiles: $l_a = 0.5$ mm, $l_b = 1$ mm.

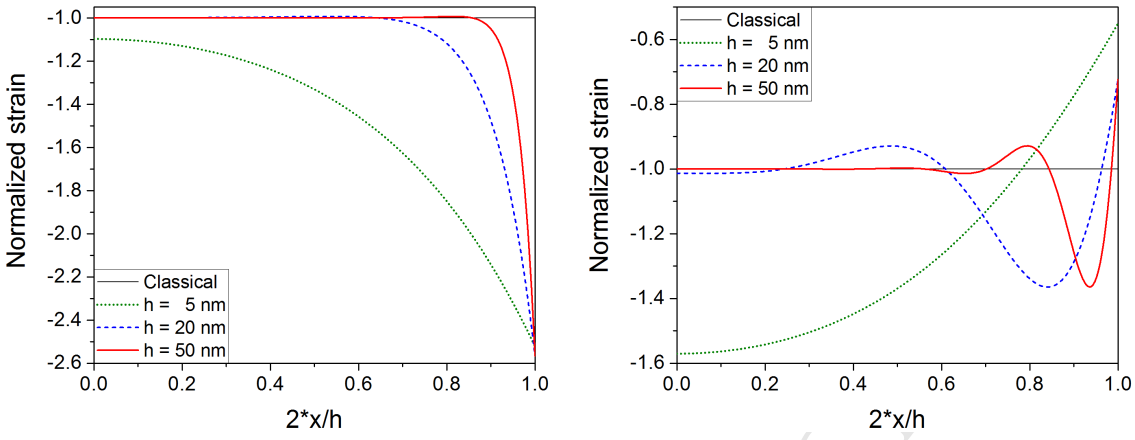

(a) $c = -0.7$ nm^2, $c_1 = 0$

(b) $c = 0.7$ nm^2, $c_1 = 0$

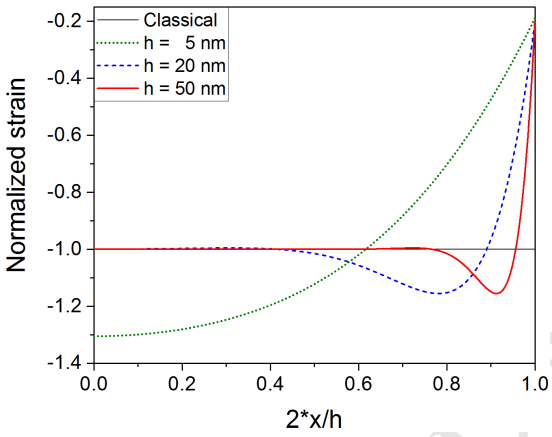

(c) $c = 0$, $c_1/\lambda = -1$ nm^2

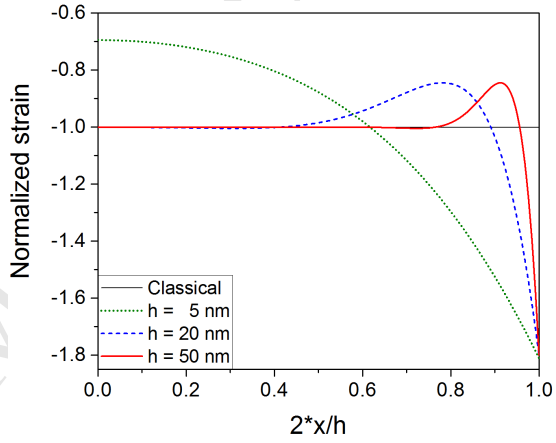

(d) $c = 0$, $c_1/\lambda = 1$ nm^2

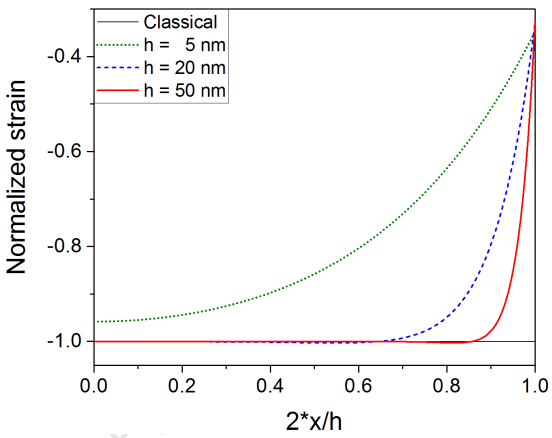

(e) $c = -0.7$ nm^2, $c_1/\lambda = -1$ nm^2

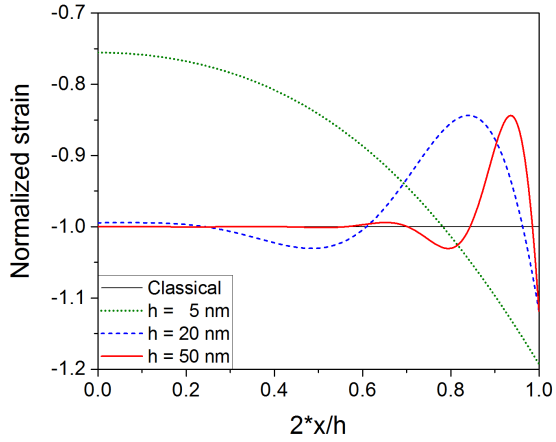

(f) $c = 0.7$ nm^2, $c_1/\lambda = 1$ nm^2

Figure 7: Strains: $l_a = 0.5$ mm, $l_b = 1$ mm.

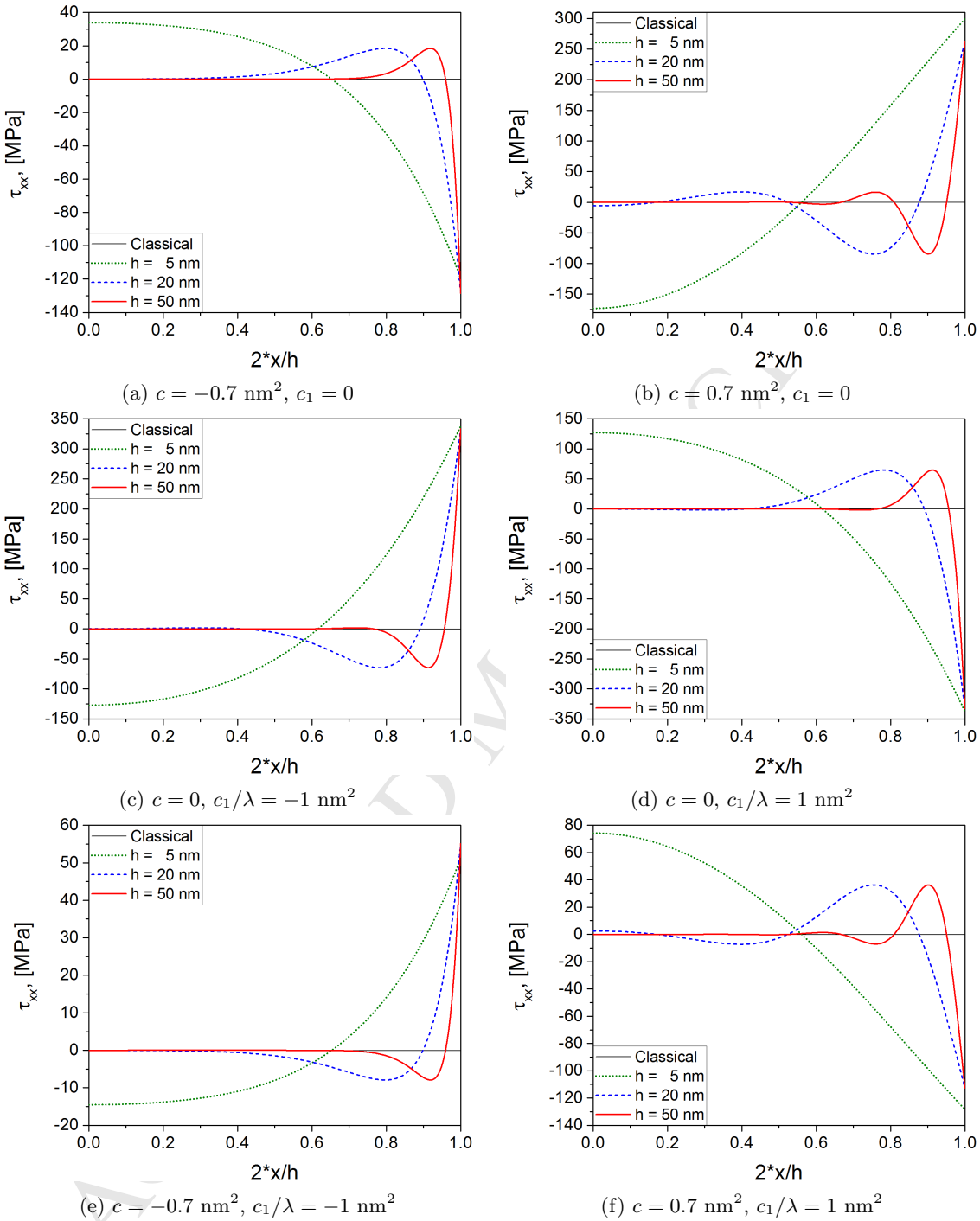

(a) $c = -0.7$ nm^2, $c_1 = 0$

(b) $c = 0.7$ nm^2, $c_1 = 0$

(c) $c = 0$, $c_1/\lambda = -1$ nm^2

(d) $c = 0$, $c_1/\lambda = 1$ nm^2

(e) $c = -0.7$ nm^2, $c_1/\lambda = -1$ nm^2

(f) $c = 0.7$ nm^2, $c_1/\lambda = 1$ nm^2

Figure 8: xx-component of the Cauchy stress tensor: $l_a = 0.5$ mm, $l_b = 1$ mm.

4.3 Effective Poisson's ratio

The effective Poisson's ratio ν^{eff} is based on measuring the boundary deformation and defined as

$$\nu^{eff} = -\frac{\varepsilon_{xx}^{eff}}{\varepsilon_{yy}}, \quad \varepsilon_{xx}^{eff} = \frac{u(h/2) - u(-h/2)}{h}, \tag{61}$$

where ε_{xx}^{eff} is the effective strain along the strip width. By substituting solution (56) with integration constants (59) into (61), one can derive the effective Poisson's ratio as a function of width and material

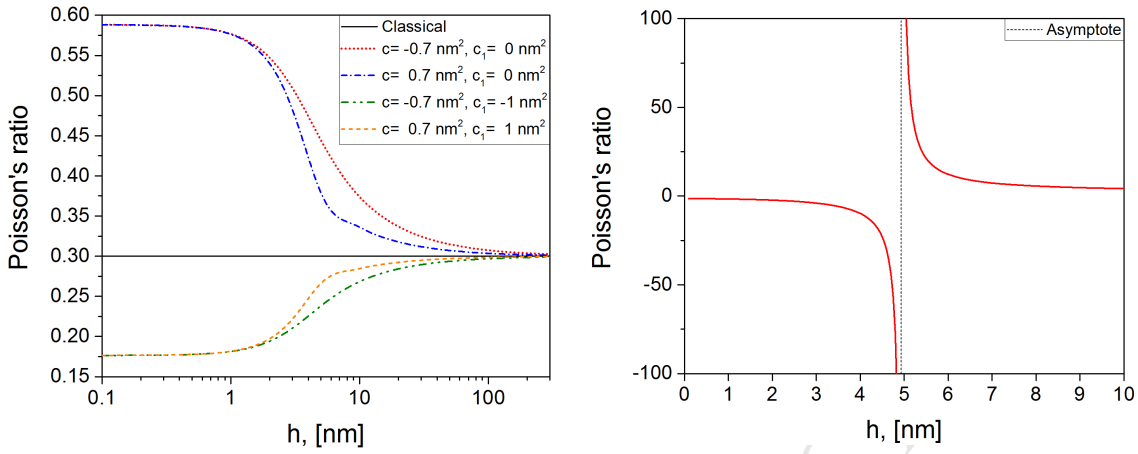

(a) (b)

Figure 9: Effective Poisson's ratio: (a) admissible parameter values, (b) forbidden parameter values ($c = -1.1$ nm^2, $c_1 = 0$).

parameters. Within the second strain gradient elasticity theory, the effective size-dependent Poisson's ratio takes the form

$$\nu^{eff} = \nu\Big(1 + \frac{2c(c_1 - \lambda c)(l_1^2 - l_2^2)}{\lambda h(l_1(l_2^2 + c)^2 \coth(\gamma_1) - l_2(l_1^2 + c)^2 \coth(\gamma_2))}\Big), \tag{62}$$

where the conventional Poissons' ratio $\nu = \lambda/(2\mu + \lambda)$ corresponds to the plane stress problem formulation. The very first analysis of the derived expression (62) reveals that there are no size-dependence when either $c_i = 0$ or $c_1 = \lambda c$ showing once again that the cross-parameters c_i are responsible for the corresponding surface effects.

The dependence of the effective Poisson's ratio on the strip width is illustrated in Fig. 9a for the material parameters defined in Subsection 4.2 and satisfying the stability conditions (49). It can be seen that for strip widths large enough all curves approach the horizontal line corresponding to the conventional modulus, i.e., $\nu = 0.3$. For small h, the effective Poisson's ratio tends to a limit value. These observations are confirmed by considering two limit cases for expression (62), i.e., when h tends to zero and plus infinity

$$\lim_{h\to 0} \nu^{eff} = \nu \frac{cc_1/\lambda - l_b^4}{c^2 - l_b^4}, \qquad \lim_{h\to +\infty} \nu^{eff} = \nu. \tag{63}$$

Indeed, when the strip width is large enough the free surface effects are negligible and the conventional, or bulk, Poisson's ratio is retrieved. For strip widths small enough, the effective Poisson's ratio takes its limit value being equal to 0.588 for $c = \pm 0.7$ nm^2, $c_1 = 0$, and equal to 0.176 for $c = -0.7$ nm^2, $c_1/\lambda = -1$ nm^2 and $c = 0.7$ nm^2, $c_1/\lambda = 1$ nm^2.

Finally, a criminal and, hence, important case is considered in Fig. 9b for $c = -1.1$ nm^2 and $c_1 = 0$. It can be seen that there exist a critical width value $h^* \approx 5$ nm for which the effective modulus tends to $\pm\infty$ depending on the approaching path, which definitely is not acceptable. In [40] (in Fig. 14), the size-dependency of the apparent Poisson's ratio has been studied by using a set of parameters lying in the forbidden parameter zone, which gives a wrong impression on the increase of the apparent Poisson's ratio. The same applies for the apparent Young's modulus in Fig. 13 of [40].

5 Surface effects in shear

In this section, we consider another illustrative and important (one-dimensional) problem, namely, shear of an infinite strip of width h. At first, we carefully analyse the material parameter space and derive a closed-form solution for two types of boundary conditions. Then, based on the derived solution

we analyse the displacement, strain and stress – Cauchy and total – profiles for the parameter values. Finally, we introduce a measure for the effective shear modulus and demonstrate its physicalness (for the case of different boundary conditions) comparing to the corresponding measure of the apparent shear modulus proposed in [40].

5.1 Simple shear problem

5.1.1 Closed-form solution

In this subsection, the analytical solution is derived for a so-called simple shear problem. It is assumed that the upper and bottom surfaces undergo applied displacements or shear loadings (considered in Appendix C), while the double and triple traction forces are equal to zero, see Fig. 25a (top). As in the previous section, this problem is formulated in a 2D Cartesian coordinate system with the abscissa axis lying at the midline of the strip.

The displacement field far from the ends and the corresponding strain field are supposed to be of the form

$$\boldsymbol{u} = u(y)\boldsymbol{e}_x, \quad \boldsymbol{\varepsilon} = \varepsilon_{xy}(y)(\boldsymbol{e}_x\boldsymbol{e}_y + \boldsymbol{e}_y\boldsymbol{e}_x). \tag{64}$$

By substituting the strain tensor from (64) with the reduced nabla operator $\nabla = \boldsymbol{e}_y\partial/\partial y$ into the simplified strain energy density (24), the last takes the following form

$$W = 2\mu(\varepsilon_{xy}^2 + l_a^2\varepsilon_{yxy}^2 + l_b^4\varepsilon_{yyxy}^2 + 2c\varepsilon_{xy}\varepsilon_{yyxy}), \tag{65}$$

where $c = c_3/(2\mu)$. The corresponding stability conditions read as $\mu > 0, \quad l_a^2 > 0, \quad l_b^4 > c^2$. It is worth noting that the cross-parameter c_3 appears in expression (65) alone unlike in problems of Sections 3 and 4. Next, the surface energy associated with modulus of cohesion b_0 gives no effect on the shear mode since the term linear in $\nabla\nabla\boldsymbol{\varepsilon}$ does naturally not appear within this problem formulation. By including the linear term into the strain energy density, we just activate the displacement component in y-direction.

The active stress tensor components are defined as derivatives of the strain energy density (keep in mind that there exist strain and stress components $\varepsilon_{yx} = \varepsilon_{xy}$ and $\tau_{yx} = \tau_{xy}$, respectively)

$$\begin{aligned}
\tau_{xy} &= \frac{1}{2}\frac{\partial W}{\partial \varepsilon_{xy}} = 2\mu(\varepsilon_{xy} + c\varepsilon_{yyxy}),\\
\tau_{yxy} &= \frac{1}{2}\frac{\partial W}{\partial \varepsilon_{yxy}} = 2\mu l_a^2\varepsilon_{yxy},\\
\tau_{yyxy} &= \frac{1}{2}\frac{\partial W}{\partial \varepsilon_{yyxy}} = 2\mu(l_b^4\varepsilon_{yyxy} + c\varepsilon_{xy}).
\end{aligned} \tag{66}$$

With the kinematical assumptions listed below, the strains take the form

$$\varepsilon_{xy} = \frac{1}{2}u', \quad \varepsilon_{yxy} = \varepsilon'_{xy} = \frac{1}{2}u'', \quad \varepsilon_{yyxy} = \varepsilon''_{xy} = \frac{1}{2}u''', \tag{67}$$

whereas the stress components can be written in terms of displacements as

$$\tau_{xy} = \mu(u' + cu'''), \quad \tau_{yxy} = \mu l_a^2 u'', \quad \tau_{yyxy} = \mu(l_b^4 u''' + cu'), \tag{68}$$

with the corresponding total stress

$$\sigma_{xy} = \mu(u' + (2c - l_a^2)u''' + l_b^4 u''''), \tag{69}$$

where prime indicates the derivative with respect to y-coordinate. As a caution, one should keep track on the second strain gradient elasticity formulations since Form I implies different kinematical relations with respect to the ones of Form II.

The resulting displacement equilibrium equation takes the form

$$(1 - l_1^2\frac{d^2}{dy^2})(1 - l_2^2\frac{d^2}{dy^2})\frac{d^2u}{dy^2} = 0, \tag{70}$$

where

$$l_{1,2}^2 = \frac{1}{2}\big(l_a^2 - 2c \pm \sqrt{(l_a^2 - 2c)^2 - 4l_b^4}\big). \tag{71}$$

The general solution of the differential equation (70) is derived in the form

$$u(y) = A_1 e^{y/l_1} + A_2 e^{-y/l_1} + A_3 e^{y/l_2} + A_4 e^{-y/l_2} + A_5 y + A_6. \tag{72}$$

A note concerning total stress σ_{xy} should be given: by substituting solution (72) into expression (69), the total stress σ_{xy} takes the reduced form being constant across the width

$$\sigma_{xy} = \mu A_5. \tag{73}$$

With the boundary conditions at $y = \pm h/2$ corresponding to the simple shear problem,

$$\begin{aligned} &\boldsymbol{u}\cdot\boldsymbol{e}_x = u = \pm U_0/2, \\ &\boldsymbol{t}_2\cdot\boldsymbol{e}_x = \mu\big((l_a^2 - c)u'' - l_b^4 u''''\big) = 0, \\ &\boldsymbol{t}_3\cdot\boldsymbol{e}_x = \mu\big(l_b^4 u''' + cu'\big) = 0, \end{aligned} \tag{74}$$

the integration constants A_i, $i = 1, ..., 6$, are explicitly defined in the form

$$\begin{aligned} &A_1 = -\frac{U_0}{4d}c(1 + \frac{c}{l_2^2})\sinh(\gamma_2), \quad A_3 = \frac{U_0}{4d}c(1 + \frac{c}{l_1^2})\sinh(\gamma_1), \\ &A_5 = \frac{U_0}{2d}\frac{1}{l_b^4}\big(l_1(l_2^2 + c)^2\cosh(\gamma_1)\sinh(\gamma_2) - l_2(l_1^2 + c)^2\cosh(\gamma_2)\sinh(\gamma_1)\big), \\ &A_2 = -A_1, \quad A_4 = -A_3, \quad A_6 = 0, \end{aligned} \tag{75}$$

where $\gamma_i = h/(2l_i)$, $i = 1, 2$ and

$$d = \frac{h}{2l_b^4}\big(l_1(l_2^2 + c)^2\cosh(\gamma_1)\sinh(\gamma_2) - l_2(l_1^2 + c)^2\cosh(\gamma_2)\sinh(\gamma_1)\big) \tag{76}$$

$$- \frac{c^2}{l_b^4}(l_1^2 - l_2^2)\sinh(\gamma_1)\sinh(\gamma_2). \tag{77}$$

It is notable that the solution (72) degenerates into the corresponding classical one $u(y) = u_0(y) = U_0 y/h$ when $c = 0$, i.e., $c_3 = 0$, even with non-zero parameters l_a and l_b (or l_1 and l_2).

5.1.2 Parameter study

As in Subsection 3.1, a parameter study starts from the analysis of the parameter space (presented in Fig. 10a) which exactly coincides with the one constructed in Subsection 3.1 except the domain of singular solutions. This zone (hatched by vertical red lines), unlike for the problem of Subsection 3.2, is spread on the other side of the "singularity" curve (red solid line implicitly defined as $l_1(l_2^2 + c)^2 = l_2(l_1^2 + c)^2$) reflecting the fact that the width of the strip acts as a characteristic length in this problem. For any set of parameters lying in the domain of singular solutions, there exists a critical thickness h^* such that the solution becomes absolutely non-physical, which is shown in Fig. 10b for the displacement profiles (for $l_a = 0.3$ nm, $l_b^4/l_a^4 = 1$, $c/l_a^2 = -1.5$). It can be seen that passing through some critical width values ($h^* \approx 13.2$ nm, in this case) the displacement profile abruptly changes the sign, which implies that some material points undergo infinite displacements. It will be illustrated for the effective shear modulus in the next subsection. This is realized for the displacement profiles in Fig. 10a of [40] but not addressed at all.

A parameter relation between the present simplified model and the corresponding one considered in [40] is given as $l_a^2 = L_1^2$, $l_b^4 = L_1^2 L_2^2$ and $c = L_1^2\eta/2$, where $L_1^2 = 2(\tilde{a}_3 + \tilde{a}_4)/\mu$, $L_2^2 = (\tilde{b}_5 + \tilde{b}_6)/(\tilde{a}_3 + \tilde{a}_4)$ and $\eta = \tilde{c}_3/(2(\tilde{a}_3 + \tilde{a}_4))$.

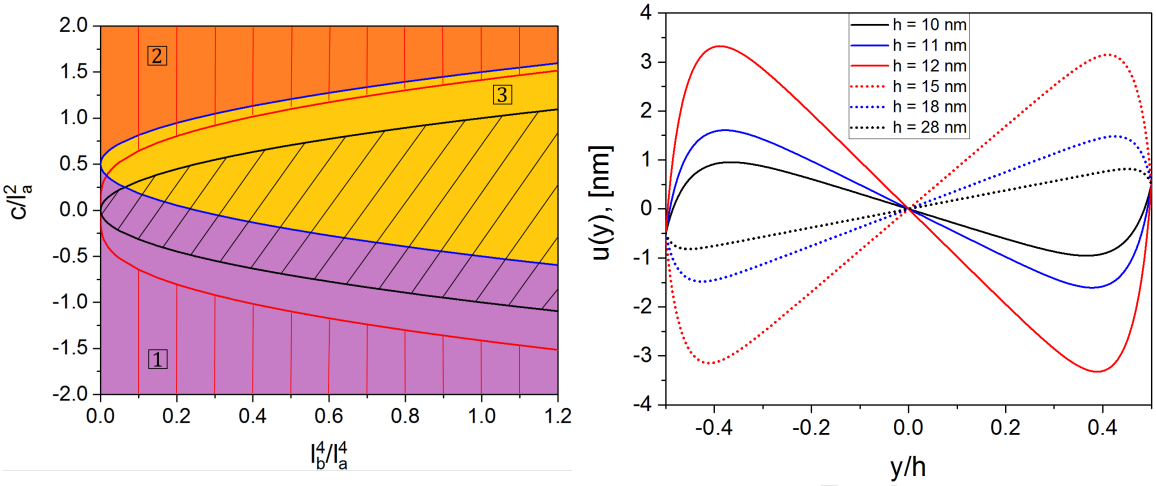

(a) (b)

Figure 10: Simple shear problem. (a) Parameter space: Zones "1", "2" and "3" are supplemented by the area of singular solutions hatched with vertical red lines. (b) Singular solution for $c/l_a^2 = -1.5$ and $l_b^4/l_a^4 = 1$: Displacement profiles for several values of a strip width h for $l_a = 0.3$ nm.

Next, we select the material parameters lying in the domain of convex strain energy density (black skew hatching): $l_a = 0.3$ nm, $l_b^4/l_a^4 = 1$, $c/l_a^2 = \pm 0.9$. The profiles of normalized displacements $u(y)/u_0(h/2)$ are shown in Fig. 11 for $h = 3, 5, 10$ nm. The normalized shear strains $\varepsilon_{xy}(y)/(0.5u_0'(h/2))$ are collected in Figs. 12a–14a for $h = 3, 5, 10$ nm, respectively. It can be seen that the surface effects are localised near the strip boundaries, whereas the bulk solution tends to the corresponding classical one. In Figs. 12b–14b, we compare the normalised Cauchy and total shear stress profiles. The normalization is performed with respect to the corresponding classical shear stress value $\tau_{xy}^{cl} = \mu U_0/h$. As shown in (73) with (75), the total stress takes the constant values, whereas the Cauchy stress demonstrates the presence of surface effects being localised near the strip boundaries. It can be also noticed that as the strip width becomes larger the Cauchy stress in the bulk part of the material at first tends to the corresponding total stress and then both stresses tends to the corresponding classical shear stress values.

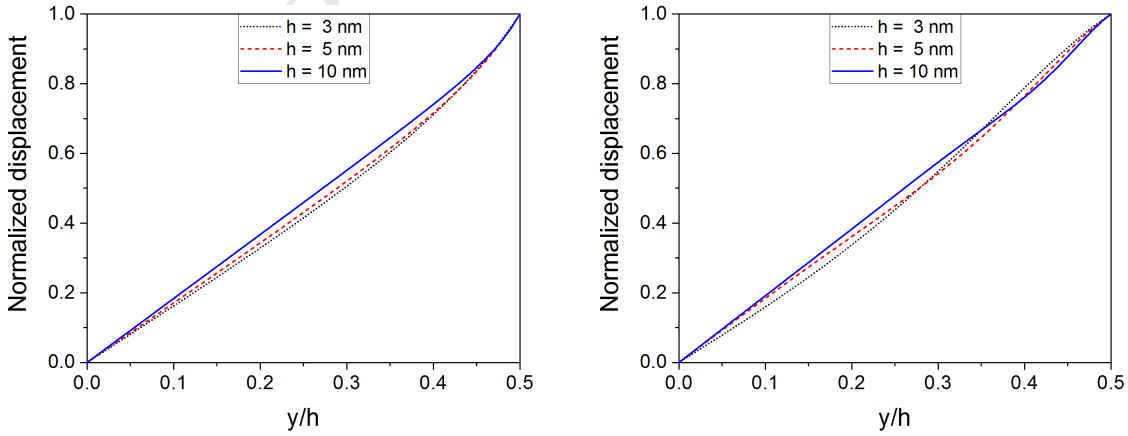

(a) $c/l_a^2 = -0.9$ (b) $c/l_a^2 = 0.9$

Figure 11: Normalized displacement profiles.

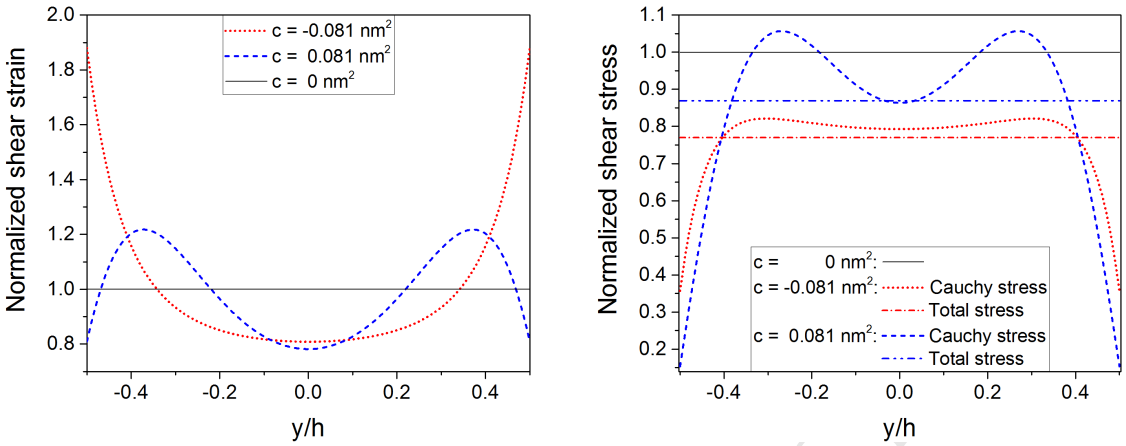

(a) Normalized shear strain (b) Normalized shear stress

Figure 12: Normalized shear strain and stress profiles for $h = 3$ nm.

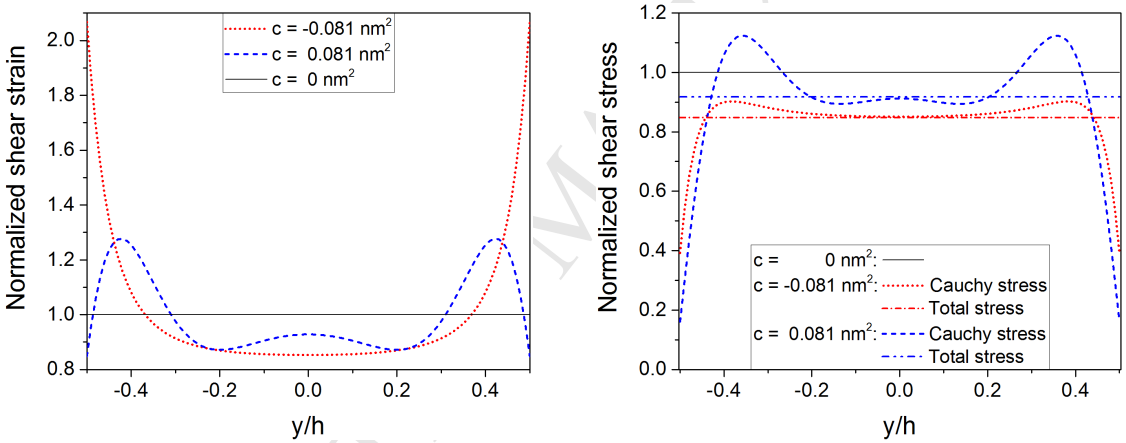

(a) Normalized shear strain (b) Normalized shear stress

Figure 13: Normalized shear strain and stress profiles for $h = 5$ nm.

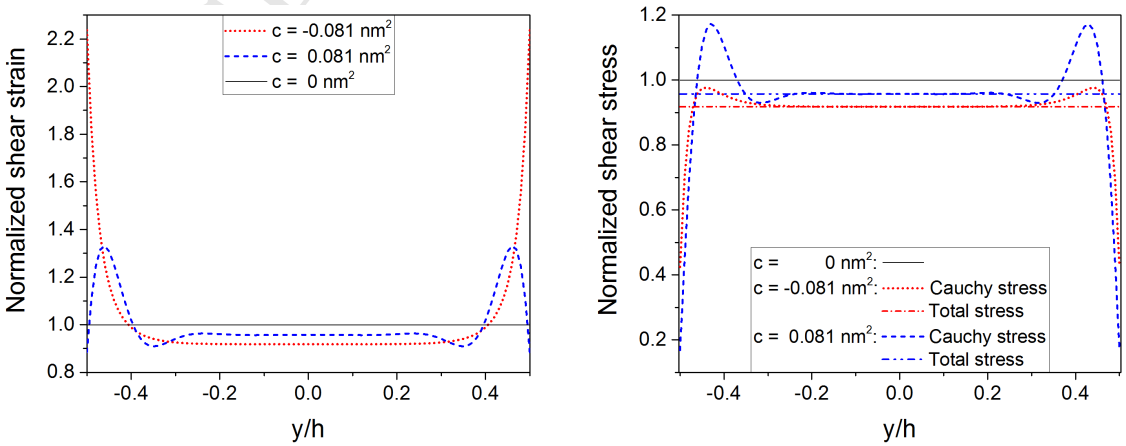

(a) Normalized shear strain (b) Normalized shear stress

Figure 14: Normalized shear strain and stress profiles for $h = 10$ nm.

5.1.3 Effective versus apparent [40] shear modulus

The effective shear modulus is defined in a classical manner as

$$\mu^{eff} = \frac{\tau}{2\varepsilon_{xy}^{eff}}, \quad \varepsilon_{xy}^{eff} = \frac{u(h/2)}{h}, \tag{78}$$

where ε_{xy}^{eff} denotes the effective shear strain and τ is the applied shear load. Within the problem formulation given in Subsection 5.1.1, we further write

$$\mu^{eff} = \sigma_{xy}(h/2)\frac{h}{U_0}, \tag{79}$$

where U_0 is the prescribed displacement and the applied shear load τ is replaced by the distributed reaction force being the total shear stress value on the boundary.

It is worth noting that the normalized effective shear modulus coincides with the normalized material macro-stiffness as well as with the normalized stored strain energy, which is formally expressed by equality

$$\frac{\mu^{eff}}{\mu} = \frac{k_{gr}}{k_{cl}} = \frac{W_{gr}}{W_{cl}}, \tag{80}$$

confirming the correctness of the effective shear modulus measure introduced in (78). Here

$$k_{cl} = \frac{\tau_{xy}^{cl}}{U_0} = \frac{\mu}{h} \quad \text{and} \quad k_{gr} = \frac{\sigma_{xy}(h/2)}{U_0}$$

denote, respectively, the reduced macro-stiffness of the classical and second strain gradient materials, while

$$W_{cl} = \frac{1}{2}\mu\frac{U_0^2}{h} = \frac{1}{2}\tau_{xy}^{cl}U_0 \quad \text{and} \quad W_{gr} = \int_{-h/2}^{h/2} W dy = \frac{1}{2}\sigma_{xy}(h/2)U_0$$

(with W defined in (65)) stand for the reduced stored strain energies of the classical and gradient materials, respectively.

By substituting (73) and (75) into (79), one can derive the effective shear modulus as a function of width and material parameters in the form

$$\mu^{eff} = \mu/(1 - \frac{2}{h}\frac{c^2(l_1^2 - l_2^2)}{l_1(l_2^2 + c)^2\coth(\gamma_1) - l_2(l_1^2 + c)^2\coth(\gamma_2)}). \tag{81}$$

In the limit cases when h tends to zero and plus infinity, we get

$$\lim_{h\to 0}\mu^{eff} = \mu(1 - \frac{c^2}{l_b^4}), \quad \lim_{h\to+\infty}\mu^{eff} = \mu. \tag{82}$$

It should be noticed that with the stability conditions, namely, $l_b^4 > c^2$, the limit effective shear modulus is always less than the corresponding conventional modulus. The normalized effective shear modulus against dimensionless strip width h/l_a is shown in Fig. 15a for $l_b^4/l_a^4 = 1$ with several dimensionless cross-parameters $c/l_a^2 = \pm 0.9, \pm 0.7, \pm 0.45$ lying in the "convex" area. It can be seen that when the strip width is getting smaller the second strain gradient material becomes softer than the corresponding classical material. For strip width large enough, the conventional or bulk shear modulus is retrieved.

An exceptional case is represented in Fig. 15b for $c/l_a^2 = -1.5$ lying in the "singularity" area. It may give the wrong impression that for h/l_a grater some value ($h/l_a \approx 44$ which for $l_a = 0.3$ nm gives the critical width value $h^* \approx 13.2$ nm, see subsection 5.1.2) the second strain gradient material becomes stiffer than the classical one (cf. Fig. 11 of [40]). In fact, such behaviour reflects the presence of singular displacements (highlighted in subsection 5.1.2), which is considered to be non-physical and unacceptable.

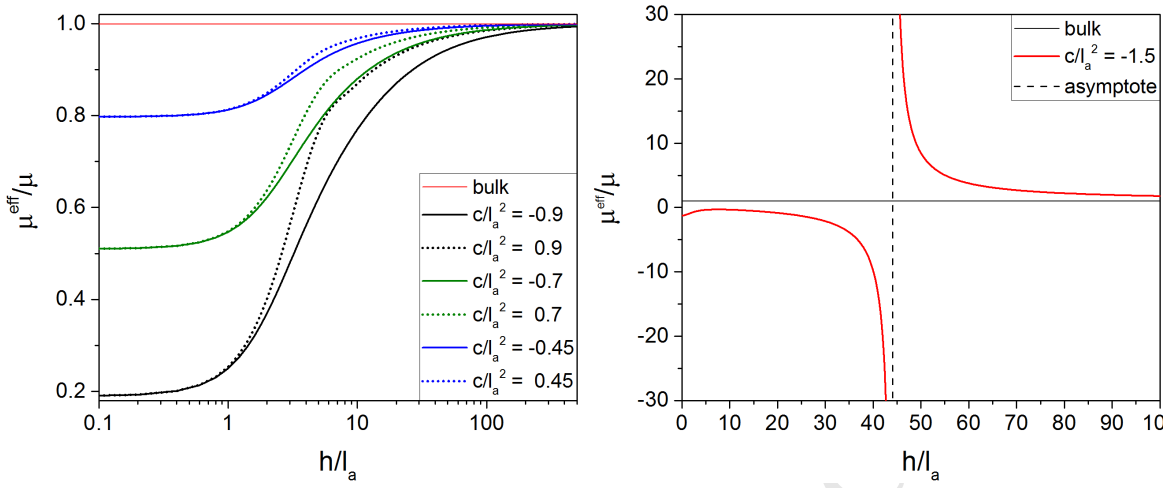

(a) (b)

Figure 15: Normalized effective shear modulus for cross-parameters c taken in the domain of (a) convex strain energy density and (b) singular solutions.

Finally, it should be noted that for the simple shear problem the derived expression (81) for the effective shear modulus coincides with the apparent shear modulus μ^{app} introduced in [40] as a proportionality factor between the averaged Cauchy shear stress and averaged shear strain

$$\int_{-h/2}^{h/2} \tau_{xy} dy = 2\mu^{app} \int_{-h/2}^{h/2} \varepsilon_{xy} dy. \tag{83}$$

A detailed comparison of these two measures for the non-conventional shear modulus is given in the next subsection.

5.2 Shear problem with rough boundaries

In this section, we consider a shear problem with the so-called rough boundaries (displacement and its normal derivative fixed), see Fig. 25a (bottom). This can be modelled by imposing the essential boundary conditions of second order (16), which leads to the boundary conditions at $y = \pm h/2$ of the form

$$\begin{aligned} \boldsymbol{u} \cdot \boldsymbol{e}_x &= u = \pm U_0/2, \\ \boldsymbol{n} \cdot \nabla \boldsymbol{u} \cdot \boldsymbol{e}_x &= u' = V_0, \\ \boldsymbol{t}_3 \cdot \boldsymbol{e}_x &= \mu\big(l_b^4 u''' + c u'\big) = 0. \end{aligned} \tag{84}$$

Further, V_0 is set to be zero implying zero shear strains at the boundaries. By substituting general solution (72) into boundary conditions (84), integration constants A_i take the form

$$\begin{aligned} A_1 &= -\frac{l_1^3}{2l_b^4} \frac{U_0 l_b^4 - V_0(h l_b^4 + c h l_2^2 - 2c l_2^3 \tanh(\gamma_2))}{h(l_1^2 - l_2^2)\cosh(\gamma_1) + 2l_2^3 \cosh(\gamma_1)\tanh(\gamma_2) - 2l_1^3 \sinh(\gamma_1)}, \\ A_3 &= -A_1 \frac{l_2^3 \cosh(\gamma_1)}{l_1^3 \cosh(\gamma_2)} \frac{U_0 l_b^4 - V_0(h l_b^4 + c h l_1^2 - 2c l_1^3 \tanh(\gamma_1))}{U_0 l_b^4 - V_0(h l_b^4 + c h l_2^2 - 2c l_2^3 \tanh(\gamma_2))}, \\ A_5 &= -2A_1 \frac{\cosh(\gamma_1)}{l_1^3} \frac{(l_1^2 - l_2^2) U_0 l_b^4 + 2V_0(l_2^3(l_b^4 + c l_1^2)\tanh(\gamma_2) - l_1^3(l_b^4 + c l_2^2)\tanh(\gamma_1))}{U_0 l_b^4 - V_0(h l_b^4 + c h l_2^2 - 2c l_2^3 \tanh(\gamma_2))}, \\ A_2 &= -A_1, \quad A_4 = -A_3, \quad A_6 = 0, \end{aligned} \tag{85}$$

where $\gamma_i = h/(2l_i)$, $i = 1, 2$. The profiles of the normalized displacements, shear strains and shear stresses are shown, respectively, in Figs. 16 and 17. The normalization is performed with respect to the corresponding classical solution as in Subsection 5.1.2. Here, we present the results obtained within the classical continuum model ($l_a = 0$, $l_b = 0$, $c = 0$), the first strain gradient continuum model ($l_a = 0.3$ nm, $l_b = 0$, $c = 0$) and the second strain gradient continuum model (3 cases: (1) $l_a = 0.3$ nm, $l_b = 0.3$ nm, $c = 0$; (2) $l_a = 0.3$ nm, $l_b = 0.3$ nm, $c/l_a^2 = -0.9$; (3) $l_a = 0.3$ nm, $l_b = 0.3$ nm, $c/l_a^2 = 0.9$). It can be seen that the shear strains are equal to zero at the strip boundaries. The same is valid for The Cauchy stresses except for cases (2) and (3) of the second strain gradient continuum model due to non-zero values for cross parameter c. The total stresses are represented in Fig. 17 (right) as solid lines with the corresponding colors.

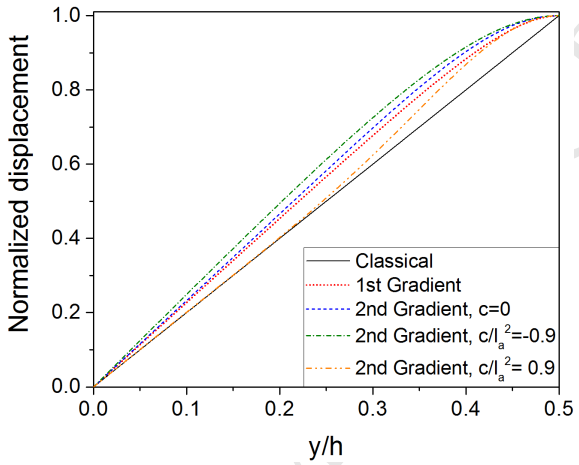

Figure 16: Normalized displacement profiles for $h = 5$ nm.

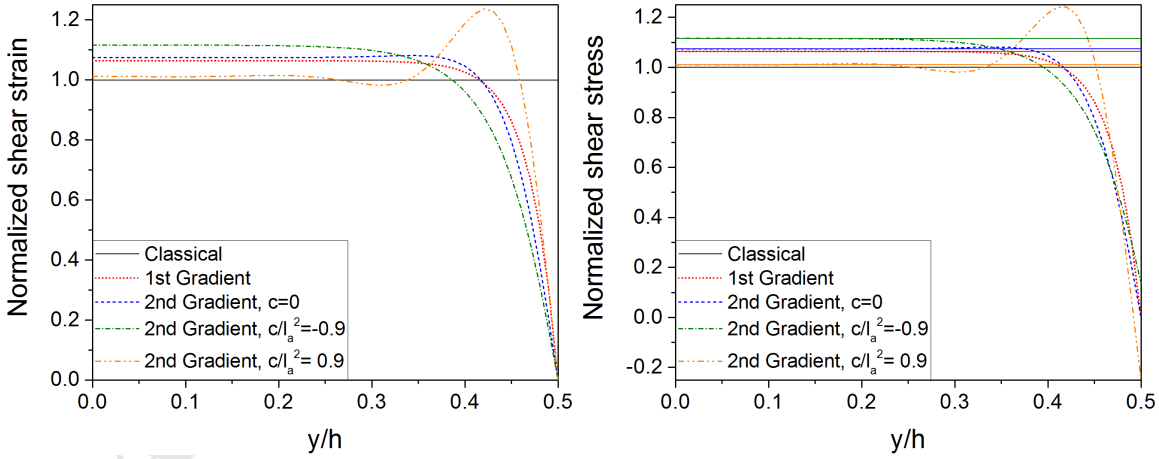

Figure 17: Normalized shear strain (left) and stress (right) profiles for $h = 10$ nm.

Of a special interest is the analysis of the measures for the non-conventional shear modulus. Let us utilize at first the measure introduced in (78) which gives the following expression for the effective shear modulus

$$\mu^{eff} = \mu h \frac{l_1^2 - l_2^2}{h(l_1^2 - l_2^2) + 2l_2^3 \tanh(\gamma_2) - 2l_1^3 \tanh(\gamma_1)} \tag{86}$$

with two limit cases (the exceptional case $l_1 = l_2$ is not considered here)

$$\lim_{h\to 0} \mu^{eff} = +\infty, \quad \lim_{h\to+\infty} \mu^{eff} = \mu. \tag{87}$$

The normalized effective shear modulus against dimensionless strip width h/l_a is illustrated in Fig. 18. In Fig. 18 (left), the normalization is performed with respect to the conventional shear modulus μ. It can be clearly seen that the strain gradient continuum models predict stiffening behaviour with respect to the classical model. In Fig. 18 (right), the normalization is accomplished with respect to the effective shear modulus μ_1 arising in the first strain gradient continuum model ($l_a = 0.3$ nm, $l_b = 0$, $c = 0$). It is notable that with parameters specified in cases (1) and (2) the second strain gradient continuum model is able to predict stiffening behaviour, whereas with parameters from case (3) the softening behaviour is observed (for $h/l_a > 2.5$).

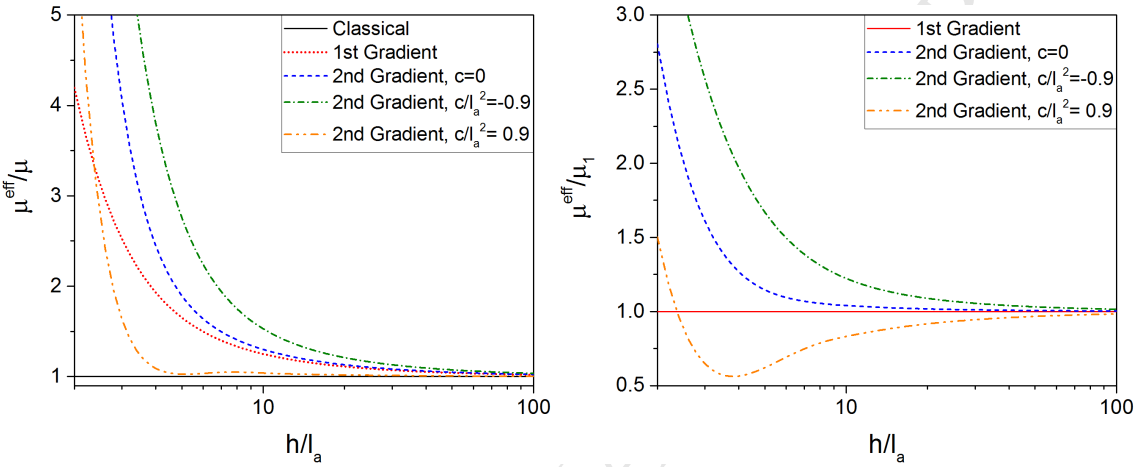

Figure 18: Normalized effective shear modulus: with respect to the classical modulus μ (left) and first strain gradient modulus μ_1 (right).

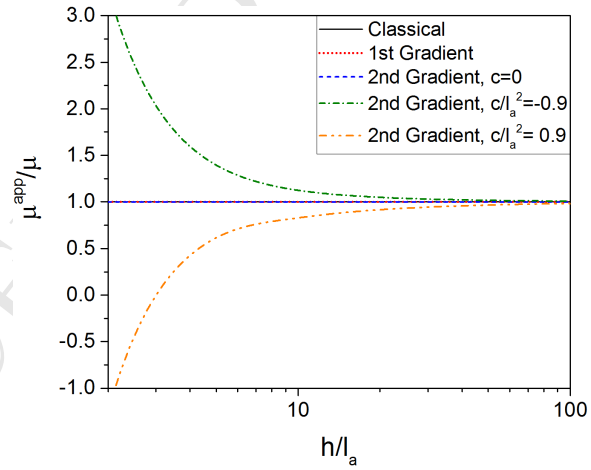

Figure 19: Normalized apparent shear modulus of [40].

The apparent shear modulus of [40] recalled in (83) is depicted in Fig. 19. It can be seen that this measure is not sensitive to the strain gradient effects when cross-parameter c is excluded from the model ($c = 0$). For negative values of c, the stiffening behaviour is predicted, whereas non-physical behaviour is observed for positive c, namely, for width small enough the apparent shear modulus becomes negative and when the width is getting larger the material softening is observed.

As a concluding remark, it is recommended to use the effective shear modulus measure introduced in (78) since this measure demonstrates physical results supported by the reasoning given in Subsection 5.1.3 and formally expressed in (80).

6 Triangular lattice structure as a second strain gradient solid

In this section, we consider one of the representatives of the micro-architectured lattice metamaterials, namely, triangular lattice structure composed of trusses in millimeter range with one-, two- and three-neighbour interactions. First, by a continualisation technique presented in [70], we define the stiffness tensor of the equivalent classical continuum media. Next, by solving the two problems discussed in Sections 4 and 5, i.e., tension and simple shear problems, we find that the triangular truss structure behaves as a second strain gradient solid. Accordingly, we calibrate the continuum model by defining the higher-order material parameters l_a, l_b and c_i, $i = 1, 2, 3$. We also show that the initial stresses prescribed on the boundary trusses can be associated to Mindlin's cohesion parameter b_0 which gives rise to surface tension.

Finally, we accomplish an eigenvalue analysis of the discrete structure evidently demonstrating the necessity of the inertia terms of higher-order. The dispersion characteristics, i.e., angular frequency, phase and group velocities against angular wavenumber, of the discrete structure are defined by the generalized continuum model. It is worth noting that although [71] presents the effective second strain gradient continuum for a 1D discrete system with one-neighbour and two-neighbour interactions, no real experiments or at least numerical evidences have been reported so far. All numerical simulations discussed in this section are accomplished within a commercial finite element software Abaqus by utilizing standard and user-defined higher-order [62] finite elements.

6.1 Description of the lattice structure

Let us consider a set of massless points placed at vertices of equilateral triangles and connected by linear trusses that form a triangular truss lattice structure which occupies an infinite domain in a two-dimensional space. A small part of this structure is schematically shown in Fig. 20a. It is assumed that each point (yellow full circle) interacts with the neighbouring points (blue, green and red full circles) located at the first (blue dotted circle), second (green dashed circle) and third (red dash-dotted circle) coordination spheres, respectively, by linear trusses of type "1" (blue lines), "2" (green springs) and "3" (red springs), see Fig. 20a.

Next, we adopt the approach presented in [70] and define the material constants of an equivalent classical continuum media. The resulting stiffness tensor (details omitted here) takes the form

$$^4\mathbf{C} = \mu(^4\mathbf{I}_1 + {}^4\mathbf{I}_2 + {}^4\mathbf{I}_3), \quad \text{with} \quad \mu = \lambda = \frac{3}{8}\frac{k_1 l_1^2 + k_2 l_2^2 + k_3 l_3^2}{V_0}, \tag{88}$$

indicating that the equivalent classical continuum media is isotropic and Lamé parameters μ and λ are equal to each other. The material properties are defined in terms of the lattice structure parameters where k_i stands for the stiffness and l_i denotes the length of the trusses with $V_0 = \sqrt{3}l_1^2/2$ being the volume, or the area, of an elementary lattice cell, represented in Fig. 20b. Truss stiffness k_i is given as $k_i = E_i A_i / l_i$, where A_i is the cross-sectional area and E_i denotes the Young's modulus of the truss. The corresponding Poisson's ratio ν and Young's modulus E of the equivalent continuum are derived from the standard expressions (within the plane stress problem formulation) $\nu = \lambda/(2\mu + \lambda)$, $E = 4\mu(\mu + \lambda)/(2\mu + \lambda)$ and with $\mu = \lambda$ take the form

$$\nu = \frac{1}{3}, \quad E = \frac{8}{3}\mu = \frac{k_1 l_1^2 + k_2 l_2^2 + k_3 l_3^2}{V_0}. \tag{89}$$

It should be noted that the bulk Poisson's ratio is equal to 1/3 independently on the truss stiffnesses and lengths. Finally, the mass density of the equivalent continuum media is defined as

$$\rho = \frac{3}{V_0}(l_1 A_1 \rho_1 + l_2 A_2 \rho_2 + l_3 A_3 \rho_3), \tag{90}$$

where ρ_i stands for the truss density.

It is worth noting that the approach in [70] is derived mainly for atomic lattices but in this article we extend the applicability area by considering truss lengths at larger scales. The list of parameters defining the geometry and behaviour of the triangular truss lattice structure is given in Table 1.

Table 1: List of parameters defining the discrete structure.

Truss type, i	l_i, [mm]	A_i, [mm^2]	E_i, [GPa]	k_i, [kN/mm]	ρ_i, [kg/m^3]
1	5	1	210	42	7850
2	8.66	1	210	24.25	7850
3	10	1	210	21	7850

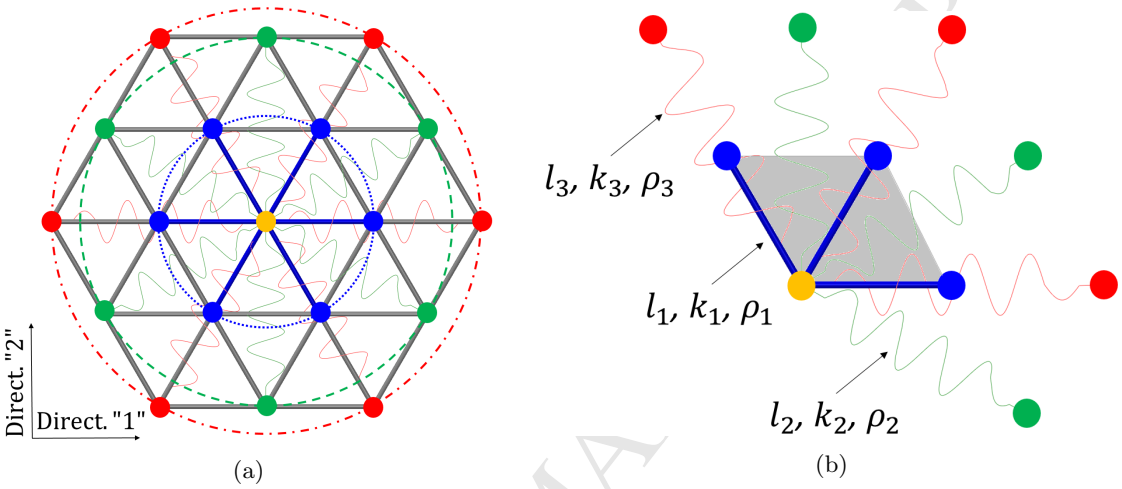

(a) (b)

Figure 20: Triangular lattice structure. For clarity, trusses of type "2" and "3" are represented as springs. (a) Truss types with corresponding coordination spheres. (b) Elementary lattice cell "V_0" (filled with grey).

6.2 Tension of a lattice structure strip

In this subsection, we consider a long strip made of the triangular truss structure introduced above with total length L and width h. The strip is stretched by a prescribed displacement U_0 which is applied at the upper end ($y = L$), while the bottom end ($y = 0$) is fixed as illustrated in Fig. 21a.

Here, we distinguish two directions of the triangular lattice illustrated in Fig. 20a. It is worth noting that strips stretched in direction "1" (Fig. 21b) behave as ones made of equivalent classical continuum. It means that the displacements of the discrete points are governed by the classical expressions $u(x) = -\nu U_0 x/L$ and $v(y) = U_0 y/L$ (see Section 4), where the material parameters are defined in Subsection 6.1. On the contrary, strips stretched in direction "2" (Fig. 21c) behave differently demonstrating the presence of free surface effects discussed below.

For simplicity, the trusses of type "2" and "3" are excluded for the tension problem of this subsection ($k_2 = k_3 = 0$) since the surface effects are already observed with trusses of type "1" (presence of trusses of type "2" and "3" affect the structure behaviour only quantitatively, not qualitatively). The numerical simulations have been accomplished for the strips composed of different numbers of "blocks" (an example is given in Fig. 21c). As can be seen in Fig. 21c, the side boundaries of the strip are of "zigzag" shape which means that (i) the width of the discrete strip is a function of y-coordinate, (ii) there exist two types of strip sections. Thereby, in order to correctly interpret the results, an effective strip section with interpolated points is defined. Coordinates and displacements of the effective points are interpolated between the corresponding points of the sections of type "A" and "B". As a result, the effective strip width, which is used for the equivalent second strain gradient continuum model, is determined as $h_i = (i - 0.5)l_1$, where $i = 2, ...$ denotes the "block" number.

In Fig. 22, we illustrate the normalized u-component of the displacement field against the dimensionless x-coordinate for four different values of the width. The normalization is performed with respect to the corresponding classical solution. Blue dots represent the discrete values, black dotted lines stand for the solution of the classical elasticity theory. By utilizing the analytical higher-order

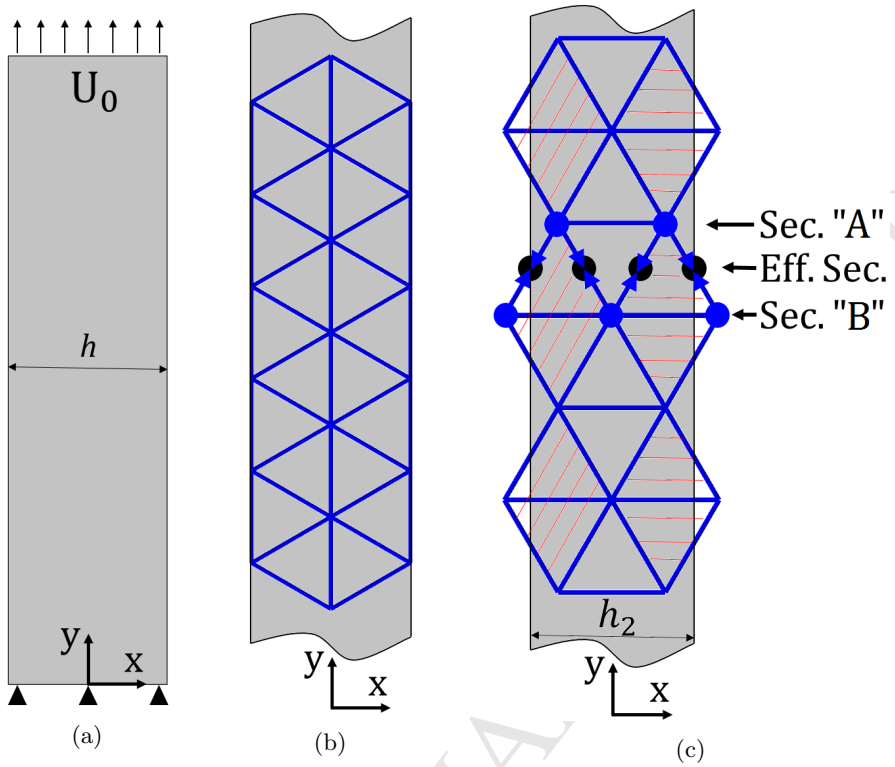

Figure 21: Tension of a strip. (a) Sketch of the problem setting. (b) Stretching in direction "1" with the straight side boundaries. (c) Stretching in direction "2" with the side boundaries of "zigzag" shape. The effective strip section is formed from black points while the points of sections of type "A" and "B" are marked in blue. The strip is composed of two "blocks": the 1st one is hatched by red skew lines, the 2nd one is hatched by red horizontal lines.

solution derived in Section 4, we have calibrated the equivalent second strain gradient continuum, i.e., we have selected higher-order parameter values $l_a = 0.1$ mm, $l_b = 0.8$ mm, $c = 0.60339$ mm^2 and $c_1/\lambda = 0.38$ mm^2 such that the corresponding solution (red solid lines) visually fits the discrete solution. The oscillating character as well as the magnitude of the solution are perfectly captured by the second strain gradient continuum model. It is worth noting that assumptions (44)–(47) adopted in Section 4 are fulfilled.

Next, by utilizing the measure for the effective Poisson's ratio introduced in Subsection 4.3 (equation (61)), we define discrete set of Poisson's ratio values as shown in Fig. 23 with blue dots for different values for the width of the strip. The black dotted line corresponds to the conventional or bulk Poisson's ratio which is equal to 1/3. Finally, by substituting the calibrated higher-order parameter values ($l_a = 0.1$ mm, $l_b = 0.8$ mm, $c = 0.60339$ mm^2 and $c_1/\lambda = 0.38$ mm^2, collected in Table 2) in equation (62), we derive the size-dependent Poisson's ratio of the equivalent second strain gradient continuum which is represented in Fig. 23 with a red solid line. It can be seen that (i) the red solid line captures the discrete values with a remarkable accuracy; (ii) for strip widths large enough, both the discrete and continuous curves tend to the horizontal line corresponding to the conventional Poisson's ratio value.

6.3 Surface tension in a lattice structure strip

Next, let us consider the same problem setting as in the previous subsection but with $U_0 = 0$. Initial stresses of 100 MPa are prescribed at each truss forming the "zigzag"-shaped boundaries (see Fig. 21c), deforming the strip structure in the x-direction.

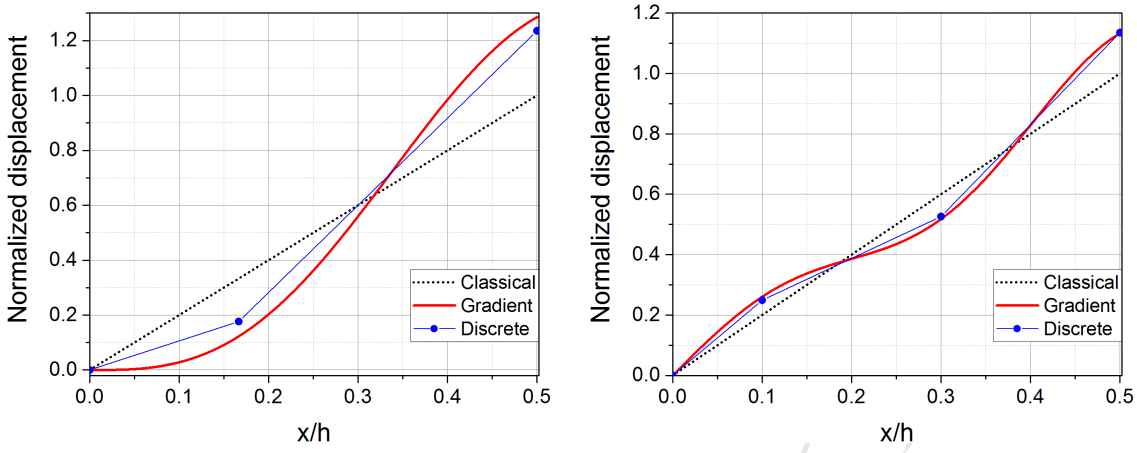

(a) $h = 7.5$ mm (b) $h = 12.5$ mm

(c) $h = 17.5$ mm (d) $h = 22.5$ mm

Figure 22: Normalized displacement profiles.

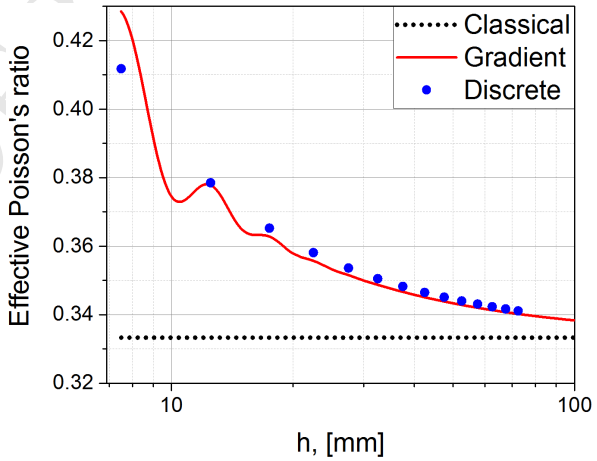

Figure 23: Size-dependent effective Poisson's ratio.

In Fig. 24, the u-component of the displacement field against the dimensionless x-coordinate is presented for four different values of the width. Blue dots represent the discrete values, whereas the red lines correspond to the second strain gradient solution derived in Subsection 3.2. With the higher-order parameters calibrated in the previous subsection (collected in Table 2) the modulus of

cohesion is calibrated to $b_0 = -6.38$ N. Negative sign reflects the fact that positive initial stresses lead to compression of the strip in the x-direction. In case of negative initial stresses (not considered here), the modulus of cohesion takes positive values, which leads to extension of the strip in the x-direction.

Table 2: Material moduli calibrated for the tension problem of Subsections 6.2 and 6.3.

E, [kN/mm]	ν	l_a, [mm]	l_b, [mm]	c, [mm^2]	c_1/λ, [mm^2]	b_0, [N]
58.2	1/3	0.1	0.8	0.60339	0.38	-6.38

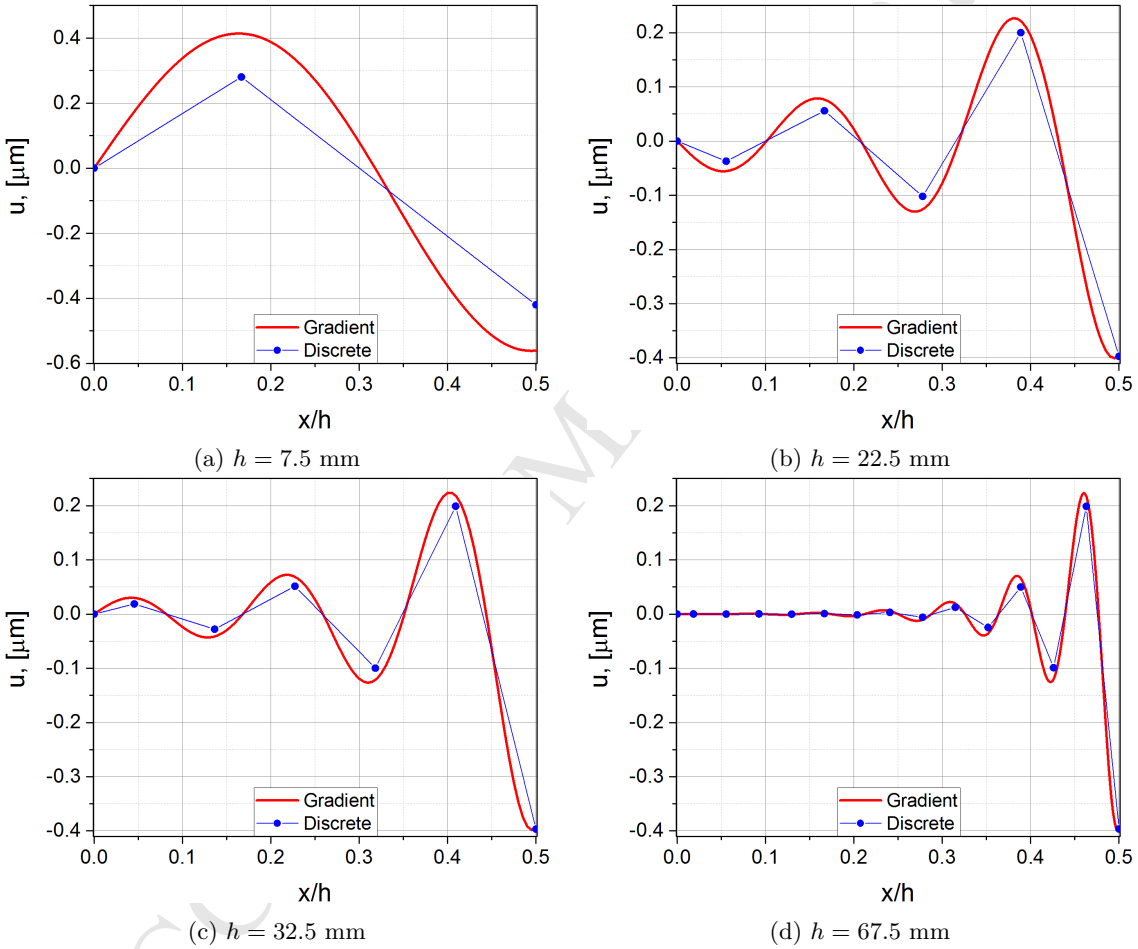

(a) $h = 7.5$ mm (b) $h = 22.5$ mm

(c) $h = 32.5$ mm (d) $h = 67.5$ mm

Figure 24: Displacement profiles.

6.4 Shear of a lattice structure strip

Let us consider a long strip made of the triangular truss structure with applied shear loadings in the lattice direction "1" (see Figs. 20a and 25b). It is worth noting that only trusses of type "3" are responsible for the free surface effects. Thereby, for simplicity, the trusses of type "2" are excluded for the shear problem of this subsection ($k_2 = 0$). The numerical simulations have been accomplished for different strip widths. An illustration of a deformed truss lattice structure composed of two "blocks" in the width direction is presented in Fig. 25b.

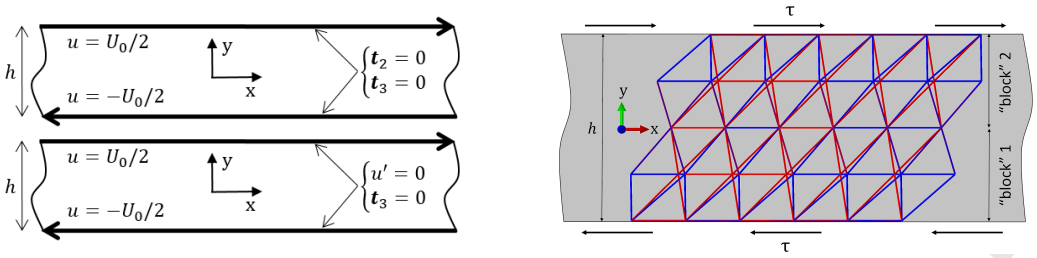

(a) (b)

Figure 25: (a) Boundary conditions for a simple shear problem (top) and shear problem with rough boundaries (bottom). (b) Deformed shape of the truss lattice structure with the width of two "blocks". Trusses of type "1" and "3" are marked, respectively, with blue and red lines.

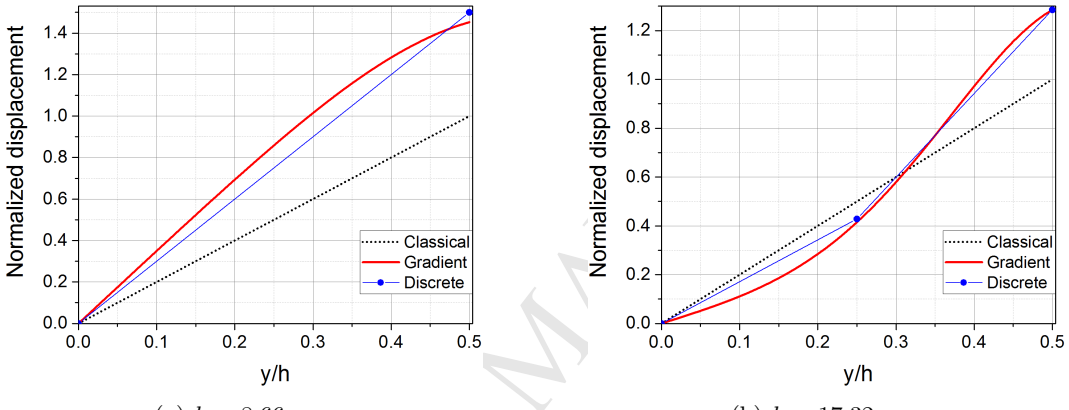

(a) $h = 8.66$ mm

(b) $h = 17.32$ mm

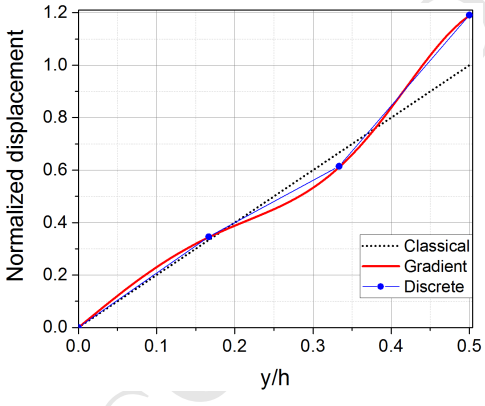

(c) $h = 25.98$ mm

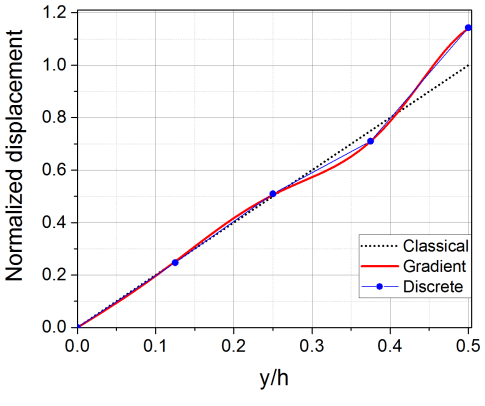

(d) $h = 34.64$ mm

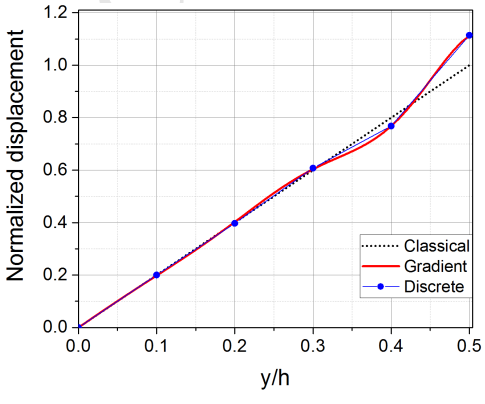

(e) $h = 43.3$ mm

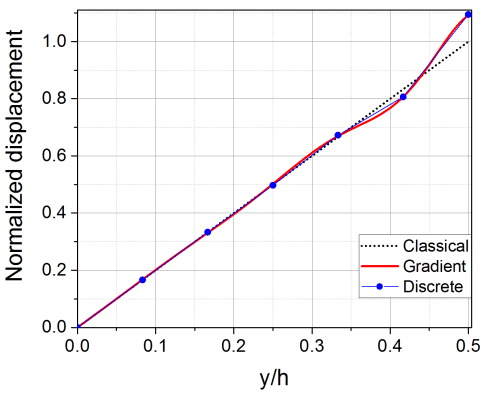

(f) $h = 51.96$ mm

Figure 26: Normalized displacement profiles.

The normalized (with respect to the corresponding classical solution) u-component of the displacement field across the strip width (along the dimensionless y-coordinate) is presented in Fig. 26. As in the previous subsection, the blue dots represent the discrete values, while the black dotted lines stand for the solution of the classical elasticity theory. Red solid lines correspond to the analytical second strain gradient solution derived in Subsection 5.1 (equation (72), see Appendix C as well) with the higher-order parameter values selected as $l_a = 1$ mm, $l_b = 1.57$ mm and $c = 2.457$ mm^2.

It can be seen that the oscillating character as well as the magnitude of the displacements of the discrete structure are captured well by the equivalent second strain gradient continuum. It is remarkable that the surface effects are localized near the strip boundaries as the strip width increases, while points inside the lattice structure undergo the classical (linear) solution.

The normalized effective shear modulus against strip width h is shown in Fig. 27. The discrete set of values (blue dots) is derived according to the measure introduced in Subsection 5.1.3 (eq. (78)). By utilizing the calibrated non-classical parameters ($l_a = 1$ mm, $l_b = 1.57$ mm and $c = 2.457$ mm^2, collected in Table 3) in eq. (81), the effective shear modulus of the equivalent second strain gradient continuum is represented with a red solid line. It is clearly seen that the discrete truss structure as well as the equivalent second strain gradient continuum obey softening behaviour as the strip becomes thinner. On the other hand, for strip widths large enough, the effective shear modulus tends to the corresponding classical one.

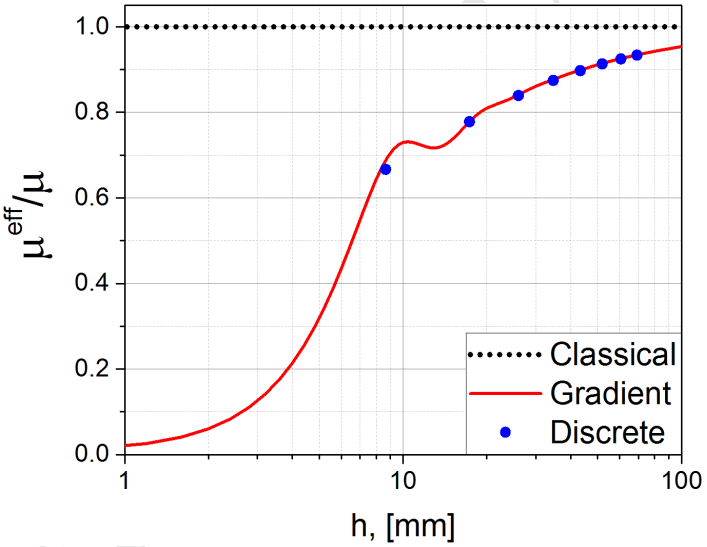

Figure 27: Normalized effective shear modulus.

6.5 Eigenvalue analysis: shear mode regime

For completeness, in this subsection we provide an eigenanalysis of the long strip made of triangular truss lattice structure considered in the previous subsection (by activating shear mode regime). The eigenvalues of the discrete model computed by the commercial finite element software Abaqus are compared to the corresponding frequencies of the following continuum models (with $E = 145.5$ kN/mm, $\nu = 1/3$, $\rho = 16316$ kg/m^2): (1) equivalent classical continuum model; (2) equivalent second strain gradient model ($l_a = 1$ mm, $l_b = 1.57$ mm, $c = 2.457$ mm^2) without higher-order inertia effects ($d_1 = d_2 = 0$ mm) and (3) with them ($d_1 = d_2 = 1$ mm), as presented in Fig. 28. The strong form, i.e., differential equation (11) and boundary conditions (13)–(15), of the second strain gradient continuum model within the simple shear problem formulation is written in terms of displacements as

$$\begin{aligned}
\mu(u + (2c - l_a^2)u'' + l_b^4 u'''')'' &= \rho(\ddot{u} - d_1^2\ddot{u}'' + d_2^4\ddot{u}'''') \quad \text{in } \Omega = (-h/2, h/2),\\
\boldsymbol{t}_1 \cdot \boldsymbol{e}_x = \mu(u + (2c - l_a^2)u'' + l_b^4 u'''')' + \rho(d_1^2\ddot{u}' - d_2^4\ddot{u}''') &= 0 \quad \text{on } \partial\Omega = \{-h/2, h/2\},\\
\boldsymbol{t}_2 \cdot \boldsymbol{e}_x = \mu((l_a^2 - c)u'' - l_b^4 u'''') + \rho d_2^4\ddot{u}'' &= 0 \quad \text{on } \partial\Omega,\\
\boldsymbol{t}_3 \cdot \boldsymbol{e}_x = \mu(l_b^4 u''' + cu') &= 0 \quad \text{on } \partial\Omega.
\end{aligned} \tag{91}$$

It is worth noting that due to the complicated structure of the strong form analytical methods are replaced by a numerical method following the weak formulation addressed in Appendix D.

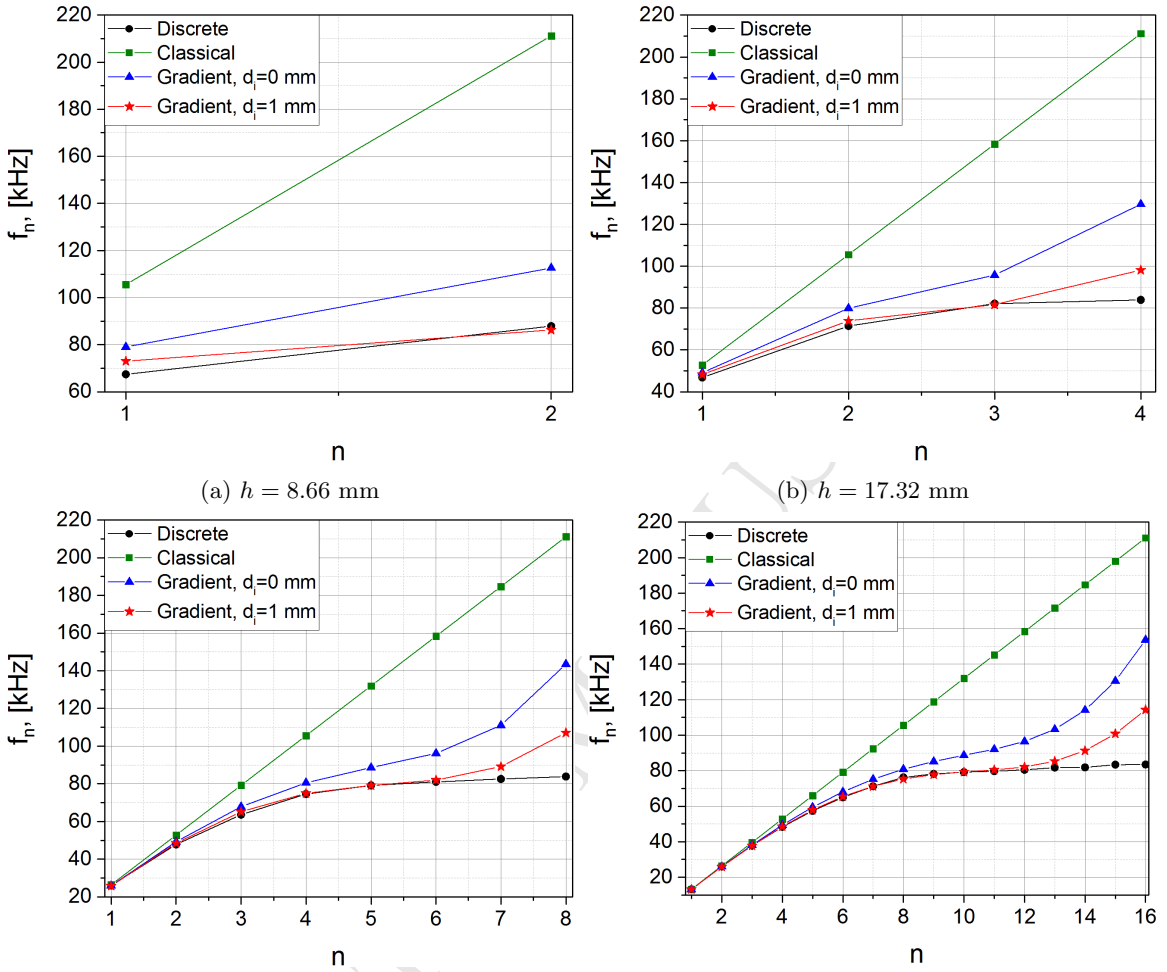

(a) $h = 8.66$ mm (b) $h = 17.32$ mm

(c) $h = 34.64$ mm (d) $h = 69.28$ mm

Figure 28: Eigenfrequencies against mode numbers.

The higher-order elastic parameters (l_a, l_b and c) have been defined in the previous subsection, whereas the higher-order inertia parameters ($d_1 = d_2 = 1$ mm) have been selected by fitting the black dotted curve (eigenvalue spectrum of the discrete model) by the red curve with star marks (eigenvalue spectrum of the equivalent higher-order continuum). It can be seen that the classical elasticity theory (green curves with square marks) fails to describe the mechanical behaviour of the discrete system. The second strain gradient continuum model (blue curves with triangle marks), instead, is able to describe the discrete behaviour, at least qualitatively. By including the higher-order inertia parameters (d_1 and d_2), the generalized continuum model demonstrates quantitative matching (red curves versus black curves) for the majority of the frequencies (the lowest 75%).

Table 3: Material moduli calibrated for the shear problem of Subsections 6.4 and 6.5.

E, [kN/mm]	ν	ρ, [kg/m^2]	l_a, [mm]	l_b, [mm]	c, [mm^2]	d_1, [mm]	d_2, [mm]
145.5	1/3	16316	1	1.57	2.457	1	1

Next, let us consider a strip of infinite width and seek for a wave form solution as $u(y,t) = u_0 e^{-ik(y-v_p t)}$, where i is the imaginary unit, k stands for the wave number, v_p denotes the phase

velocity and u_0 is the wave amplitude. By substituting this solution in the motion equation (91), one can derive the dispersion relation of the form

$$\omega = v_0 k \sqrt{\frac{1 + (l_a^2 - 2c)k^2 + l_b^4 k^4}{1 + d_1^2 k^2 + d_2^4 k^4}}, \tag{92}$$

where ω is the angular frequency and $v_0 = \sqrt{\mu/\rho}$ stands for the phase velocity in the classical continuum solid. The corresponding phase and group velocities are derived, respectively, as

$$v_p = \frac{\omega}{k} \xrightarrow{k\to+\infty} v_0 \left|\frac{l_b^2}{d_2^2}\right|, \quad v_g = \frac{\partial \omega}{\partial k} \xrightarrow{k\to+\infty} v_0 \left|\frac{l_b^2}{d_2^2}\right|. \tag{93}$$

In Fig. 29, it can be seen that (i) for the selected higher-order parameter values long waves propagate with a velocity smaller than the classical one ($v_p < v_0$ and $v_g < v_0$), (ii) the phase and group velocities tend to the limit values given in (93).

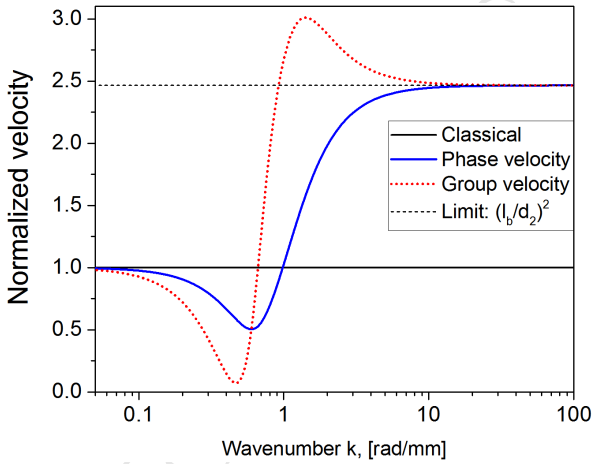

Figure 29: Normalized (with respect to $v_0 = \sqrt{\mu/\rho}$) phase and group velocities against angular wavenumber.

Finally, we show that for this truss structure, being a discrete system, there exists a threshold value for the wave length. First, it is worth noting that, within the higher-order problem formulation (91), the corresponding expression for k_n is extremely complicated. Therefore, as a rough estimation, let us use the classical expression for the wave number in the case of a finite domain: $k_n = \pi n/h$, where n stands for the frequency number. For the minimum allowable width ($h_{\min} = 8.66$ mm), the maximum number of the degrees of freedom (excluding rigid body motion) is $N = 2$ (see Fig. 28a). For the structure with width $h = mh_{\min}$, the maximum number of the degrees of freedom increases to $N = 2m$ (shown in Fig. 28) leading to $k_N = 2\pi/h_{\min}$. Thus, by letting m tend to infinity, i.e., by considering an infinite domain, one can conclude that $k_{\max} = 2\pi/h_{\min} \approx 0.73$ rad/mm giving the following estimation for the minimum length wave: $\lambda_{\min} = 2\pi/k_{\max} = h_{\min} = 8.66$ mm. Thereby, by using the second strain gradient continuum model, the dispersion relation for the truss lattice structure appears as depicted in Fig. 30a with the corresponding phase and group velocities shown in Fig. 30b.

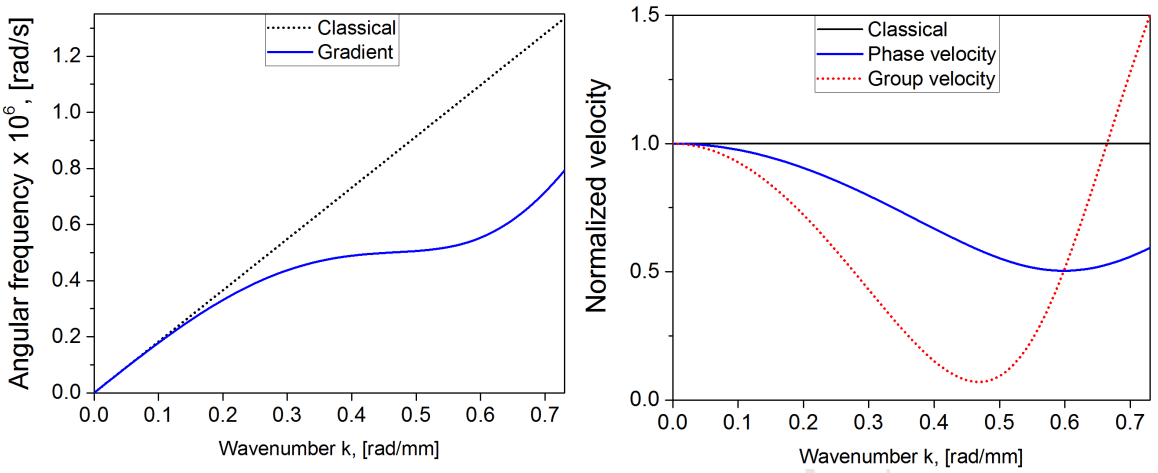

Figure 30: Triangular truss lattice structure. (a) Dispersion relation. (b) Normalized phase and group velocities.

7 Conclusions

Brief summary

Hamilton's principle has been applied for deriving the so-called strong form of the second strain gradient elasticity theory with the second velocity gradient inertia, i.e., the governing equation of motion with the corresponding sets of natural (traction, or Neumann) and essential (displacement, or Dirichlet) boundary conditions. The Form II second strain gradient elasticity model along with the corresponding constitutive relations has been, for the first time, explicitly defined for isotopic solids with surface tension. Furthermore, a simplified variant has been proposed, still capable of accounting for free surface effects and surface tension.

Within the proposed simplified model, the affect of surface tension in solids occupying both half-space and narrow-space domains have been studied. The free surface effects (in the absence of surface tension) have been analyzed in shear and tension/compression problems. Physically appropriate measures for the effective shear modulus and Poisson's ratio have been introduced. Accordingly, a strong size-dependency of both effective moduli has been demonstrated. For each of the benchmark problems, a stability analysis guaranteeing physical solutions has been accomplished.

A fairly general triangular lattice structure of linear springs has been shown, for the first time, to behave as a second strain gradient solid introducing a new mechanical metamaterial. In static cases (tension/compression and shear problems), it has been approved that surface effects appearing at free boundaries of the lattice structure can be adequately captured (qualitatively and quantitatively) and described only by coupling parameters c_i. By performing a free vibration eigenanalysis, the necessity of higher-order inertia parameters (two coefficients in the simplied model) has been demonstrated.

Concluding remarks

1. Stability analyses for the higher-order material parameters (insufficiently accomplished in the related earlier study [40]) in Sections 3, 4 and 5 of the present work demonstrates that for non-admissible parameter values solutions become singular leading to absolutely nonphysical material behaviour (befallen but not exclusively disputed in [40], rather endorsed by vague argumentation and leaving the question open), which impugns many of the results presented in [40]. Such material response is a direct consequence of the violation of the positive definiteness of the strain energy. Although there are examples of negative values of certain higher-order material parameters (cf. [30]), the positive definiteness is a necessary condition for stable material behaviour. It is remarkable that the calibrated higher-order parameters associated to the triangular lattice structure studied in Section 6 of the present work keep the strain energy density positive definite.

2. It has been shown that upon shear deformations (studied in Section 5) coupling parameter

c_3 is responsible for free surface effects, whereas upon tensile/compressive deformations (studied in Section 4) certain combinations of cross-parameters c_1 and c_2 are needed. These issues have not been revealed until now.

3. The second strain gradient elasticity model has been successfully applied for modelling the behaviour of a fairly general macro-scale lattice structure – albeit the analysis remains valid at any length-scale – approving that the critical higher-order effects encountered are not limited to nano-scale alone.

4. Effective material moduli, namely the shear modulus and Poisson's ratio, of the triangular lattice structure have been, for the first time, described by equations of the second strain gradient elasticity theory and found to be size-dependent.

5. It has been demonstrated that for lattice structures the "modulus of cohesion" (coefficient b_0, [17]) can be associated to the initial stresses prescribed on the lattice boundaries (see Subsection 6.3). The compressive/tensile character of the initial stress defines the sign of parameter b_0.

6. A finite element analysis based on the so-called isogeometric pradigm has been performed, for the first time, for simulating free vibrations of a second strain gradient material with non-zero coupling and higher-order inertia parameters.

7. A material parameter identification procedure for the corresponding second strain gradient mechanical metameterials is proposed in the following form: by accomplishing a full-scale finite element modelling of the considered structure (i) higher-order material parameters l_a, l_b, c_i are calibrated upon static simulations (cf. Subsection 6.4), (ii) higher-order inertia length-scale parameters d_1 and d_2 are defined upon eigenvalue analyses (cf. Subsection 6.5).

Acknowledgements

Authors have been supported by Academy of Finland through the project *Adaptive isogeometric methods for thin-walled structures* (decision numbers 270007, 273609, 304122). Access and licenses for the commercial FE software Abaqus have been provided by CSC – IT Center for Science (https://www.csc.fi/)

Appendices

A Relation to Form I of the second strain gradient theory

The Form I strain energy density proposed in 1965 (in index notation) by Mindlin [17] takes the following form in tensor notation

$$\begin{aligned}\tilde{W} = {} & \frac{1}{2}\lambda(tr\boldsymbol{\varepsilon})^2 + \mu\boldsymbol{\varepsilon} : \boldsymbol{\varepsilon} + \tilde{a}_1\nabla(\nabla\cdot\boldsymbol{u})\cdot\nabla(\nabla\cdot\boldsymbol{u}) + \tilde{a}_2\Delta\boldsymbol{u}\cdot\nabla(\nabla\cdot\boldsymbol{u}) \\ & + \tilde{a}_3\Delta\boldsymbol{u}\cdot\Delta\boldsymbol{u} + \tilde{a}_4\nabla\nabla\boldsymbol{u}\vdots\nabla\nabla\boldsymbol{u} + \tilde{a}_5\nabla\nabla\boldsymbol{u}\vdots\boldsymbol{u}\nabla\nabla + \tilde{b}_1(\Delta\nabla\cdot\boldsymbol{u})^2 \\ & + \tilde{b}_2\nabla\nabla(\nabla\cdot\boldsymbol{u}) : \nabla\nabla(\nabla\cdot\boldsymbol{u}) + \tilde{b}_3\Delta\nabla\boldsymbol{u} : \nabla\nabla(\nabla\cdot\boldsymbol{u}) + \tilde{b}_4\Delta\nabla\boldsymbol{u} : \Delta\boldsymbol{u}\nabla \\ & + \tilde{b}_5\Delta\nabla\boldsymbol{u} : \Delta\nabla\boldsymbol{u} + \tilde{b}_6\nabla\nabla\nabla\boldsymbol{u} :: \nabla\nabla\nabla\boldsymbol{u} + \tilde{b}_7\nabla\nabla\nabla\boldsymbol{u} :: \boldsymbol{u}\nabla\nabla\nabla \\ & + \tilde{c}_1(tr\boldsymbol{\varepsilon})\Delta(\nabla\cdot\boldsymbol{u}) + \tilde{c}_2\boldsymbol{\varepsilon} : \nabla\nabla(\nabla\cdot\boldsymbol{u}) + \tilde{c}_3\boldsymbol{\varepsilon} : \Delta\nabla\boldsymbol{u} + \tilde{b}_0\Delta(\nabla\cdot\boldsymbol{u}). \end{aligned} \tag{94}$$

From (94), (9) and (4), the corresponding constitutive equations follow:

$$\begin{aligned}
\tilde{\boldsymbol{\tau}}_1 &= 2\mu\boldsymbol{\varepsilon} + \lambda(\mathrm{tr}\boldsymbol{\varepsilon})\mathbf{I} \\
&\quad + \tilde{c}_1\Delta(\nabla\cdot\boldsymbol{u})\mathbf{I} + \tilde{c}_2\nabla\nabla(\nabla\cdot\boldsymbol{u}) + \frac{1}{2}\tilde{c}_3(\Delta\nabla\boldsymbol{u} + \Delta\boldsymbol{u}\nabla), \qquad (95)\\
\tilde{\boldsymbol{\tau}}_2 &= 2\tilde{a}_1{}^4\mathbf{I} : \nabla(\nabla\cdot\boldsymbol{u})\mathbf{I} + \tilde{a}_2{}^4\mathbf{I} : (\mathbf{I}\nabla\nabla\cdot\boldsymbol{u} + \Delta\boldsymbol{u}\mathbf{I}) \\
&\quad + 2\tilde{a}_3\mathbf{I}\Delta\boldsymbol{u} + 2\tilde{a}_4\nabla\nabla\boldsymbol{u} + \tilde{a}_5(\boldsymbol{u}\nabla\nabla + \nabla\boldsymbol{u}\nabla), \qquad (96)\\
\tilde{\boldsymbol{\tau}}_3 &= \frac{2}{3}\tilde{b}_1\Delta(\nabla\cdot\boldsymbol{u})^4\mathbf{I} + \frac{2}{3}\tilde{b}_2\nabla\nabla(\nabla\cdot\boldsymbol{u}) : {}^6\mathbf{I} \\
&\quad + \frac{1}{6}\tilde{b}_3[(\Delta\nabla\boldsymbol{u} + \Delta\boldsymbol{u}\nabla) : {}^6\mathbf{I} + 2\nabla\cdot{}^4\mathbf{I}\nabla(\nabla\cdot\boldsymbol{u})] \\
&\quad + \frac{2}{3}\tilde{b}_4\Delta\boldsymbol{u}\cdot{}^4\mathbf{I}\nabla + \frac{2}{3}\tilde{b}_5\Delta\nabla\cdot{}^4\mathbf{I}\boldsymbol{u} + 2\tilde{b}_6\nabla\nabla\nabla\boldsymbol{u} \\
&\quad + \frac{2}{3}\tilde{b}_7(\boldsymbol{u}\nabla\nabla\nabla + \nabla\boldsymbol{u}\nabla\nabla + \nabla\nabla\boldsymbol{u}\nabla) \\
&\quad + \frac{1}{3}\tilde{c}_1(\mathrm{tr}\boldsymbol{\varepsilon})^4\mathbf{I} + \frac{1}{3}\tilde{c}_2\boldsymbol{\varepsilon} : {}^6\mathbf{I} + \frac{1}{3}\tilde{c}_3{}^4\mathbf{I}\cdot\boldsymbol{\varepsilon} + \frac{1}{3}\tilde{b}_0{}^4\mathbf{I}, \qquad (97)
\end{aligned}$$

where ${}^4\mathbf{I} = {}^4\mathbf{I}_1 + {}^4\mathbf{I}_2 + {}^4\mathbf{I}_3$, ${}^6\mathbf{I} = {}^6\mathbf{I}_1 + {}^6\mathbf{I}_2 + {}^6\mathbf{I}_3$, ${}^4\mathbf{I}_1 = \mathbf{II} = \boldsymbol{e}_i\boldsymbol{e}_i\boldsymbol{e}_j\boldsymbol{e}_j$, ${}^4\mathbf{I}_2 = \boldsymbol{e}_i\boldsymbol{e}_j\boldsymbol{e}_i\boldsymbol{e}_j$, ${}^4\mathbf{I}_3 = \boldsymbol{e}_i\mathbf{I}\boldsymbol{e}_i$, ${}^6\mathbf{I}_1 = {}^4\mathbf{I}_2\mathbf{I}$, ${}^6\mathbf{I}_2 = \boldsymbol{e}_i\boldsymbol{e}_j\boldsymbol{e}_i\boldsymbol{e}_k\boldsymbol{e}_j\boldsymbol{e}_k$, ${}^6\mathbf{I}_3 = \boldsymbol{e}_i\boldsymbol{e}_j\boldsymbol{e}_k\boldsymbol{e}_i\boldsymbol{e}_j\boldsymbol{e}_k$.

Material parameters of the Form I and Form II second strain gradient theories are coupled as follows:

$$\begin{aligned}
&\hat{a}_1 = 2\tilde{a}_2 - 4\tilde{a}_3, \quad \hat{a}_2 = \tilde{a}_1 - \tilde{a}_2 + \tilde{a}_3, \\
&\hat{a}_3 = 4\tilde{a}_3, \quad \hat{a}_4 = 3\tilde{a}_4 - \tilde{a}_5, \quad \hat{a}_5 = -2\tilde{a}_4 + 2\tilde{a}_5, \\
&\hat{b}_1 = \tilde{b}_1, \quad \hat{b}_2 = \tilde{b}_2 - \tilde{b}_4 + \tilde{b}_5, \quad \hat{b}_3 = \tilde{b}_3 - 2\tilde{b}_4 + 2\tilde{b}_5, \quad \hat{b}_4 = 2\tilde{b}_5, \qquad (98)\\
&\hat{b}_5 = 4\tilde{b}_4 - 4\tilde{b}_5, \quad \hat{b}_6 = 3\tilde{b}_6 - \tilde{b}_7, \quad \hat{b}_7 = -2\tilde{b}_6 + 2\tilde{b}_7, \\
&\hat{b}_0 = \tilde{b}_0, \quad \hat{c}_1 = \tilde{c}_1, \quad \hat{c}_2 = \tilde{c}_2, \quad \hat{c}_3 = \tilde{c}_3.
\end{aligned}$$

B Index notation for Form II model

The Form II strain energy density (21) proposed in Subsection 2.2 in index notation takes the form

$$\begin{aligned}
\hat{W} &= \frac{1}{2}\lambda\varepsilon_{ii}\varepsilon_{jj} + \mu\varepsilon_{ij}\varepsilon_{ij} + \hat{a}_1\hat{\varepsilon}_{iij}\hat{\varepsilon}_{jkk} + \hat{a}_2\hat{\varepsilon}_{ijj}\hat{\varepsilon}_{ikk} + \hat{a}_3\hat{\varepsilon}_{iik}\hat{\varepsilon}_{jjk} \\
&\quad + \hat{a}_4\hat{\varepsilon}_{ijk}\hat{\varepsilon}_{ijk} + \hat{a}_5\hat{\varepsilon}_{ijk}\hat{\varepsilon}_{kji} + \hat{b}_1\hat{\varepsilon}_{iijj}\hat{\varepsilon}_{kkll} + \hat{b}_2\hat{\varepsilon}_{ijkk}\hat{\varepsilon}_{ijll} \\
&\quad + \hat{b}_3\hat{\varepsilon}_{iijk}\hat{\varepsilon}_{jkll} + \hat{b}_4\hat{\varepsilon}_{iijk}\hat{\varepsilon}_{lljk} + \hat{b}_5\hat{\varepsilon}_{ijjk}\hat{\varepsilon}_{klli} + \hat{b}_6\hat{\varepsilon}_{ijkl}\hat{\varepsilon}_{ijkl} \\
&\quad + \hat{b}_7\hat{\varepsilon}_{ijkl}\hat{\varepsilon}_{iljk} + \hat{c}_1\varepsilon_{ii}\hat{\varepsilon}_{jjkk} + \hat{c}_2\varepsilon_{ij}\hat{\varepsilon}_{ijkk} + \hat{c}_3\varepsilon_{ij}\hat{\varepsilon}_{kkij} + \hat{b}_0\hat{\varepsilon}_{iijj}, \qquad (99)
\end{aligned}$$

The corresponding constitutive equations are written as

$$\begin{aligned}
\hat{\tau}_{pq} &= \lambda\varepsilon_{ii}\delta_{pq} + 2\mu\varepsilon_{pq} + \hat{c}_1\hat{\varepsilon}_{iijj}\delta_{pq} + \hat{c}_2\hat{\varepsilon}_{pqii} + \hat{c}_3\hat{\varepsilon}_{iipq}, \\
\hat{\tau}_{pqr} &= \hat{a}_1(\hat{\varepsilon}_{iip}\delta_{qr} + \frac{1}{2}\hat{\varepsilon}_{rii}\delta_{pq} + \frac{1}{2}\hat{\varepsilon}_{qii}\delta_{pr}) + 2\hat{a}_2\hat{\varepsilon}_{pii}\delta_{qr} \\
&\quad + \hat{a}_3(\hat{\varepsilon}_{iir}\delta_{pq} + \hat{\varepsilon}_{iiq}\delta_{pr}) + 2\hat{a}_4\hat{\varepsilon}_{pqr} + \hat{a}_5(\hat{\varepsilon}_{rqp} + \hat{\varepsilon}_{qpr}), \\
\hat{\tau}_{pqrs} &= 2\hat{b}_1\hat{\varepsilon}_{iijj}\delta_{pq}\delta_{rs} + 2\hat{b}_2\hat{\varepsilon}_{pqii}\delta_{rs} + \hat{b}_3(\hat{\varepsilon}_{rsii}\delta_{pq} + \hat{\varepsilon}_{iipq}\delta_{rs}) \\
&\quad + 2\hat{b}_4\hat{\varepsilon}_{iirs}\delta_{pq} + \frac{1}{2}\hat{b}_5(\hat{\varepsilon}_{siip}\delta_{qr} + \hat{\varepsilon}_{siiq}\delta_{pr} + \hat{\varepsilon}_{riip}\delta_{qs} + \hat{\varepsilon}_{riiq}\delta_{ps}) \\
&\quad + 2\hat{b}_6\hat{\varepsilon}_{pqrs} + \frac{1}{2}\hat{b}_7(\hat{\varepsilon}_{psqr} + \hat{\varepsilon}_{prqs} + \hat{\varepsilon}_{qspr} + \hat{\varepsilon}_{qrps}) \\
&\quad + \hat{c}_1\varepsilon_{ii}\delta_{pq}\delta_{rs} + \hat{c}_2\varepsilon_{pq}\delta_{rs} + \hat{c}_3\varepsilon_{rs}\delta_{pq} + \hat{b}_0\delta_{pq}\delta_{rs}, \qquad (100)
\end{aligned}$$

where δ_{ij} is the Kronecker delta.

Density of kinetic energy (30) and the corresponding momenta (31) in index notation take, respectively, the forms

$$T = \frac{1}{2}\rho(\dot{u}_i\dot{u}_i + d_1^2\dot{u}_{j,i}\dot{u}_{j,i} + d_2^4\dot{u}_{k,ij}\dot{u}_{k,ij}), \tag{101}$$

$$p_i = \rho\dot{u}_i, \quad p_{ij} = \rho d_1^2\dot{u}_{j,i}, \quad p_{ijk} = \rho d_2^4\dot{u}_{k,ij}. \tag{102}$$

C Simple shear problem with traction boundary conditions

In case of applied shear loading T, the boundary conditions at $y = \pm h/2$ in (74) take the form

$$\begin{aligned} &\boldsymbol{t}_1 \cdot \boldsymbol{e}_x = \sigma_{xy} = \mu A_5 = T, \\ &\boldsymbol{t}_2 \cdot \boldsymbol{e}_x = \mu\big((l_a^2 - c)u'' - l_b^4 u''''\big) = 0, \\ &\boldsymbol{t}_3 \cdot \boldsymbol{e}_x = \mu\big(l_b^4 u''' + cu'\big) = 0, \end{aligned} \tag{103}$$

leading to integration constants A_i, $i = 1, ..., 6$, of the form

$$\begin{aligned} A_1 &= -\frac{T}{2\mu}\frac{cl_1^2(l_2^2 + c)}{\sinh(\gamma_1)(l_1(l_2^2 + c)^2\coth(\gamma_1) - l_2(l_1^2 + c)^2\coth(\gamma_2))}, \\ A_3 &= -\frac{l_2^2(l_1^2 + c)\sinh(\gamma_1)}{l_1^2(l_2^2 + c)\sinh(\gamma_2)}A_1, \\ A_2 &= -A_1, \quad A_4 = -A_3, \quad A_5 = T/\mu, \quad A_6 = 0, \end{aligned} \tag{104}$$

where $\gamma_i = h/(2l_i)$, $i = 1, 2$. It can be seen that solution (72) degenerates into the corresponding classical one $u(y) = u_0(y) = yT/\mu$ when $c = 0$, i.e., $c_3 = 0$.

D Weak formulation of the eigenvalue problem

The variational, or weak, formulation of the strong form (91), by assuming that the solution of the corresponding differential equation takes the classical form $u(y, t) = e^{i\omega t}u(y)$, reads as follows:
Find $u \in U \subset H^3(\Omega)$ such that

$$a(u, v) = \omega^2 m(u, v) \quad \forall v \in V \subset H^3(\Omega), \tag{105}$$

where bilinear forms a and m: $U \times V \to \mathbb{R}$, respectively, are defined as

$$a(u, v) = \int_\Omega \mu(u'v' + (l_a^2 - 2c)u''v'' + l_b^4 u'''v''')d\Omega, \tag{106}$$

$$m(u, v) = \int_\Omega \rho(uv + d_1^2 u'v' + d_2^4 u''v'')d\Omega. \tag{107}$$

For the problem formulation given in (91), the trial and test function sets consist of $H^3(\Omega)$ functions satisfying a suitable normalization conditions. A conforming Galerkin formulation for the corresponding weak problem reads as follows: Find $u_h \in U_h \subset U$ such that

$$a(u_h, v) = \omega^2 m(u_h, v) \quad \forall v \in V_h \subset V. \tag{108}$$

Further implementation issues with all details are described in [62].

References

[1] D. Sander, Surface stress: implications and measurements, Current Opinion in Solid State and Materials Science 7 (2003) 51–57.

[2] R. Dingreville, J. Qu, M. Cherkaoui, Surface free energy and its effect on the elastic behavior of nano-sized particles, wires and film, Journal of the Mechanics and Physics of Solids 53 (2005) 1827–1854.

[3] S. Cuenot, C. Frétigny, S. Demoustier-Champagne, B. Nysten, Surface tension effect on the mechanical properties of nanomaterials measured by atomic force microscopy, Physical Review B 69 (2004) 165410–1–5.

[4] C. Q. Chen, Y. Shi, Y. S. Zhang, J. Zhu, Y. J. Yan, Size dependence of Young's modulus in ZnO nanowires, Physical Review Letters 96 (2006) 075505–1–4.

[5] G. Y. Jing, H. L. Duan, X. M. Sun, Z. S. Zhang, J. Xu, Y. D. Li, J. X. Wang, D. P. Yu, Surface effects on elastic properties of silver nanowires: Contact atomic-force microscopy, Physical Review B 73 (2006) 235409–1–6.

[6] C.-Y. Nam, P. Jaroenapibal, D. Tham, D. E. Luzzi, S. Evoy, J. E. Fischer, Diameter-dependent electromechanical properties of GaN nanowires, Nano Letters 6 (2006) 153–158.

[7] K. B. Gavan, H. J. R. Westra, E. W. J. M. van der Drift, W. J. Venstra, H. S. J. van der Zant, Size-dependent effective Young's modulus of silicon nitride cantilevers, Applied Physics Letters 94 (2009) 233108–1–3.

[8] J. Sun, L. He, Y.-C. Lo, T. Xu, H. Bi, L. Sun, Z. Zhang, S. X. Mao, J. Li, Liquid-like pseudoelasticity of sub-10-nm crystalline silver particles, Nature Materials 13 (2014) 1007–1012.

[9] S. Nikolov, C.-S. Han, D. Raabe, On the origin of size effects in small-strain elasticity of solid polymers, International Journal of Solids and Structures 44 (2007) 1582–1592.

[10] V. P. Smyshlyaev, N. A. Fleck, The role of strain gradients in the grain size effect for polycrystals, Journal of the Mechanics and Physics of Solids 44 (1996) 465–495.

[11] D. C. C. Lam, F. Yang, A. C. M. Chong, J. Wang, P. Tong, Experiments and theory in strain gradient elasticity, Journal of the Mechanics and Physics of Solids 51 (2003) 1477–1508.

[12] D. Polyzos, G. Huber, G. Mylonakis, T. Triantafyllidis, S. Papargyri-Beskos, D. E. Beskos, Torsional vibrations of a column of fine-grained material: A gradient elastic approach, Journal of the Mechanics and Physics of Solids 76 (2015) 338–358.

[13] R. A. Toupin, Elastic materials with couple-stresses, Archive for Rational Mechanics and Analysis 11 (1962) 385–413.

[14] R. Mindlin, H. Tiersten, Effects of couple-stresses in linear elasticity, Archive for Rational Mechanics and Analysis 11 (1962) 415–448.

[15] R. A. Toupin, Theories of elasticity with couple-stress, Archive for Rational Mechanics and Analysis 17 (1964) 85–112.

[16] R. D. Mindlin, Micro-structure in linear elasticity, Archive for Rational Mechanics and Analysis 16 (1964) 51–78.

[17] R. D. Mindlin, Second gradient of strain and surface-tension in linear elasticity, International Journal of Solids and Structures 1 (1965) 417–438.

[18] R. D. Mindlin, N. N. Eshel, On first strain-gradient theories in linear elasticity, International Journal of Solids and Structures 4 (1968) 109–124.

[19] A. C. Eringen, E. S. Suhubi, Nonlinear theory of simple microelastic solids: I, International Journal of Engineering Science 2 (1964) 189–203.

[20] A. C. Eringen, E. S. Suhubi, Nonlinear theory of simple microelastic solids: II, International Journal of Engineering Science 2 (1964) 389–404.

[21] A. E. Green, R. S. Rivlin, Multipolar continuum mechanics, Archive for Rational Mechanics and Analysis 17 (1964) 113–147.

[22] M. E. Gurtin, A. I. Murdoch, Continuum theory of elastic-material surfaces, Archive for Rational Mechanics and Analysis 57 (1975) 291–323.

[23] M. E. Gurtin, A. I. Murdoch, Surface stress in solids, International Journal of Solids and Structures 14 (1978) 431–440.

[24] G. Rosi, L. Placidi, V.-H. Nguyen, S. Naili, Wave propagation across a finite heterogeneous interphase modeled as an interface with material properties, Mechanics Research Communications 84 (2017) 43–48.

[25] A. Eringen, On differential equations of nonlocal elasticity and solutions of screw dislocation and surface waves, Journal of Applied Physics 54 (1983) 4703–4710.

[26] G. A. Maugin, Generalized continuum mechanics: What do we mean by that?, in: G. A. Maugin, A. V. Metrikine (Eds.), Mechanics of Generalized Continua, One Hundred Years After the Cosserats, Springer, 2010, pp. 3–14.

[27] G. A. Maugin, A historical perspective of generalized continuum mechanics, in: H. Altenbach, G. A. Maugin, V. Erofeev (Eds.), Mechanics of Generalized Continua, Springer, 2011, pp. 3–14.

[28] H. Askes, E. C. Aifantis, Gradient elasticity in statics and dynamics: An overview of formulations, length scale identification procedures, finite element implementations and new results, International Journal of Solids and Structures 48 (2011) 1962–1990.

[29] A. Javili, F. dell'Isola, P. Steinmann, Geometrically nonlinear higher-gradient elasticity with energetic boundaries, Journal of the Mechanics and Physics of Solids 61 (2013) 2381–2401.

[30] R. Maranganti, P. Sharma, A novel atomistic approach to determine strain-gradient elasticity constants: Tabulation and comparison for various metals, semiconductors, silica, polymers and the (ir) relevance for nanotechnologies, Journal of the Mechanics and Physics of Solids 55 (2007) 1823–1852.

[31] T. Böhme, W. Dreyer, W. H. Müller, Determination of stiffness and higher gradient coefficients by means of the embedded-atom method–an approach for binary alloys, Continuum Mechanics and Thermodynamics 18 (2007) 411–441.

[32] H. M. Shodja, A. Zaheri, A. Tehranchi, Ab initio calculations of characteristic lengths of crystalline materials in first strain gradient elasticity, Mechanics of Materials 61 (2013) 73–78.

[33] N. C. Admal, J. Marian, G. Po, The atomistic representation of first strain-gradient elastic tensors, Journal of the Mechanics and Physics of Solids 99 (2017) 93–115.

[34] L. Placidi, U. Andreaus, A. D. Corte, T. Lekszycki, Gedanken experiments for the determination of two-dimensional linear second gradient elasticity coefficients, Zeitschrift für angewandte Mathematik und Physik 66 (2015) 3699–3725.

[35] L. Placidi, U. Andreaus, I. Giorgio, Identification of two-dimensional pantographic structure via a linear d4 orthotropic second gradient elastic model, Journal of Engineering Mathematics 103 (1) (2017) 1–21.

[36] D. K. Trinh, R. Janicke, N. Auffray, S. Diebels, S. Forest, Evaluation of generalized continuum substitution models for heterogeneous materials, International Journal for Multiscale Computational Engineering 10 (6) (2012) 527–549.

[37] R. A. Toupin, D. C. Gazis, Surface effects and initial stress in continuum and lattice models of elastic crystals, in: Lattice Dynamics. Proceedings of the International Conference Held at Copenhagen, Denmark, August 5–9, 1963, 1965, pp. 597–605.

[38] H. M. Shodja, F. Ahmadpoor, A. Tehranchi, Calculation of the additional constants for fcc materials in second strain gradient elasticity: behavior of a nano-size Bernoulli-Euler beam with surface effects, Journal of Applied Mechanics 79 (2012) 021008–1–8.

[39] F. Ojaghnezhad, H. M. Shodja, A combined first principles and analytical determination of the modulus of cohesion, surface energy, and the additional constants in the second strain gradient elasticity, International Journal of Solids and Structures 50 (2013) 3967–3974.

[40] N. M. Cordero, S. Forest, E. P. Busso, Second strain gradient elasticity of nano-objects, Journal of the Mechanics and Physics of Solids 97 (2016) 92–124.

[41] I. Vardoulakis, G. Exadaktylos, E. Aifantis, Gradient elasticity with surface energy: Mode-III crack problem, International Journal of Solids and Structures 33 (1996) 4531–4559.

[42] B. S. Altan, E. C. Aifantis, On some aspects in the special theory of gradient elasticity, Journal of the Mechanical Behavior of Materials 8 (1997) 231–282.

[43] M. Lazar, G. A. Maugin, E. C. Aifantis, Dislocations in second strain gradient elasticity, International Journal of Solids and Structures 43 (2006) 1787–1817.

[44] C. Polizzotto, A hierarchy of simplified constitutive models within isotropic strain gradient elasticity, European Journal of Mechanics A/Solids 61 (2017) 92–109.

[45] C. Polizzotto, A second strain gradient elasticity theory with second velocity gradient inertia – Part II: Dynamic behavior, International Journal of Solids and Structures 50 (2013) 3766–3777.

[46] S. Papargyri-Beskou, D. Polyzos, D. E. Beskos, Wave dispersion in gradient elastic solids and structures: A unified treatment, International Journal of Solids and Structures 40 (2009) 385–400.

[47] S. Deng, J. Liu, N. Liang, Wedge and twist disclinations in second strain gradient elasticity, International Journal of Solids and Structures 44 (2007) 3646–3665.

[48] X.-L. Gao, S. Park, Variational formulation of a simplified strain gradient elasticity theory and its application to a pressurized thick-walled cylinder problem, International Journal of Solids and Structures 44 (2007) 7486–7499.

[49] S. Khakalo, J. Niiranen, Gradient-elastic stress analysis near cylindrical holes in a plane under bi-axial tension fields, International Journal of Solids and Structures 110–111 (2017) 351–366.

[50] X. Zhang, P. Sharma, Inclusions and inhomogeneities in strain gradient elasticity with couple stresses and related problems, International Journal of Solids and Structures 42 (2005) 3833–3851.

[51] X. L. Gao, H. M. Ma, Solution of Eshelby's inclusion problem with a bounded domain and Eshelby's tensor for a spherical inclusion in a finite spherical matrix based on a simplified strain gradient elasticity theory, Journal of the Mechanics and Physics of Solids 58 (2010) 779–797.

[52] X. L. Gao, M. Q. Liu, Strain gradient solution for the Eshelby-type polyhedral inclusion problem, Journal of the Mechanics and Physics of Solids 60 (2012) 261–276.

[53] C. Liebold, W. H. Müller, Applications of higher-order continua to size effects in bending: theory and recent experimental results, in: H. Altenbach, S. Forest (Eds.), Generalized Continua as Models for Classical and Advanced Materials, Springer, 2016, Ch. 12, pp. 237–260.

[54] J.-J. Alibert, P. Seppecher, F. Dell'Isola, Truss modular beams with deformation energy depending on higher displacement gradients, Mathematics and Mechanics of Solids 8 (2003) 51–73.

[55] H. Askes, A. V. Metrikine, Higher-order continua derived from discrete media: continualisation aspects and boundary conditions, International Journal of Solids and Structures 42 (2005) 187–202.

[56] A. Madeo, L. Placidi, G. Rosi, Towards the design of metamaterials with enhanced damage sensitivity: second gradient porous materials, Research in Nondestructive Evaluation 25 (2014) 99–124.

[57] P. Seppecher, J.-J. Alibert, F. dell'Isola, Linear elastic trusses leading to continua with exotic mechanical interactions, Journal of Physics 319 (2011) 012018–1–13.

[58] F. dell'Isola, T. Lekszycki, M. Pawlikowski, R. Grygoruk, L. Greco, Designing a light fabric metamaterial being highly macroscopically tough under directional extension: first experimental evidence, Z. Angew. Math. Phys. 66 (2015) 3473–3498.

[59] Y. Rahali, I. Giorgio, J. F. Ganghoffer, F. dell'Isola, Homogenization à la Piola produces second gradient continuum models for linear pantographic lattices, International Journal of Engineering Science 97 (2015) 148–172.

[60] J. Niiranen, S. Khakalo, V. Balobanov, A. H. Niemi, Variational formulation and isogeometric analysis for fourth-order boundary value problems of gradient-elastic bar and plane strain/stress problems, Computer Methods in Applied Mechanics and Engineering 308 (2016) 182–211.

[61] J. Besson, G. Cailletaud, J.-L. Chaboche, S. Forest, M. Blétry, Non-Linear Mechanics of Materials. Series: Solid Mechanics and Its Applications, vol. 167, Springer, 2009.

[62] S. Khakalo, J. Niiranen, Isogeometric analysis of higher-order gradient elasticity by user elements of a commercial finite element software, Computer-Aided Design 82 (2017) 154–169.

[63] R. Makvandi, J. C. Reiher, A. Bertram, D. Juhre, Isogeometric analysis of first and second strain gradient elasticity, Computational Mechanics, (2017) doi:10.1007/s00466-017-1462-8.

[64] A. E. H. Love, A treatise on the mathematical theory of elasticity, Fourth edition, Cambridge: University Press, 1927.

[65] C. Polizzotto, A second strain gradient elasticity theory with second velocity gradient inertia – Part I: Constitutive equations and quasi-static behavior, International Journal of Solids and Structures 50 (2013) 3749–3765.

[66] C. Polizzotto, A gradient elasticity theory for second-grade materials and higher order inertia, International Journal of Solids and Structures 49 (2012) 2121–2137.

[67] F. Dell'Isola, P. Seppecher, The relationship between edge contact forces, double forces and interstitial working allowed by the principle of virtual power, Comptes rendus de l'Académie des sciences. Série IIb, Mécanique, physique, astronomie (1995) 7.

[68] F. dell'Isola, A. Madeo, P. Seppecher, Cauchy tetrahedron argument applied to higher contact interactions, Archive for Rational Mechanics and Analysis 219 (2016) 1305–1341.

[69] R. J. D. Tilley, Crystals and Crystal Structures, Wiley, 2006.

[70] E. A. Ivanova, A. M. Krivtsov, N. F. Morozov, A. D. Firsova, Description of crystal packing of particles with torque interaction, Mechanics of Solids 38 (2003) 76–88.

[71] D. Polyzos, D. I. Fotiadis, Derivation of Mindlin's first and second strain gradient elastic theory via simple lattice and continuum models, International Journal of Solids and Structures 49 (2012) 470–480.

Highlights

- Simplified model of Mindlin’s second strain gradient theory of elasticity is introduced
- This model is able to account for free surface effects and surface tension in solids
- Parameter limits from stability analyses disallow non-physical material behavior
- New second strain gradient mechanical metamaterial is introduced
- Effective shear modulus and effective Poisson's ratio are shown to be size-dependent
- Free vibration eigenanalysis determines the higher-order inertia parameters